UNIVERSIDADE DE SÃO PAULO

ESCOLA POLITÉCNICA

Atena Amanati Shahri

Microwave-based microfluidic biosensors:

from the design and implementation to real-time sensing

São Paulo

2023

Atena Amanati Shahri

Microwave-based microfluidic biosensors:

from the design and implementation to real-time sensing

Versão Corrigida

Tese apresentada à Escola Politécnica da Universidade de São Paulo para a obtenção do título de Doutora em Ciências.

Área de Concentração :Microeletrônica

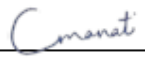Orientador: Profa. Dra. Ariana Maria da Conceição Lacorte Caniato Serrano

São Paulo

2023

Este exemplar foi revisado e corrigido em relação à versão original, sob responsabilidade única do autor e com a anuência de seu orientador.

São Paulo, __08__ de ____fevereiro____ de __2023__

Assinatura do autor: _____

Assinatura do orientador: _____

Catalogação-na-publicação

" Because technology provides the tools and biology the problems, the two should enjoy a happy marriage."

Stanley Fields

Acknowledgments

Resumo

Observar materiais biológicos é um passo crucial em aplicações médicas. As técnicas convencionais de estudo celular são muito bem estabelecidas e eficazes. No entanto, os métodos de detecção são baseados em técnicas de imagem de fluorescência e coloração que podem ser invasivas para as células. A espectroscopia dielétrica em frequências de micro-ondas é uma metodologia analítica nova e não destrutiva para investigar matérias biológicas sem ligação química ou preparação e manipulação prévias que eliminam a modificação do conteúdo. Além disso, oferece a vantagem atraente de monitoramento em tempo real. Esta tese teve como objetivo desenvolver biossensores microfluídicos integrados baseados em micro-ondas capazes de medir as propriedades dielétricas de matérias biológicas como glicose e suspensões celulares para caracterização celular. Depois de revisar os métodos atuais de análise do estado da arte, focamos no desenvolvimento de biossensores de micro-ondas de alta sensibilidade para investigar questões biológicas. Durante o desenvolvimento, a concepção das estruturas dos circuitos em micro-ondas juntamente com a parte fluídica, bem como seus processos de fabricação foram otimizados para melhorar o desempenho dos biossensores em relação à sensibilidade e repetibilidade. Primeiro, a evolução do desempenho do biossensor foi avaliada medindo-se as mudanças de amplitude, fase e frequência nas frequências ressonantes em função das concentrações de glicose em soluções aquosas. O sensor proposto distingue variação de concentrações de glicose em torno de 5,2 GHz e é considerado simples, fácil de operar e bastante sensível (0,32 MHz/(mg/dL). Em seguida, a pesquisa seguiu investigando estruturas biológicas mais complexas, e células vivas foram individualmente detectadas em seu meio de cultura num fluxo em tempo real para fins de quantificação de células. As variações nos parâmetros de espalhamento foram medidas ao longo do tempo na frequência ressonante para conduzir a medição dielétrica de suspensões de células, resultando em sensores com alto desempenho sensibilidade e repetibilidade. O dispositivo proposto neste trabalho distinguiu as células de seu meio medindo uma diferença de aproximadamente 23º na fase do sinal transmitido. Este biossensor pode detectar as células em seu meio de cultura mesmo em fluxo rápido em tempo real e, portanto, pode ser usado como uma ferramenta de diagnóstico precoce e monitoramento de doenças.

Palavras-chave: Glicose, Célula viva única, Biossensor de micro-ondas, Espectroscopia dielétrica, Biossensores, alterações na permissividade relativa

Abstract

Observing biological matters is a crucial step in medical applications. Conventional techniques of cell study are very well established and effective. However, their detection method is based on fluorescence imaging techniques and staining that can be invasive to cells. Microwave dielectric spectroscopy is a novel and non-destructive analytical methodology to investigate biological matters without chemical binding or prior preparation and manipulation that eliminates the modification of the content. Furthermore, it provides the attractive advantage of real-time monitoring. This thesis aimed to develop microfluidic integrated microwave-based biosensors capable of measuring the dielectric properties of biological matters such as glucose and cell suspensions for cell characterization. After reviewing the current state of art analysis methods, we focused on developing high-sensitivity microwave biosensors to investigate biological matters. During the development, the microwave components, design structures, and fabrication processes were optimized to improve the performance of the biosensors regarding sensitivity and repeatability. First, the evolution of the biosensor performance was assessed by measuring the amplitude, phase, and frequency shifts at the absorption peak as a function of glucose concentrations in water solutions. Our sensing device distinguishes the variation of glucose concentrations around 5.2 GHz and is considered to be simple, easy to operate and highly sensitive (0.32 MHz/(mg/dL). Then the research followed by investigating more complex biological structures, and single living cells in culture medium were detected in their flow stream for cell quantification purposes. The changes in the S-parameter were measured over time at the resonant frequency to conduct the dielectric measurement of cell suspensions. The device proposed in the present work distinguished cells from the medium measuring a difference of approximately 23º in the phase of the transmitted signal. This biosensor could detect rapid flowing cells in their biological medium in real-time and hence can be used as an early diagnosis and monitoring tool for diseases.

Keywords: Glucose, Single living cell, Microwave Biosensor, Dielectric spectroscopy, Biosensors, changes in relative permittivity

Table of Figures

List of abbreviations

BGL   Blood Glucose Level

CPW   CoPlanar Waveguide

CSSR   Complementary Split Ring Resonator

DMSO   DiMethylSulfOxide

DR   Dielectric Resonator

DSSR   Double Split Ring Resonator

DUT   Device Under Test

IDC   InterDigitated Capacitor

IgG   Immunoglobulin G

LOD   Limit Of Detection

MUT   Material Under Test

PBS   Phosphate-Buffered Saline

PDMS   PolyDiMethylSiloxane

PMMA   PolyMethyl MethAcrylate

POC   Point Of Care

PTFE   PolyTetraFluoroEthylene

SIR   Stepped Impedance Resonators

SRR   Split Ring Resonator

SUT   Sample Under Test

TMP   Tissue-Mimicking Phantoms

VNA   Vector Network Analyzer

Table of Contents

Chapter 1. INTRODUCTION

The ability to characterize biomaterials in a timely manner is a crucial element of effective medical diagnosis and treatment. Observing and investigating biological matter is a common approach used in clinical and medical research. The biological matter here can be biomolecules, such as proteins, hormones, medically relevant analytes such as glucose, biological systems like cells, or medical parameters, including pulse, heartbeat, etc.

Monitoring blood glucose levels is the most critical part of managing diabetes. Diabetes is a global epidemic affecting an estimated 537 million people worldwide (ÖZTÜRK et al., 2017). According to the International Diabetes Federation, the total number of patients with diabetes is predicted to be 783 million by 2045. Furthermore, diabetes was responsible for 6.7 million deaths in 2021 (IDF DIABETES ATLAS | TENTH EDITION). Diabetes patients must maintain their glucose level in a safe range to avoid diabetic complications such as kidney failure, heart disease, and nerve damage by frequently monitoring blood glucose as an essential part of their diabetic management (LUCISANO et al., 2017).

Furthermore, observing and investigating cells is common in medical applications such as pharmaceuticals, biotechnology, and other clinical/medical research activities. Characterizing cells promptly is a crucial element of effective medical diagnosis and treatment. Assessment of cell counting is an essential step in the characterization of cells. Currently, cell counting is being performed either manually or automatically. Manual cell counting suffers from various shortcomings, such as time-consuming preparations, accuracy due to the subjectivity of counts, and device misuse. Automated cell counters, on the other hand, offer more reliable and reproducible results.

1.1. Conventional Methods for Glucose Monitoring

Generally, laboratory-based testing techniques measure a broad range of glucose concentrations with high specificity and sensitivity. On the other hand, home monitoring

techniques use ambulatory devices by applying a drop of blood to a disposable strip with a chemical reagent system, which is then inserted into an electronic blood glucose meter. These point-of-care (POC) devices are also accurate and reliable in self-assessment situations. In these standard methods, the glucose level is determined from blood, plasma, or serum samples, which makes them inconvenient. Thus, many researchers have tried to demonstrate the feasibility of different non-destructive biosensing technologies to monitor glucose levels (GONZALES; MOBASHSHER; ABBOSH, 2019).

1.2.Conventional Methods for Cell Studies

Conventionally, optical detection systems are utilized for cell analysis due to their high efficiency and specificity on account of fluorochromes and antibodies used for attachment in the cells. In cell biology, microscopy and flow cytometry have been employed extensively and successfully over the last two decades. Microscopy uses optical imaging techniques to observe cells through a microscope. The obtained images allow the analysis of the morphology of the cell or its intracellular environment using stains or fluorescent dyes. The advances in microscopy deepened the knowledge about either fixed cells or living states. They can image cells, making them the standard of practice for biologists and physicians. Microscopic imaging of cells provides valuable information on a single-cell constitution for investigating biological processes. A certain number of microscopes have been developed to allow the observation of cells. Two families of optical microscopes and electric microscopes have mainly been distinguished (KARP; IWASA; MARSHALL, 2016).
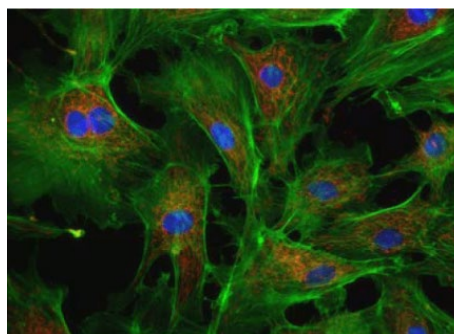
Figure 1. Cells stained with three dyes highlighting the nucleus (blue), actin (green), and mitochondria (red)

Source: (ARTIS et al., 2015)

In optical microscopy, living cells can be studied directly. However, observing biological structures is challenging because cells are usually too small and transparent to visible light. In this content, as illustrated in Figure 1, fluorescence microscopy utilizes different dyes simultaneously to highlight intracellular structures, such as the nucleus in blue, the actin in green, and the mitochondria in red. The study of whole cell structure is possible in electric microscopy. But the cells are dead; they must be treated by the methods known as fixation to be analyzed.

Flow cytometry is a well-established technique for quantifying and identifying cells or particles in suspension used in various applications such as pharmacology, hematology, immunology, microbiology, etc. A flow cytometer is composed of a fluidic system to transport the cells to be analyzed from the sample tube to the flow cell, an optical system to emit and collect light signals, and an electronic and computer system to convert collected optical signals to electronic signals and digitize and process them for computer analysis. The intensity of the collected signals correlates to cell properties(MCKINNON, 2018).

- Forward scatter (FSC) identifies the relative cell size from light scattering past the cell along the laser path.
- Side scatter (SSC) helps to provide information on the complexity of the cell by measuring the light scattering at a ninety-degree angle relative to the laser.

A Process called hydrodynamic focusing forces the cells to line up in a single file in the stream. When each cell passes through a laser path, multiple parameters, such as forward and side light scatter, are measured. It offers several unique advantages, such as fast, relatively quantitative, multiparametric analysis of cell populations at the single-cell level.

Although traditional diagnosis with contemporary methods is very efficient with very high specificity, these methods are considered invasive for observing cells due to labeling techniques to analyze intracellular structures. At the same time, cells must first be fixed, permeabilized, stained, and then analyzed by flow cytometry or microscopy. The procedure is time-consuming and also destructive for the cells. These labels and markers may modify cells, resulting in undesirable and inaccurate detection. They need time to interact with the cells; therefore, real-time monitoring is not an option. Also, the need for costly equipment for further analysis and information extraction poses unique challenges. Thus, the development of

techniques that would be non-invasive or label-free has the potential to improve biological discovery remarkably.

There is a significant interest in developing real-time non-destructive biological sensing and analysis methods that can bring consequences at the fundamental level and for therapy. This could result in a superior understanding of biological processes, early diagnosis of disease, and rapidly evaluating of the effectiveness of treatment. The use of biosensors for biomaterial characterization can prevent traditional difficulties. Therefore, biosensing technology represents a promising solution to enhance biological and medical applications due to its ease of use and cost-effective production.

1.3.Recent Advances in Biosensing Technology

The evolution and development of sensing technology and devices have significantly impacted medical practices and biomedical research over the years. Biosensors are quite present in many applications, such as diagnosis monitoring, treating different diseases, and drug delivery (BHALLA et al., 2016). Various techniques have been used for the development of biosensors. Lately, biosensing has experienced enormous growth by deploying electrical, mechanical, optical, and microwave technologies for healthcare applications. They can successfully detect and measure various biological matters. Advances in microfabrication and technological approaches with new material and design techniques aim to provide biosensing tools to improve the quality of life by changing health care delivery. Therefore, these biosensors are popular in developing point-of-care testing (POCT), from monitoring of treatment to disease progression.

Over the past few years, POCT or bedside testing – medical diagnostic near or at the patient's location in non-laboratory conditions– has been improving rapidly. It attracts researchers to develop new approaches that can be easy, reliable, miniaturized, real-time, and less costly than Lab-based testing. The key objective of POCT is to provide a more rapid, high-accuracy result so that appropriate treatment can be considered, leading to an improved clinical outcome (CHIN; LINDER; SIA, 2012; GUHA; JAMAL; WENGER, 2017). This attracts researchers to also arrive at a comprehensive solution by applying suitable sensitive integrated

characterization techniques such as optical, electrochemical analysis (SALITERMAN, 2006), and bio-impedancemetry using microwave frequencies (GUARITI et al., 2013).

1.3.1. Biosensing types

A biosensor is an analytical device incorporating a biological sensing element either intimately connected to or integrated within a transducer. The purpose of developing a biosensor is to rapidly provide accurate and reliable information about an analyte of interest in real-time, preferably without requiring the addition of other reagents or pretreatment of the sample (TURNER; KARUBE; WILSON, 1987). The components of a biosensor are illustrated in Figure 2.

It is composed of a bioreceptor to ensure the recognition of the biological matter and a transducer to convert the biological signal into a measurable signal. Biosensors can be categorized by type of bioreceptor, whether a labeling process is involved during the detection or not. Label-based biosensors depend on labeling materials to perform the biosensing process. On the other hand, label-free biosensors measure the transduced signal without any labels or complicated sample preparation steps. Generally, four main types of biosensors can be classified as electrical, mechanical, optical, and RF/microwave-based due to the nature of their transducers. The following section summarizes various signal transduction methods utilized in biosensing applications.
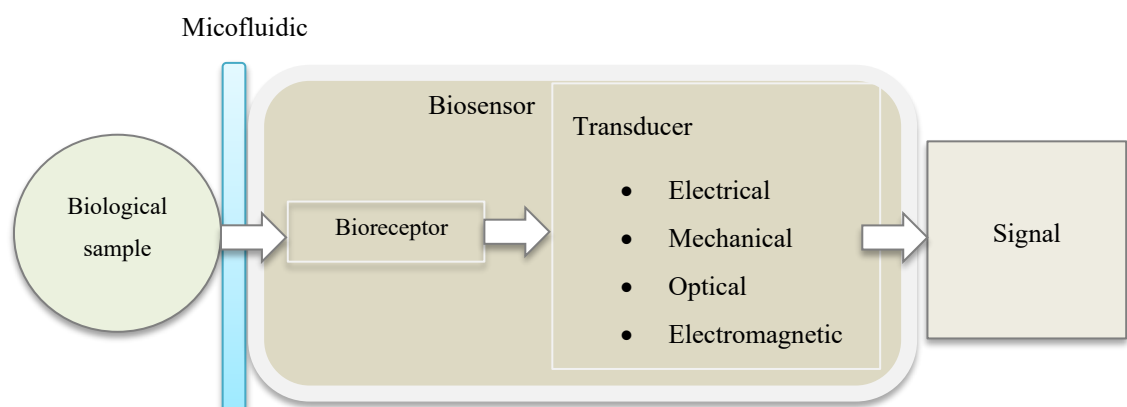
Figure 2. Schematic representation of a biosensor

1.3.1.1. Electrical biosensors

Electrical biosensors generally measure currents or voltages to detect a target biomaterial (DANIELS; POURMAND, 2007). Electrical biosensors can be subdivided based on the manner in which the electrical measurement is performed, such as impedance biosensors that measure the electrical impedance(MADURAIVEERAN; SASIDHARAN; GANESAN, 2018; SUHITO; KOO; KIM, 2021). Impedance can be measured with a minimum of two electrodes. A small sinusoidal voltage at a defined frequency will be applied to a biological material while measuring the resulting current. Hence different target substances due to impedance changes can be detected. Impedance biosensors have been mainly utilized in the detection of glucose levels (NADERI ASRAMI et al., 2018), tumor cells (CHUNG et al., 2011), protein disease biomarkers (LUO; DAVIS, 2013), blood coagulation (LI et al., 2018b), and monitoring cholesterol levels (KAUR; TOMAR; GUPTA, 2018). However, this technique is generally applied to low frequencies below 100MHz. Electrochemical-based biosensors became another research subject and dominated the commercial market (TANG et al., 2004). The interactions between analytes and bioreceptors on the electrodes or probes are acquired. Enzyme-Electrochemical glucose methods have been used in commercial glucose meters. The main advantages of the electrical detection technique are ease of implementation, low power consumption, and flexibility in sensor size.

1.3.1.2. Mechanical biosensors

Mechanical biosensors measure forces, displacements, and mass changes from cellular and subcellular processes, for instance, quartz crystal microbalance (QCM) or resonant cantilever, as a detection technique. QCM-based biosensors investigate the changes in the frequency of a piezoelectric crystal, such as quartz-based, on adherence to a target molecule. The target biological substance is attached to the microcantilever with two detection modes in the latter.

In static mode, the surface of the microcantilever bends, and its deflection depends on the stress induced by the analyte binding reaction at the interface. In dynamic detection mode, the change in the resonance frequency of the beam is caused by the mass of the analyte. According to the mode, with the binding of the target molecule, either the deflection or vibration

of the microcantilever changes the resonant frequency. The resulting signal is then further analyzed (CHALKLEN; JING; KAR-NARAYAN, 2020; FRITZ, 2008). Mechanical biosensors are employed for the detection of virus infections (HUANG et al., 2013; KIM et al., 2015), cancer biomarkers (WANG et al., 2014; WU et al., 2001), and protein-membrane(NIELSEN; OTZEN, 2019). However, unprecedented challenges of mechanical biosensing systems are the need to improve intrinsic device performance, fabrication reproducibility, and system integration (ARLETT; MYERS; ROUKES, 2011).

1.3.2.3. Optical biosensors

The interaction of an optical field with biological material is studied in optical biosensing (CHEN; WANG, 2020). Light can be reflected or absorbed according to reacting materials, and its intensity is proportionate to the concentration of the measured substance (CARRASCOSA; HUERTAS; LECHUGA, 2016; ESPINA PALANCO et al., 2016; KEISER, 2016). As an example, a surface plasmon resonance (SPR) based biosensor can be utilized to characterize interactions between biomolecules by measuring the angle shift of reflected light (SANSONE et al., 2018; SANTANGELO et al., 2015; WANG; ZHAO, 2018; YOO; LEE, 2016). The majority of optical biosensors are based on fluorescence detection. These techniques use fluorescent molecules as markers to obtain sufficient sensitivity and specificity. For instance, a biosensor composed of a biochip to detect E. coli bacteria was proposed using fluorescently-labeled antibodies (STOKES; GRIFFIN; VO-DINH, 2001). The major drawback of these techniques is the use of marker-specific material, which makes handling (sample preparations) more prolonged, more complex, and more expensive. Nevertheless, the lack of standards, manufacturing protocols, and the cost of many photonic biosensors are the general issues of this type of biosensing.

1.3.1.4. Microwave biosensors

This new biosensing method uses microwave frequencies to study the electrical parameters of biological samples. Microwave biosensors usually consist of microwave transmission networks fabricated on a substrate for sensing purposes. The scattering parameters

are then obtained, and the shift in resonant frequency or change in the amplitude (attenuation) delivers valuable information about the biological target.

The use of electromagnetic (EM) waves in the frequency range of GHz to THz in biosensors as a well-established detection technique for the characterization of biological suspensions and biomolecules was reported successfully (MEHROTRA; CHATTERJEE; SEN, 2019) thanks to Dr. Schwan, who first identified the frequency-dependent behavior of biological materials in the presence of an electromagnetic field (SCHWAN, 1957). This sensing method can identify the changes in the concentration of the biomolecules or distinguish cancerous cells by studying the unique permittivity spectrum of biomolecules or cells. As a result, any abnormalities and disorders could be pointed out. A number of human and animal tissues were characterized at the frequencies of microwaves up to 20 GHz (GABRIEL; LAU; GABRIEL, 1996).

In summary, electrical biosensors focus on low-cost, simple solutions in exchange for lower sensitivity. Even though electrochemical-based biosensors are highly sensitive, they are still considered costly and inconvenient for the patient. Impedance techniques are subject to the labeling process, and the use of nanoparticles tends to be invasive. Although mechanical biosensors provide high sensitivity, they are considered complex and uncertain. There is a long history of using optical biosensors, while some have been commercially used (PIRES et al., 2014). Optical biosensors are highly sensitive; however, these devices are primarily based in laboratories, present significant costs, and require the pre-preparation of samples.

Microwave technology has the potential to address these issues by eliminating the need for physical or chemical modification of the biological sample while operating at higher frequencies (i.e., GHz). Microwave biosensors have become popular among researchers, and electromagnetic waves have been employed to differentiate biological materials relying on detecting dielectric properties due to benefits such as being minimally invasive and cost-effective for many years now (ARTIS et al., 2015; COLE; COLE, 2004; FOSTER; SCHWAN, 1989; GABRIEL; LAU; GABRIEL, 1996; SCHWAN, 1985). Microwave biosensors also offer high sensitivity and real-time monitoring of biological materials (ZARIFI, 2018). Furthermore, they offer label-free detection as opposed to some optical biosensors that utilize labeling techniques for detection purposes.

In addition, the possibility of fabricating complex structures at the micrometric scale provides the opportunity of detecting the presence of microorganisms at the single-cell level.

This miniaturization can pave the way for developing novel medical devices to measure the property of a single cell. Therefore, these biosensors are beneficial in developing POCT, from monitoring treatment to disease progression.

1.4.Microwave Dielectric Spectroscopy Method

Microwave dielectric spectroscopy (MDS) is a real-time, compact, non-destructive analytical methodology that can probe dynamic processes over a broad range of frequencies up to hundreds of gigahertz. Therefore, it has been used to characterize biological materials, from which one may extract the relative permittivity, ε_r, of the material as a function of frequency (KAATZE; FELDMAN, 2005; WOLF et al., 2011). The response from a dielectric material exposed to an external electromagnetic field is schematically depicted in Figure 3, with the material being represented by its complex relative permittivity, ε_r:

$$\varepsilon_r = \varepsilon_r{'} - j\varepsilon_r{''} \tag{1}$$
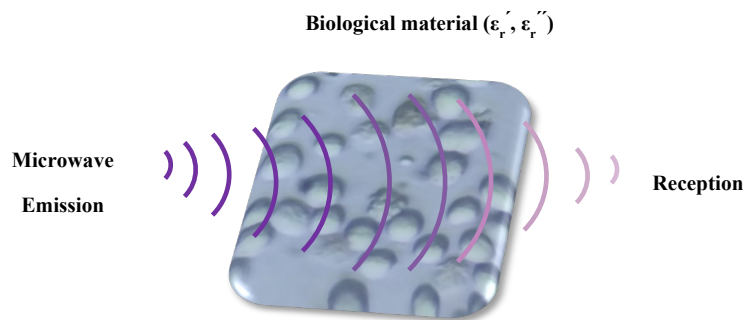
Figure 3. Characterization of material with its dielectric properties

Generally, the real component of the relative permittivity ($\varepsilon_r{'}$) is referred to as the dielectric constant that is a measure of the ability of each material to store electric field energy, while the imaginary relative permittivity ($\varepsilon_r{''}$) can be called loss factor, dissipation factor or dielectric loss that is related to the fraction of energy dissipated in the material per unit length. The effect of structure influencing parameters on the dielectric spectral response can be investigated by measuring dielectric properties. Due to changes in permittivity, the material modifies the transmitted signal, thus allowing one to characterize the physical and chemical properties of the biological material, particularly at radio and microwave frequencies. The

frequency of choice is based on the information of interest. Depending on the characteristic of the material under test (MUT), microwave dielectric spectroscopy can be performed in reflection or transmission mode.
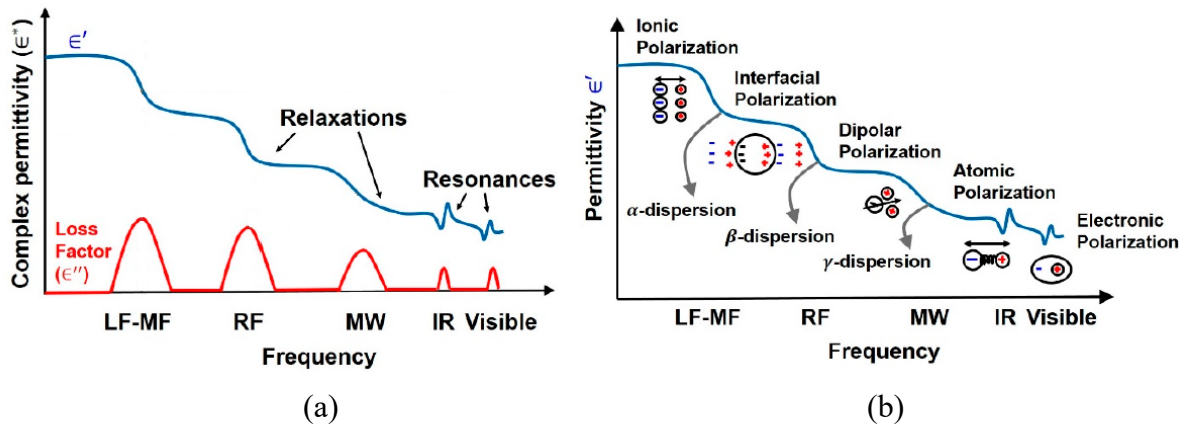
Figure 4. (**a**) The dielectric behavior, and (**b**) The order of polarization and relaxation mechanisms observed in the presence of an alternating electric field.

Source: (MEHROTRA; CHATTERJEE; SEN, 2019)

The complex relative permittivity of biological matter can be obtained due to the occurrence of various polarization phenomena in different frequency ranges from kilo to a few terahertz, as demonstrated in Figure 4. This can be divided into relaxation and resonance of the complex permittivity, which permits the characterization of the sample with its frequency-dependent dielectric properties. The relaxations named α, β, and γ are related to the different polarization phenomena. They are more often referred to by the term dispersion observable over a wide range of frequencies (MEHROTRA; CHATTERJEE; SEN, 2019). The main relaxation phenomena observed from biological tissue are as follows:

o α dispersion occurs in the range of low frequencies up to a few kilohertz. Under the influence of an electric field, the dispersion is associated with ionic diffusion processes occurring at the surface of the cell membrane and resulting in the appearance of a dipole across the cell. The membranes have a capacitive behavior that prevents the current passes into the intracellular medium.

o β dispersion occurs in the frequency range 500 kHz – 20 MHz. This dispersion is mainly due to the polarization of the membrane plasma. At these frequencies, the membrane is no longer insulating: it allows the circulation of a current in the intracellular medium.

o γ dispersion occurs in the microwave frequency range. This dispersion is caused by the high water content in the cells. The dipole orientation of free water molecules relaxes at 20 GHz. The plasma membrane is electrically transparent to these frequencies and gives access to the intracellular environment.

In higher frequencies, there are no longer any dispersions but the resonances induced by atomic and electronic polarization. A detailed explanation of the different relaxation phenomena can be found in (ASAMI, 2002), which is not in the remit of this thesis.

In the presence of an external alternating electric field, the dipole moment occurs with the separation of positive and negative charges on a molecule yielding the overall polarity. At higher frequencies, dispersion happens when the molecules do not have enough time to align with the alternating electric field fully and fail to follow the fast-changing electric field resulting in a sharp drop in the permittivity spectrum, considered a loss in electromagnetic energy. Microwave dielectric spectroscopy assesses these dispersions for measuring the electrical permittivity of a material. The unique dielectric signature of materials is provided by the permittivity spectrum that can be employed for sensing purposes and facilitates understanding different biological phenomena.
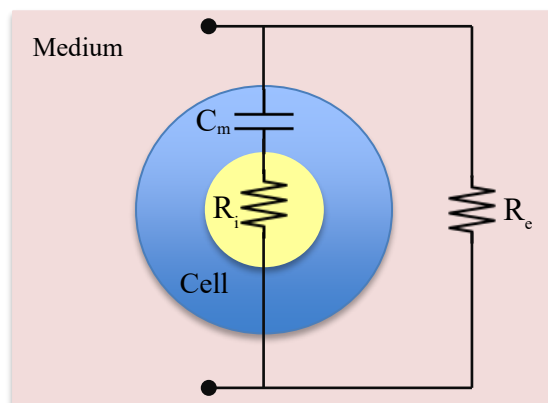
Figure 5. The electrical equivalent circuit model for a single cell in suspension.

For example, the method of characterization of cells based on their dielectric properties determines the modeling and classification of cell properties. A simplified electrical equivalent circuit model of the cell suspension is composed of passive electrical elements (resistor, capacitor) connected in series and in parallel. As illustrated in Figure 5, capacitance (C_m) representing the cell membrane in series with a resistance (R_i) representing the intracellular medium and the extracellular medium is modeled by a resistance (R_e)(FRICKE; MORSE, 1925).

The interaction of electromagnetic waves with cell suspensions is shown in Figure 6. At low frequencies (below 100 MHz), the electrical properties of the membrane that has very low conductivity predominate, preventing the current flow cell. As the frequency increases, the membrane becomes electrically transparent; therefore, current flows through the cell. Thus, the short wavelength and penetration ability of microwaves make the dielectric characterization of the intracellular environment possible. Moreover, cell discrimination and dynamic biological mechanisms can be observed in this range.
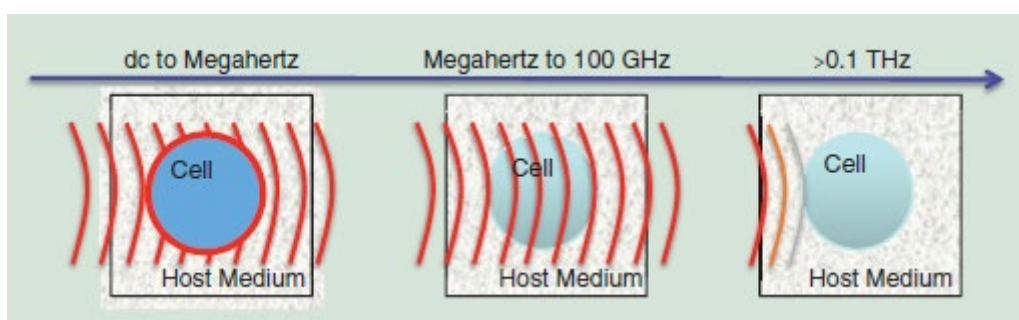
Figure 6. The interaction of electromagnetic waves with cell suspensions.

Source:(ARTIS et al., 2015)

For instance, α-dispersion and β-dispersion regions are best for sensing the changes in the potential of the cell membrane. At the same time, γ-dispersion has a superior function in obtaining intercellular information and determining the concentration of biomolecules. In this range, the dispersion is due to the polarization of water molecules which is the principal constituent of cells. The sensing ability of each dispersion is summarized in Table 1.1.

Table 1.1. Sensing abilities of the dispersions and their applications

Frequency Range	Sensing abilities	Application
α and β dispersion	Extra cellular properties, such as changes in cell membrane potential and thickness	Characterization of different types of blood cells
γ dispersion	Intracellular properties, such as changes in cell content	Detection of biomolecules (glucose), Population of cancerous cell

1.4.1. Methodology and instrumentation

Radio Frequency (RF) and microwave (MW) biosensors utilize capacitive sensing to study permittivity to provide the dielectric property. In these sensors, capacitance or scattering

parameters are measured using components such as interdigitated capacitors, coplanar waveguide (CPW) lines, resonators like a split ring or cavity, and microstrip structures, including open and shunt stub. These components are generally part of an oscillator circuit. They can be modeled as a series or parallel resistor, inductor, and capacitor (RLC) resonant circuit where the capacitance is a permittivity function. Thus, with changes in permittivity, the capacitance and hence, the resonant frequency in these circuits change that can be sensed. The variation of concentrations of biomolecules or content of biological matters changes the permittivity due to the interpretation of the water content, thus resulting in changes in capacitance or shift in the resonant frequency.

Changes in the permittivity are observed either over a wide range of frequencies (broad band) or a small frequency band (narrow band). Therefore, the choice of the components depends on whether a narrow band or a broad band study is preferred. For instance, CPW-based sensors are employed in broad-band detection. On the other hand, for narrowband detection, resonators are utilized.

Resonator-based sensors enable the detection of changes in the dielectric properties of the material under test with higher sensitivity in terms of changes in magnitude and shifts in the frequency of S-parameters at resonance frequencies. They are relatively small depending on the resonant frequency, and can be miniaturized. They can easily integrate with microfluidic systems and offer real-time measurements and fast responses. Resonant-based methods cannot yield a continuous permittivity spectrum as broadband methods since they provide data in discrete frequencies. For instance, CPW-based biosensors have provided broad-band dielectric characterization of a cell using frequency-dependent parameters, i.e., complex permittivity. But for detecting cells in their biological medium, the similar curves make it difficult to distinguish between them unless there is high dielectric permittivity contrast between the cells and the surrounding medium. Hence when the continuous dielectric spectrum is not required, resonators extract narrow-band dielectric information.

The location of the MUT plays a significant role in the sensitivity of the sensor. Therefore the MUT should be positioned where the electric field is highly confined and mainly concentrated, considering their planar structures, the electric field distribution, and the interaction between the tested materials and the electric field of the sensor. These factors need to be considered to make the sensor highly sensitive for detecting the changes in the concentrations, even in small-volume samples.

Furthermore, in the measurement of dielectric properties of a biological matter, the high relative permittivity of the MUT is another critical design parameter. The key challenge in enhancing the sensitivity is measuring materials with high ε_r, for instance, water, the major constituent of a biological cell and its culture medium. Although the relative permittivity of water varies with frequency(LIEBE; HUFFORD; MANABE', 1991), it is much higher than general commercially available microwave substrates. Therefore, different structures are considered to investigate the dielectric properties of bioanalytes and cell suspensions.
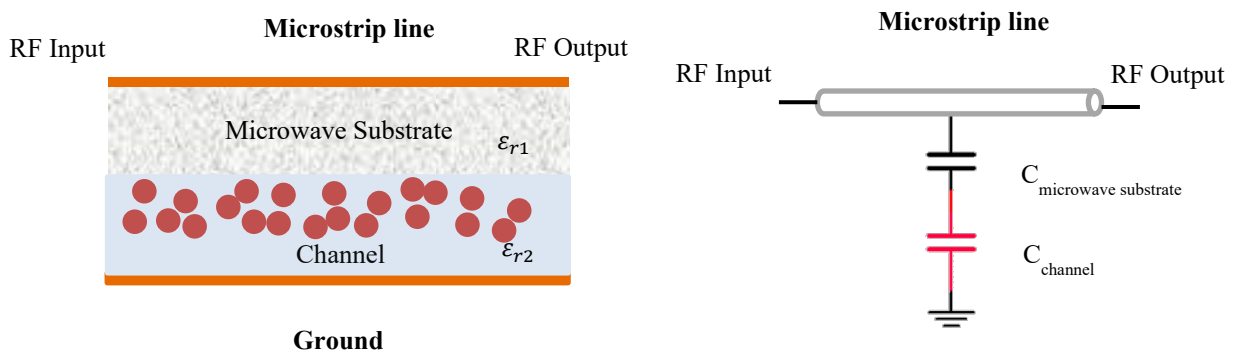
Figure 7. (a) A drawing of a microstrip line with mixed substrates (b) its equivalent electrical model.

As an example, Figure 7(a) illustrates a drawing of a simple microstrip line configuration utilized for the characterization of water solutions in a channel. A commercial substrate layer acts as a support layer for the transmission line. The channel is positioned in the highly confined electric field underneath the line as a part of substrate. Therefore, the channel should be placed between the support, a commercial substrate, and the ground. An equivalent circuit model of this configuration is demonstrated in Figure 7(b). In the circuit model, $C_{\text{microwave substrate}}$ and C_{channel} represent the mixed dielectrics in between the signal line (above) and the ground (below) with permittivity ε_{r1} for commercial substrate and ε_{r2} for water solutions in the channel.

when two capacitors ($C_{\text{microwave substrate}}$ and C_{channel}) are connected in series, the equivalent capacitance (C_{Total}) is calculated as:

$$\frac{1}{C_{Total}} = \frac{1}{C_{\text{microwave substrate}}} + \frac{1}{C_{\text{channel}}} \qquad (2)$$

The total capacitance is, therefore,

$$C_{Total} = \frac{C_{\text{microwave substrate}} C_{\text{channel}}}{C_{\text{microwave substrate}} + C_{\text{channel}}} \tag{3}$$

where the capacitance can be obtained using the following:

$$C = \varepsilon_0 \varepsilon_r \frac{A}{d} \tag{4}$$

ε_0 is the permittivity of free space, ε_r expresses the permittivity of the dielectric material, A represents the parallel plate area, and d is the distance between the two conductive plates of each capacitor. Assuming that both capacitors have the same area (A) and distance (d), from equation (3), the equivalent capacitance is:

$$C_{Total} = \varepsilon_0 \left(\frac{\varepsilon_{r1} \varepsilon_{r2}}{\varepsilon_{r1} + \varepsilon_{r2}}\right) \frac{A}{d} \tag{5}$$

The permittivity of a commercial microwave substrate is normally in a range between 2 and 10 and water solutions may vary between 20 and 80. By replacing a random number for permittivity of the microwave substrate and water solutions for instance ε_{r1} =6 and ε_{r2} =80 in equation (4), we have

$$C_{\text{microwave substrate}} = 6\varepsilon_0 \frac{A}{d} \qquad\qquad C_{\text{channel}} = 80\varepsilon_0 \frac{A}{d}$$

And,

$$C_{Total} \approx 5.6\varepsilon_0 \frac{A}{d}$$

Note that $\varepsilon_{r1} < \varepsilon_{r2}$, the equivalent capacitance is always less than the smallest individual capacitance in the network. Thus, the effect of the material with lower relative permittivity is dominant on the total equivalent capacitance. Therefore, to study the changes in the permittivity of water solutions by positioning MUT as a part of the substrate to enhance sensitivity the microwave substrate should be eliminated.

One approach to measuring a change in permittivity due to varying concentrations of biomolecules is to use a bio-receptor and fix it on the surface of the biosensor to trap target analytes, named immobilization. However, insulation limits the functionality of such as method. If the layer is not insulated correctly, it leads to short-circuiting the sensor system. Furthermore, the preparation process is time-consuming. Another approach is to incorporate microfluidic channels in the sensor where the solutions flow in a sensing area, and a change in permittivity can be sensed.
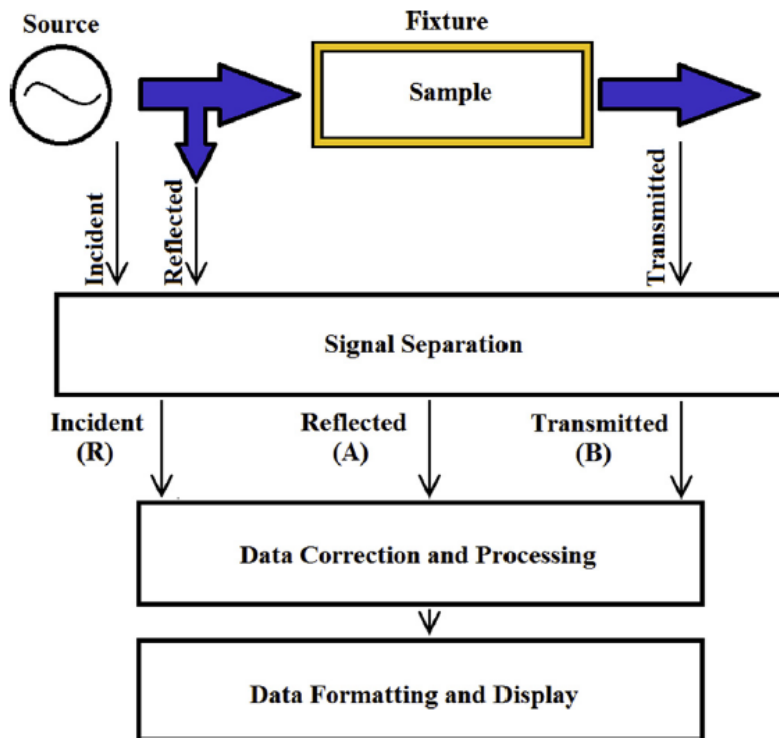
Figure 8. Schematic of a VNA

Source:(BLAKEY; MORALES-PARTERA, 2016)

A measurement using the Transmission/Reflection method involves placing a sample in the presence of the microwave source and measuring the two ports' complex scattering parameters with a vector network analyzer (VNA). The method involves measurement of the reflected (S_{11} or S_{22}) and transmitted signal (S_{21} or S_{12}) (see Appendix). The first number in the subscript refers to the responding port, while the second number refers to the incident port. Thus, S_{21} means the response at port 2 due to a signal at port 1. It is a complex number therefore it is possible to measure the response of the sensor in terms of magnitude and phase.

Generally, VNA consists of a signal source, a receiver, computational components, and a display screen, as shown in Figure 8. The signal source provides the network stimulus to the ports connected directly to the device under test (DUT). They typically have two connections at the input and the output to the DUT; however, the possibility of using more ports for use with systems that have multiple connections exists. The source can sweep over the frequency range of the test instrument. The receiver is tuneable but locked to the same frequency the source propagates. It receives the signals from the signal separators and processes them in terms of reflected and transmitted waves compared to the incident wave. These results are passed into

the processor and displayed. Recognition depends on scattering parameter responses. The measured response is a spectrum where both the amplitude and phase of the high-frequency signal are captured at each frequency point. It is possible to display the network analysis results in various formats, including the Smith chart, Cartesian format, and real and imaginary values. Calibration needs to be routinely assessed to correct systematic measurement errors. The procedure is relatively easy to carry out and is required to ensure the VNA makes precise measurements.

1.5.Justification and Motivation

The microwave-based dielectric investigation is an emerging biosensing method, and it is still evolving. Previous studies confirmed that the relative permittivity varies between different biological tissues. However, these studies were carried out on the scales of organs (liver, for example) or tissues (centimetric samples of organs or skin). Investigations at the single cell scale in the field of microwaves have appeared very recently. Microwave-based biosensors have been integrated with microfluidic working in GHz range frequencies, as reviewed in chapter 2, to investigate different biomolecules and cells. However, studying higher frequencies (>30GHz) results in more complexity and cost in the fabrication process. Furthermore, one aspect not widely considered or deeply explained is the field distribution in the microfluidic system around the resonator.

The microstrip-based biosensor is considered as a biosensing tool in this research because of its features and advantages. Considering the quasi-mode of traveling waves, a smaller portion of waves travel in the air above the substrate. Therefore integrating microfluidic channels underneath the transmission line results in more sensitive responses considering the electric field distribution in the medium under test (MUT) in the microstrip line. The significant advantage of this integration is miniaturization. Furthermore, the ease of fabrication and the low-cost and simple geometry of microstrip resonators make them suitable for commercializing as an easy-to-use sensing device.

Hence, in this work, label-free, sensitive, miniaturized sensing platforms were developed by integrating microwave and microfluidic systems for superior performance in

sensing biomaterials. This fundamental, application-based research is intended to provide an enabling tool for new Lab-on-a-chip platforms.

1.6.Objectives

We designed and fabricated biosensors to detect and distinguish the concentration of biological materials at microwave frequencies. For this purpose, a narrowband characterization technique based on microwave dielectric measurements at the cellular scale was proposed for real-time observation of living cells in their flowing stream. This technique offers a label-free and real-time assessment and monitoring of cells and differentiation glucose concentrations; hence can be used as an early diagnosis and monitoring tool. Simple biosensors to extract biological matters such as glucose and cells were designed to access health data without peripherals. In this regard, the capability of high frequency in miniaturizing the sensor was attractive.

Therefore, this thesis aims to optimize and establish a dielectric measurement and integration technique of microwave and microfluidic biosensors to evaluate the dielectric signature of biological matters such as glucose and cells providing high sensitivity considering the high permittivity of the MUT. We aimed to take advantage of the uniform and concentrated field distribution by integrating a microfluidic channel underneath the transmission line. Using technologies and approaches compatible with biological and electromagnetic fields, we have designed and modeled sensors to enhance sensitivity. The final sensors are simple, rapid, and reliable devices requiring minimal preparation. The principle behind these POC devices was based on the change in relative permittivity.

1.7.Thesis Overview

The presented text is organized into five chapters. This chapter provides the problem statement, the research objective, and contributions to this field. The outline of the thesis was also included in this chapter; after this introduction, the thesis will cover specific topics in detail in the following chapters.

Chapter 2 presents a bibliography study of microwave biosensing focusing on planar transmission lines used in biomolecules and bioanalyts studies with their associated advantages and disadvantages and explains the motivation behind the idea of using a microstrip resonator as an alternative for biomaterial characterization in healthcare applications.

The research carried out for the thesis starts with Chapter 3 with a description of developing a label-free, sensitive, low-cost microwave system that can be integrated with microfluidic platforms for glucose level detection. It includes the methodology proposed to design and fabricate this microstrip-based glucose sensor. Initially, a basic theoretical concept of the microstrip line is described. Then a detailed methodology is presented, followed by a description of characterization methods to compute the measured shift in resonance frequency caused by variations in relative permittivity of the varying glucose concentrations. 3D EM simulations are provided to design a sensing system based on a microstrip line. The fabrication and assembly processes are discussed, followed by some experiments, and the results are presented for the fabricated sensor and analyzed compared to the simulation to verify system accuracy.

Chapter 4 demonstrates a sensing platform for single-cell detection. This chapter details the design, modeling, and fabrication procedure of a microwave-based microfluidic cell-detecting biosensor using metallic nanowire-filled membrane technology. This microwave sensor operates at microwave frequency based on the changes in the permittivity of the cell and its medium. A fundamental of the theoretical concept of the quarter wavelength stub resonator is presented, followed by a description of the methodology. 3D EM simulations are provided for designing the sensing platform. Then the fabrication and assembly processes are detailed. The results of real-time experiments for the fabricated sensor are presented and analyzed. The extended studies of the developed platform on cell discriminations for medical purposes are described. The text finally concludes with Chapter 5, which presents a conclusion of the developed work and makes recommendations for future academic studies based on the knowledge, experience, and observations gained throughout the thesis.

Chapter 2. BACKGROUND AND STATE-OF-THE-ART

2.1. Introduction

Biosensors have been utilized in different applications, from detecting vital signs such as respiration and heart rate, identifying cancerous cells in skin, blood, or liver (QUAZI, 2022) to detecting biomarkers (CHEN et al., 2014b) such as prostate-specific antigen (PSA) and detection of proteins and other biomolecules such as glucose, cortisol, heparin.

The electromagnetic wave interaction provides the frequency-dependent dielectric signature of the biological material constituents (SCHWAN, 1957). First, Organs and tissues, which are bigger and contain more liquids, were the subject of research studies tissues. Microwave technology has been successfully used to detect cancer by distinguishing between the tumor and the surrounding healthy tissues (LAZEBNIK et al., 2007; O'ROURKE et al., 2007; SHA; WARD; STROY, 2002). Some common applications of RF/Microwave biosensors are the detection of glucose, DNA, other biomolecules, and vital signs. Therefore, it is reported as a safe biosensing tool (REJINOLD; JAYAKUMAR; KIM, 2015) in different application areas such as cancer ablation (VANDER VORST; ROSEN; KOTSUKA, 2006) and, more recently, microwave cancer imaging (MOLONEY et al., 2021; NIKOLOVA, 2011). In addition, it offers label-free, rapid, and real-time identification and characterization (LI et al., 2016).

Several design methods and techniques, frequency ranges, and applications have been proposed in the literature for characterizing material properties at microwave frequency and utilized for this purpose with high accuracy(AFSAR et al., 1986; GABRIEL; LAU; GABRIEL, 1996; KRUPKA, 2006; MURATA; HANAWA; NOZAKI, 2005). Among all microwave measurement methods, cavity waveguide perturbation (ORLOFF et al., 2014), free-space transmission (SKOCIK; NEUMANN, 2015), open-ended coaxial probe(LA GIOIA et al., 2018), and planar transmission line technique (HARNSOONGNOEN; WANTHONG, 2017) have been used to determine the dielectric properties of cells and tissues of the human body. Moreover, biosensors based on planar technology utilized to detect and analyze biomaterials gained considerable interest. They are compact, cost-effective diagnostic tools considering their

small size and low manufacturing cost. These biosensors have been employed to study permittivity changes through components such as resonators and microstrip structures with high accuracy. They have advantages, such as low cost, easy fabrication, and being small and light (ALAHNOMI et al., 2021). Resonant-based methods are good examples of sensitive narrowband detection of biomarkers, DNA, the concentration of biomolecules and beads in liquid solutions, and biological cells in several applications(ADHIKARI; KIM, 2016; FOK et al., 2015; GENNARELLI et al., 2013). Resonant-based detection techniques can distinguish the changes in relative permittivity of the MUT, observing shifts in the frequency of S-parameters at resonance frequencies. Microstrip resonators can be a convincing biosensor component due to their physical and electrical properties(LEE et al., 2010, 2012a; LEE; YOOK, 2008).

There are different discussions on using lower or higher frequencies. Generally, there is no specific reason behind selecting the operating frequency in the literature. It is considered based on parameters such as resonator size, cost of the electronic components, or license-free frequency bands for industrial, scientific, and medical equipment (ISM band). The higher the frequency, the smaller the resonator; the components and measurement systems are generally more expensive. However, the possible choice of frequency for the characterization of biomaterials using dielectric measurements depends on the biomaterial of interest. For instance, the short wavelength and penetration ability of microwaves make the dielectric characterization of the intracellular environment of cells possible; therefore, this frequency range has been suitable for investigating cells.

In addition, a wide variety of two main types of broadband and narrowband techniques have been deployed to extract the permittivity of the biological materials as a function of frequency. Moreover, the sensing techniques are either based on a labeling process or a microfluidic channel to study the changes in permittivity due to variations in the concentration.

Microfluidics refers to devices, systems, and methods for manipulating the flow of small volumes of fluids to control chemical, physical, and biological processes. Microfluidic technology is a valuable and powerful tool that allows precise and localized application of fluids due to the behavior of confined fluids. These microscale systems can significantly reduce analysis or experiment time while offering low sample consumption, leading to a new way of acquiring information.

Over the past decade, microfluidics has experienced strong growth and is popularized in biology research thanks to the fabrication technologies in the microelectronics industry facilitating its development. Microfluidic systems offer numerous advantages, including micro-scale features that match the scale of many biological systems (THORSEN; MAERKL; QUAKE, 2002). For instance, microfluidic systems have been used to trap, culture, sort, and single image cells (LECAULT et al., 2012). In addition to miniaturization, the superior control and precise delivery of fluid due to the unique laminar flow properties in microfluidic systems enable the extraction of high-quality data from experimentation possible in fundamental biological research. Furthermore, they allow the use of microscopy tools for vision purposes. Consequently, microfluidics will reduce costs (LIU; LU, 2016).

Development in microfluidics has significantly contributed to the expansion of biosensing devices capable of outperforming biological and medical studies. Microfluidics enables the analyte to effortlessly pass the sensing area through the channels or in the selected region where a bioreceptor is immobilized to study the changes in permittivity. They also facilitate mimicking the cell environment at the cellular resolution that enables accessing the properties of biomolecules and cells in well-controlled small dimensions (as low as the microliter or even smaller) at a low cost and high fabrication volumes without the drawback of manual handling.

A microfluidic system consists of a microchannel network that can be integrated with various sensor configurations. Strong interactions between cells and the fluid flow in the microchannels result from their similar scales in the order of hundreds of microns. Due to the small dimensions of microfluidic devices, they facilitate the implementation of new characterization methods in single-cell analysis, which was not accessible with macroscale devices. However, adding sensitive non-destructive techniques to an analysis device in a liquid medium can be challenging.

Microwave-based biosensors provide rapid and highly sensitive measurements. Microfluidic technology, on the other hand, offers advantages such as low cost and real-time detection even in micro/nanoliter sample volumes. From the point of care view, microfluidics-integrated microwave sensing results in sensitive, reproducible, and portable detection. This method has been employed in a wide range of interdisciplinary research in biological and medical applications such as cell analysis(CHEN et al., 2014a), biomolecule and bioassays detection, and diagnostics(SISTA et al., 2008). We limit the rest of the literature review to

biosensors based on planar technology designed in the frequency region from radio frequency up to a few gigahertz.

2.1.1. Glucose biosensors

Considerable studies proposed microwave sensors for glucose monitoring, and planar technology has been widely used in biosensors to detect and analyze glucose levels. The capability of microwave-based sensors to non-destructively distinguish and measure the parameters inside the liquid sample volumes make it a great alternative to the invasive daily monitoring techniques of glucose (ALAHNOMI et al., 2021).

Some glucose sensors are based on the coplanar transmission line; however, most of them use a microstrip line to detect changes in the glucose concentrations to improve diagnostic methods for better treatment plans for diabetes and to reduce lifetime or even fatal complications. Some researchers prepared glucose solutions using different glucose concentrations in the physiological range from normal glucose levels to those that occur in diabetes. Yet, others use higher unrealistic concentrations in their tests. Some use phantoms mimicking skin, fat, muscle, etc., while some perform measurements on glucose in water samples.

Abedeen et al. proposed a microwave glucose analyzer by embedding interdigital (IDT) structures in the center of the CPW transmission line on an FR4 board (ABEDEEN; AGARWAL, 2018). A Poly-DiMethyl-Siloxane (PDMS) cavity was integrated on the top of the IDT structures, acting as a sensing area. The frequency shift and attenuation variation of S_{11} and S_{12} for the glucose concentration ranging from 0 g/mL to 1 g/mL were observed, showing that the proposed planar analyzer has great potential to quantitatively determine glucose.

Harsoongnoen et al. presented a glucose sensor composed of a CPW transmission line coupled with an electric-LC (ELC) resonator (HARNSOONGNOEN; WANTHONG, 2017). A cylindrical plastic sample chamber was placed on top of the gap in the middle branch of the ELC resonator, and the solutions were applied to the chamber using a micropipette. The variation of transmission coefficient (S_{21}) based on different glucose concentrations in deionized water and phosphate-buffered saline (PBS) varying from 0%-20% (w/V) in the range of 2.5-6 GHz was measured and analyzed. The experimental results confirmed that the proposed sensor could linearly detect glucose concentration.

Mason et al. introduced a glucose sensor consisting of a resonant co-planar type structure with a discontinuity in the ring to enhance the field (MASON et al., 2013). A tuning system was used to remove the errors, adjust the resonant peak frequency, and increase the sensitivity in that particular frequency. To evaluate the sensor feasibility, glucose-diluted solution ranges between 180-1800 mg/dL were studied. The solution entered the polymethyl methacrylate (PMMA) tube placed across the center of the ring section on the top of the ring discontinuity. The transmitted signal (S_{21}) at 3.64 GHz was monitored. This sensing method was suggested as an alternative to the time-consuming laboratory-based methods for analyzing different fluids.

J. Roelvink et al. proposed a coplanar transmission configuration fabricated on a FR4 laminate to measure the permittivity of liquids and gelatin samples in a broad band ranging from 1 to 5 GHz (ROELVINK; TRABELSI; NELSON, 2013). Hamzah et al. designed a microwave sensor for microfluidic sensing of several common solvents using a split ring resonator (SRR) with an active gap operating at 2.5 GHz (HAMZAH; LEES; PORCH, 2018). This device can sense based on the pH changes of the solutions.

Parsamyan et al. designed a metamaterial microstrip line sensor modeled by a modified Hilbert-shaped closed curve to distinguish different glucose concentrations in the frequency ranging from 5.5-6.5 GHz (PARSAMYAN et al., 2018). A cylindrical vial containing different glucose concentrations in aqueous solutions ranging from 0 up to 250 mg/dL was placed on the top of the resonator, and changes in the insertion loss due to glucose content in the aqueous solution were studied. The calculated biosensor sensitivity is 9.8×10^{-2} dB / (mg /dl). It was concluded that such a structure could detect the glucose concentration in the solution.

Juan et al. have used an open-loop microstrip resonator to characterize the glucose concentration of water–glucose solutions of 0%, 5%, and 10% in mass (JUAN et al., 2019). A varying size Polytetrafluoroethylene (PTFE) liquid holder (5–25μL volume) was glued onto the gap between the open end of the resonator fabricated on Taconic TLX-8 substrate to measure changes in the Q factor and the peak value of the S_{21} parameter at the resonance frequency. The sensor was tested at frequencies around 2, 5, and 7 GHz. Finally, the Q factor is chosen as a suitable sensing parameter instead of the S_{21} peak.

Ebrahimi et al. developed a reflective microwave microfluidic glucose sensor by measuring the return loss and shift in the frequency on Rogers, RO4350 substrate (EBRAHIMI; SCOTT; GHORBANI, 2020). The sensor was made of an open-ended microstrip transmission

line with a complementary split-ring resonator (CSRR). A PDMS channel was attached to the upper side of the CSRR. Microfluidic tubes are connected to the inlet and outlet of the channel for investigating glucose samples ranging from 0–500 mg/dL. The resonance frequency and S_{11} level for each sample were presented in the frequency range of 2.4–2.6 GHz. They suggested that using glucose concentrations in the physiological levels and interpreting the measured results showed this biosensor had a good potential to distinguish glucose levels.

Govind et al. proposed a microwave microfluidic sensor to investigate glucose concentration in aqueous solutions (GOVIND; AKHTAR, 2019). The SRR implemented on the Rogers RT6006 substrate was incorporated with an interdigital capacitor (IDC) in its gap to enhance the electric field distribution. The glucose solutions ranged from 0 to 5000 mg/dL passing the sensing area through a non-planar PDMS microfluidic channel placed over the IDC region of the SRR. The sensitivity was 2.6×10^{-2} MHz/ (mg/dL) at 4.18 GHz.

Yilmaz presented a patch resonator as a wearable glucose sensor operated in the 2.45 GHz (ISM band between 2.40–2.48 GHz) using tissue-mimicking phantoms (TMPs) replicating the dielectric properties of wet skin, fat, blood, and muscle tissues (YILMAZ; FOSTER; HAO, 2014). However, the purpose was to use these TMPs in investigations of blood glucose levels. The dielectric properties of the blood-mimicking material were investigated in a wide band for the 0.3 to 20 GHz frequency range. Then the realistic glucose amounts were added to TMP, and the changes in the input impedance of the patch resonator concerning the glucose level were studied in the blood layer. This study examined the effect of other physiological processes on the dielectric constant of the tissue while the blood glucose level (BGL) was changing.

A microstrip line-based glucose sensor for non-invasive continuous glucose monitoring (human finger as MUT) has been proposed by Huang et al. using the main field (HUANG et al., 2019). The performance of this sensor, illustrated in Figure 9, was analyzed between 100–500 MHz and 1.4–1.9 GHz, measuring the magnitude of the reflected signal at the input of the sensor as a characterization tool. It was concluded that the structure had shown better sensitivity (1.8×10^{-3} dB / (mg /dl) average) in the frequency range between 1.4 GHz and 1.9 GHz. In these type of sensors, Figure 9(b), which were developed as wearable glucose monitoring sensors, the frequency of choice rely on the position of the sensor and accordingly requires penetration depth for accurate measurement. Therefore, one common error in the measurement of this type of sensor is the motion of the body part, which changes the magnitudes in the sensor.

Also, factors such as various skin thickness, hydration, sweat, dirt, body temperature can affect the sensitivity of this sensor.

(a)   (b)
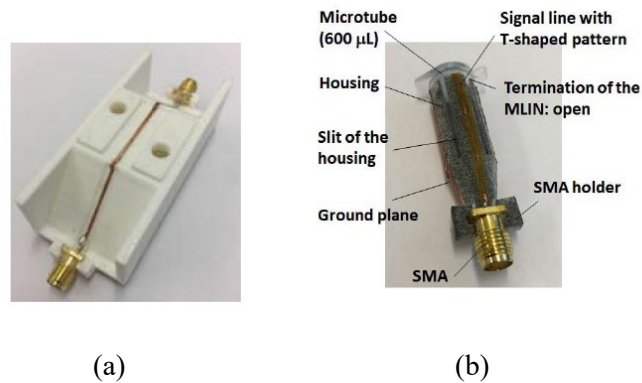
Figure 9. Photos of the fabricated MLIN-based structures for glucose sensing by Huang et al.

Source: Ref. (HUANG et al., 2019)

It was observed in the literature that the changes in scattering parameters (S-parameters) significantly depend on the glucose concentration. Moreover, those sensors mostly explore the magnitude of the S-parameters. Though external uncontrolled parameters and equipment uncertainties may limit the sensitivity of the measurements, only a few glucose sensors are reported in the literature using the changes in the relative permittivity (frequency or phase) to detect different concentrations.

2.1.2. Biomolecules and analytes biosensors

Investigating cells at a single scale in the field of microwaves is emerging. Studying cells based on their dielectric properties facilitates understanding different biological phenomena. Within the last decade, techniques for analyzing single cells have become a fast-growing field while scientists focus on having a more profound understanding of cell characteristics. Single-cell characterization eases the differentiation between cells, facilitating diagnosis and treatment plans for patients. The ability to miniaturize the devices adapts to the analysis of single cells, and different characterizations of the cell can be revealed regarding the analysis frequency. Yet, few applications related to single-cell analysis in microwaves were introduced. In this frequency range, waves can penetrate inside the cell, providing helpful information from the intracellular environment and label-free characterization. This section

summarizes the biosensors based on the planar transmission line technique with the capability of biological analysis operating at microwave frequencies.

Liu et al. presented a microwave hairpin resonator on a quartz substrate to obtain B16F10 melanoma cells characteristics in a liquid medium. The biosensor consists of stepped impedance resonators (SIR) in the form of a hairpin microstrip, a PDMS cover plate, and SU-8 cell trapping structures (LIU; WANG; JANG, 2018). It measures the reflected coefficient at a resonant frequency of 2.17 GH and concludes that the hairpin biosensor has the potential to distinguish cells.

A microwave system capable of measuring the complex permittivity of various types of cancer cells was examined by Nerguizian et al. (NERGUIZIAN et al., 2017). A capillary tube was inserted in the center of a two-port rectangular resonant cavity which later will be loaded by the samples. Changes in measurement of the resonant frequency of the transmitted signal of the empty and loaded capillary tube were studied in the range of 2-4.5 GHz. It was suggested that this technique enabled the extraction of the signature dielectric property of different cancer cells with a microfluidic device at microwave frequencies.

Dalmay et al. presented a planar microwave resonator structure for dielectric spectroscopy analysis of polystyrene particles in a liquid medium (DALMAY et al., 2014). The wall of the microfluidic channel is built using photosensitive SU-8 resist, and a transparent polymer (PDMS) is mechanically squeezed on the walls as a top cover for the microchannel. The bead is trapped in the coupling capacitor gap inside a sensitive region. The S-parameters of the sensor loaded with polystyrene particles were compared to when only the liquid was in the channel for a frequency range of up to 6 GHz. From these measurements, it was possible to extract the relative permittivity of beads (2.8 ± 0.2) by studying the capacitive change.

Jaruwongrungsee et al. introduced a microfluidic biosensor for real-time immunoglobulin G (IgG) detection. The biosensor consists of two gold SRR electrodes fabricated on the RT/duroid 6010.2LM laminates (JARUWONGRUNGSEE et al., 2015). A PDMS microfluidic channel was integrated and aligned on top of the gap of electrodes. The S_{21} under different loading conditions was measured at 1.75 GHz, and a shift in resonant frequency was observed in the presence of IgG. Yet a biofunctional building block for antibody immobilization on the gold surface of electrodes was required.

Chen et al. proposed a microwave CPW-based transmission line biosensor for detecting various densities of cancer cells (HepG2) based on their dielectric properties (CHEN et al., 2014b). The magnitude of S_{21} was considered the measuring parameter, and the dielectric constant of each sample was extracted. The gold CPW transmission line was fabricated on a glass substrate. The center of the signal line was etched and acted as the detection area. A SU-8 protection layer was placed on the biosensor surface to create a microchamber. Different samples of HepG2 cells with concentrations up to 2×10^3 cells/μL were characterized in the very wide bandwidth of 1-40 GHz. The sensitivity of the biosensor is associated with the cell density. The lowest detection limit reported was 20 cells/μl. The biomedical protocol needed a long preparation time, and the biosensor can be reused after a wash with water only.
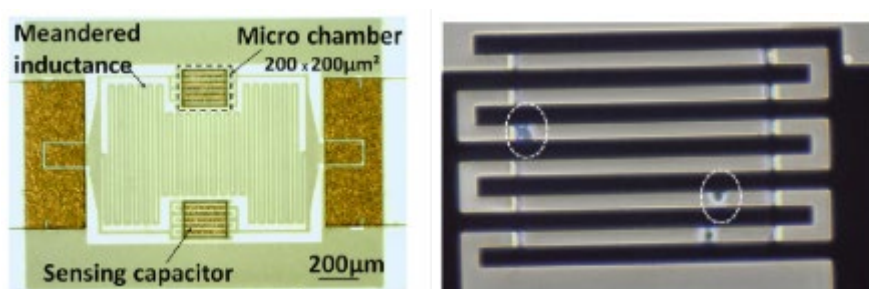
Figure 10. LC resonator configuration and deposited cells onto the interdigitated capacitor by Zhang et al.

Source: Ref. (ZHANG et al., 2014)

Zhang et al. proposed microwave LC resonators to characterize colorectal tumor cells, from low to high-grade tumors, based on their dielectric permittivity (ZHANG et al., 2014). A microwave coplanar waveguide configuration consisted of a meandered inductor, and two IDC capacitors were fabricated on a fused silica substrate, as shown in Figure 10. Two SU-8 polymer microchambers where cells should be concentrated were patterned on the sensing capacitors. S_{21} parameter was chosen as the sensing parameter, and frequency response between 5-14 GHz was studied in which the sensor provided the dielectric signature of the cells. The results confirmed a shift in resonant frequency regarding the degree of aggressiveness of malignant cells, which was related to the ability of microwaves to penetrate inside cells and interact with their intracellular content. However, the culture medium was removed, and the cells were directly deposited and grown on the biosensor surface. A limited number of cells can be characterized, yet the prolonged biochemical preparation and confirmation of the position of

the cells in the sensing area are inevitable. The author discussed it should be a practical approach for characterizing a large number of cells.

In research by Lee et al., a planar split-ring resonator operating at about 10 GHz was designed to determine biomolecules such as prostate-specific antigen (PSA) and cortisol stress hormone (LEE et al., 2012b). This biosensor consists of a microstrip line with local high-impedance and a planar SRR. The high-impedance microstrip line was employed to excite the resonator intensively. The device was fabricated on printed circuit board technology. To define a biosensing region, the whole device except for the SRR element was coated with a mask layer. Then anti-PSA and anti-cortisol were immobilized on the surface of the SRR element. The sensor surface was treated with fluorescent stains to examine and observe the reactions of MUT. In experiments, S_{21} was studied, and attenuation and shift in resonant frequency due to the various concentration of target biomolecules ranging from 0.1-100 ng/ml after the binding process was reported. The concentration of 100 pg/ml is reported as a Limit of detection (LOD) of this biosensor.
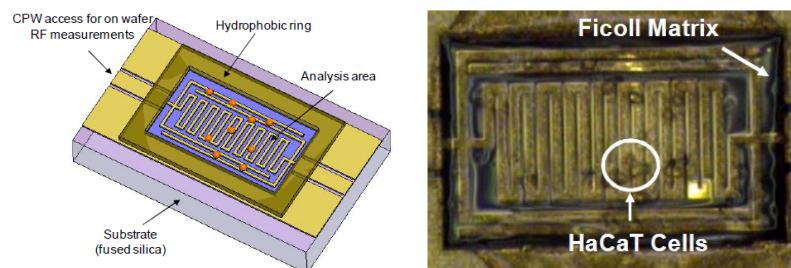
Figure 11. Design view of the proposed micro biosensor by Dalmay et al.

Source: Ref. (DALMAY et al., 2009)

A sub-millimetric size label-free planar structure was proposed by Dalmay et al. to detect and identify two different human cell types: glial (U87 type) and neuronal cells (SH-SY5Y) in the frequency range from 15 to 35 GHz (DALMAY et al., 2009). This coplanar band-stop RLC resonator was composed of a meandered inductor coupled to an inter-digital capacitor on a fused silica substrate. The sensing area was confined by a 20μm thick SU-8 polymer layer, as illustrated in Figure 11. The cells were protected in a particular support media based on a polymer matrix (ficoll). First, the transmitted signal of the unloaded sensor was measured, and then the sensor was filled with cell suspensions, and the shift in the resonant frequency of the loaded sensor was compared with the unloaded one. It is reported that the minimum number of

10 cells was sufficient to detect the shift in the resonant frequency compared to pure ficoll. However, the number and position of the cells were uncontrolled due to the lack of a microfluidic channel, and the cells were not in their living medium.

Another label-free biosensor was developed by Delamy et al. to identify glioblastoma cell (U87) cells based on their electrical properties (DALMAY et al., 2010a). This biosensor comprises a meandered inductor and an interdigital capacitor fabricated on a fused silica substrate that behaves as a band-stop resonator. A SU-8 polymer layer was used to confine the microchamber where the cell migrates and adheres to the sensing area on the fused silica substrate. To avoid the effect of the biological medium, the cells were grown directly on the sensor. To this end, the sensor chip was submerged in media culture for a few days until sufficient cells adhered to the sensor surface. Then the sensor was put out of the culture medium and washed and dried before measurements. Both reflected (S_{11}) and transmitted (S_{21}) signals were measured and showed that the resonant frequency of reflected signal S_{11} shifted toward lower frequencies after the cell adhesion on the device. The biosensor could identify one single cell where a 13 MHz frequency shift at around 12.5 GHz has been observed for the loaded sensor compared to unload.

One more published study by C. Dalmay et al. demonstrated cell analysis by impedance spectroscopy of microwave (DALMAY et al., 2010b). Two poles coplanar waveguide of 5μm thickness golden microstrips fabricated on a fused silica substrate. Thick SU-8 was used to build a microchamber to hold samples during the test. Measurement is indicated by the scattering parameter of reflection S_{11} over a frequency range of up to 16 GHz. The presence of targeted cells caused a frequency shift equal to 100 MHz. They concluded an impedance difference amid measured cell ranks. They considered cell permittivity as an indicator of the degree of cell differentiation. This method in both studies requires complex biochemical preparation for an extended period of time, up to several days. Moreover, individual cell type recognition needs more clarification and explanation. Another potential concern is the possibility of destroying the cell sample after the process of culturing or adhering cells to the capacitive sensing area, followed by chemical fixation.

Grenier et al. proposed a coplanar waveguide structure fabricated on the quartz substrate to differentiate the concentration of cells in suspension. A PDMS microfluidic channel was placed on top of CPW (GRENIER et al., 2009). Human umbilical vein endothelial cells (HUVEC) were tested with concentrations of 1.25×10^{8} cells/ml. The S-parameters were

measured in the frequency range 400 MHz-35GHz. Subsequently, the results when the sensor was loaded with the biological medium were compared to those when the sensor was loaded with cell suspension. The dielectric spectrum was extracted regarding a de-embedding technique for a small volume sample. The changes in the measured relative permittivity of cell suspension suggested the possible use of such a sensor for biological quantification.

Later the same microwave biosensor was used to determine the dielectric signatures of different concentrations of tumorous cells up to 40 GHz (GRENIER et al., 2011). The biosensor was able to identify B-lymphoma cells (NHL) in suspension. The permittivity was observed for cell concentrations up to 100 million cells/ml, and the correlation of cell density with the real part of the permittivity was reported successfully. By measuring cells in suspension, they concluded that biological medium does not delimit the microwave detection analysis. However, to increase sensitivity, they reduced the effect of the aqueous suspending medium by using highly concentrated cell suspensions. Furthermore, this microwave biosensor could discriminate three subpopulations of B lymphoma cell lines, the OCI-LY7, OCI-LY10, and OCI-LY18 ones, based on their different dielectric properties (GRENIER et al., 2018).

Seo et al. presented a finite ground coplanar waveguides (FG-CPW) sensor for wideband permittivity measurements of cell suspensions (SEO et al., 2008). A SU-8 reservoir to be filled with a few microliters sample under test (SUT) was manifested on the top of the sensor. First, the performance of the fabricated sensor on the glass substrate was verified by reference liquids such as methanol and isopropanol measurements. Then human embryonic kidney cells harvested and treated with dimethylsulfoxide (DMSO) were characterized over the frequency range of 1 to 32 GHz. The S-parameters were measured, and the complex permittivity was extracted. It is concluded that the permittivity of treated cell samples decreased with frequency as the time increased.

A similar CPW approach has been presented by Li et al. to differentiate and characterize suspensions of live and heat-killed Escherichia coli cells over a broad frequency range of 0.5-20 GHz (LI et al., 2018a). The CPW was patterned on a quartz substrate, and a removable PDMS microfluidic channel was clamped on the top of the substrate. The return loss $|S_{11}|$ and insertion loss $|S_{21}|$ of both E. coli-free media and E. coli suspensions were measured. The lowest detection limit reported was 15 individual bacteria. This sensor could discriminate the live cell from the dead cell concerning the decrease of cytoplasmic conductivity and permittivity upon

cell death. Removable PDMS cover to clean the substrate and reuse the CPW chip may cause restrictions.
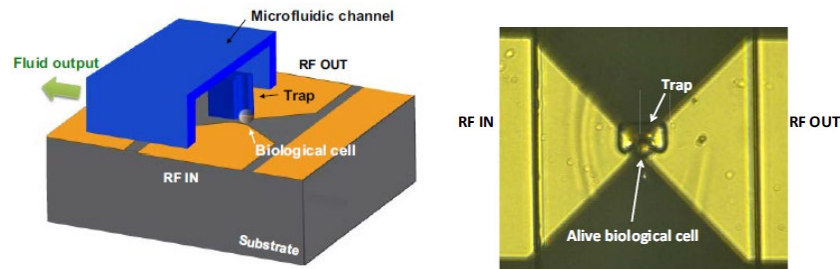
Figure 12. Microwave-based biosensor schematic by Chen et al. and photography of a single trapped cell.

Source: Ref. (CHEN et al., 2013)

Dielectric spectroscopy of a single living B lymphoma cell was performed in its culture medium by Chen et al. in a frequency range of up to 40 GHz (CHEN et al., 2013). The biosensor was made of a coplanar line with a capacitive gap at its center. To form the gap in the size of the cell, two taper transitions were used to narrow the central conductor. A microfluidic channel was placed on top of the capacitive gap to mechanically trap the cell in flow and to eliminate the effect of culture medium, as shown in Figure 12. The coplanar structure was on a quartz substrate, and the microfluidic channel and trap were realized in PDMS. S-parameters were measured, and complex admittance elements of the capacitor were extracted. The maximum contrast was obtained around 5 GHz.

Watts et al. proposed a coupled-resonator biosensor operating around 10 GHz for measuring single-flowing cells in an aqueous environment (WATTS et al., 2020). A double split-ring resonator (DSRR) was inductively coupled with a cylindrical dielectric resonator (DR) via the aperture in the lid of the cavity, as shown in Figure 13. The DR was placed inside a cylindrical copper cavity directly underneath an aperture in the cavity lid. The DSRR was deposited on a glass coverslip and positioned on top of the cover. A PDMS microfluidic channel was manually aligned between the gaps of the DSRR. Three different biological cell types, such as murine myoblasts (C2C12 cell line), human mesenchymal stem cells (hMSCs), and human peripheral blood monocytes (THP-1 cell line), were tested. The dielectric resonator was excited at $f_{DR} = 9.81$ GHz. The insertion loss was measured, and the resonance frequency of the

device when the channel was empty and loaded with samples was studied. They used a camera to monitor the capacitive gap visually and concluded that the resonance shift could be correlated to target cells passing through the sensing area.
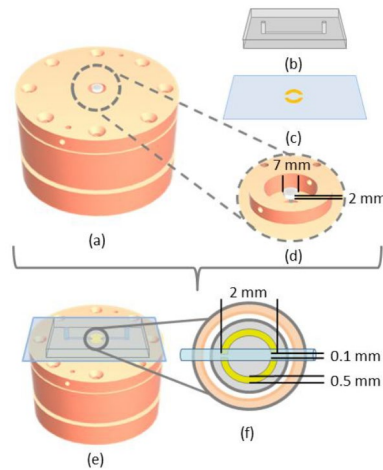
Figure 13. Schematics of the dielectric resonator (DR) sensor, both resonators, and the microfluidic chip assembly on top of the aperture by Watts et al.

Source: Ref. (WATTS et al., 2020)

2.2. Chapter Summary

Here we reviewed various biosensors, focusing on microwave biosensing in the fluid by different techniques according to the material under test and the challenges presented. Aside from the challenges mentioned above, satisfactory progress was accomplished alongside significant development in microelectronics and microfabrication technologies. Microwave biosensing has valuable advantages, such as offering rapid, and label-free detection, and has the potential to be implemented commercially.

A variety of microwave planar resonator techniques were proposed to detect and characterize the biomaterials such as glucose and living cells. Each offers its own advantages and drawbacks. The simple design and fabrication with the potential to minimize the circuit size is the primary advantage of this technique. However, limitations such as sensitivity,

performance, and electric field distribution may restrict their application in the characterization of biomaterials.

Therefore crucial factors need to be considered to make the response of the sensor highly sensitive for a small sample volume. For instance, in glucose sensors, the sensitivity of the sensor that did not have a microfluidic system to control the flow and volume of the liquid sample is ambiguous. Another drawback is the low electric field confinement. In most of the designs in the literature, the fluidic systems were integrated on the top surface of the transmission line resulting in less sensitive responses considering the low electric field distribution in the MUT. This restricts and limits the range of permittivity detection. Therefore, the electric field must be highly confined in the desired area to achieve high sensitivity in detecting the concentrations.

For cell characterization, a significant focus was on coplanar waveguides with operating frequencies up to 40GHz as biosensor devices. Split ring resonators and hairpin resonator-based biosensors were also studied. Mechanical components and circuits have also been utilized to enhance the sensitivity and discuss the dielectric properties of biological cells.

Several challenges were revealed in the reviewed literature, including integrating the microfluidic system and using complicated, slow, time-consuming, and expensive preparation work. These cause some drawbacks, such as the high cost of fabrication to improve the selectivity and sensitivity of the biosensors. However, new biosensing technology should represent a promising solution to enhance biological and medical applications as a rapid diagnostic tool that needs a small volume of samples. To serve as a point-of-care device, it should be simple, miniaturized, and cost-effective while providing real-time measurement.

Yet the sensitivity of the biosensor is the main limitation. For this purpose, the size of the lines/ electrodes should be fine-tuned to match the cell size to eliminate the effect of the surrounding liquid or area. In addition, measuring the cell in flow stream in the microfluidic channel was another difficulty, and biochemical and mechanical elements were used to trap the cell and increase selectivity. This will add more complexity to the fabrication process hence more cost.

Moreover, real-time monitoring is incredibly beneficial as it provides dynamic information about the target material. It paves the way for continuous glucose sensing applications to monitor the speed and trend of your glucose levels leading to improved

treatment. In the cell study, the repeated measurements of the same population of cells over time provide more insightful data reducing the burden of days of preparation. One other significant advantage of real-time monitoring is accountability.

In this thesis, we developed high-sensitivity microfluidic devices based on microstrip resonators operating in microwave frequency, distinguishing biomaterials such as glucose in aqueous solutions and cells in their biological medium. Due to the easy fabrication, resonators based on microstrip transmission lines are more appropriate for accurate characterization and rapid proof of the microwave biosensing principle for this particular application. The detection techniques are based on studying the dielectric properties of biological matter, such as glucose and living cells. It started with the study of changes in the relative permittivity of glucose solutions at lower frequencies (around 5 GHz), followed by the detection of cells at higher frequencies (about 11 GHz), which is the heart of our research.

Chapter 3. A LABEL-FREE MICROWAVE-BASED GLUCOSE SENSOR

This chapter describes the design, modeling, and fabrication processes of a microwave-based resonator for glucose sensing. Furthermore, the fabrication and integration of a microfluidic system and biosensor assembly will be defined, and the optimization process will be detailed in this chapter.

3.1. Concept of the Biosensor Dedicated to Microwave Dielectric Measurement

Microwave biosensing requires the use of transmission line networks that are constructed in different forms, such as microstrip lines. The microstrip line is ideal for biosensing and point-of-care applications due to its flat shape and electromagnetic properties. It operates in different frequency ranges, which is beneficial for healthcare applications. In this thesis, microwave-based biosensors are constructed based on a microstrip line considering its simplicity and planar structure. It can be easily miniaturized and integrated with microwave devices making it a common choice of transmission line for developing sensing platforms.

3.1.1. Microstrip line properties

The structure of the microstrip line is shown in Figure 14(a). A microstrip is a type of transmission line fabricated on planar technology. It consists of a conductor of width W fabricated on a dielectric substrate of thickness h with a metal bottom plane that acts as the ground plane. The dielectric material has unique characteristics such as relative permittivity (ε_r) and loss tangent ($\tan\delta$) that change the electrical behavior of the microstrip line. When a microwave signal propagates in a dielectric material, they are slowed down by a factor roughly equal to the square root of the relative permittivity, which implies that the wavelength decreases by the same amount. The guided wavelength can be calculated as follows:

$$\lambda_g = \frac{\lambda}{\sqrt{\varepsilon_r}} \tag{6}$$

Where ε_r is the relative permittivity of the microstrip line and λ is the free-space wavelength. Considering that

$$\lambda = \frac{c}{f} \tag{7}$$

where f is the frequency, equation (6) of guided wavelength can be rewritten as:

$$\lambda_g = \frac{c}{f\sqrt{\varepsilon_r}} \tag{8}$$

The permittivity of a material determines the relative speed that an electrical signal can travel in that material. The good approximation of phase velocity and propagation constant are as follows, respectively (COLLIN, 2001).

$$v_P = \frac{\omega}{\beta} = \frac{c}{\sqrt{\varepsilon_r}} \tag{9}$$

$$\beta = \frac{2\pi}{\lambda_g} \tag{10}$$

Where c is the speed of light.

In a microstrip line considering electric field distribution, in Figure 14(b), most of the electrical field passes through the substrate between the line and the ground. At the same time, a smaller portion distributes in the air above the substrate. Here, this feature contributes to the design of microwave-based microfluidic biosensors and the position of MUT to enhance sensitivity.
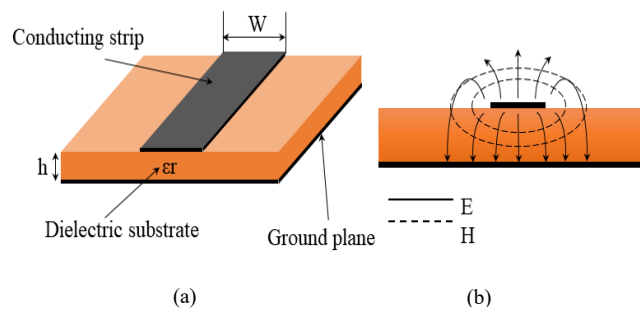
Figure 14. Microstrip Structure (a) Geometry and (b) Electric and magnetic field distribution.

Source: Reproduced (POZAR, 2012)

Because of the field distribution, the effective dielectric constant is approximated by

$$\varepsilon_e = \frac{\varepsilon_r+1}{2} + \frac{\varepsilon_r-1}{2} \frac{1}{\sqrt{1+12(\frac{h}{W})}} \tag{11}$$

which satisfies $1<\varepsilon_e<\varepsilon_r$ and depends on the relative permittivity of the (ε_r), the substrate thickness (h), the conductor Width (W), and the frequency (f).

3.2. Design and Implementation

The aim was to develop a simple, sensitive, low-cost microwave sensor capable of conducting glucose concentration measurements without chemical bindings. The sensing devices used a simple microstrip transmission line and an integrated microfluidic system to detect variations in the glucose component of the glucose water solutions.

In the sensing devices in the literature using a microstrip line, the location of the MUT is usually considered to be above the microstrip line, above the coupling area or gap of the coupled microstrip structures, or on the pattern etched in the microstrip ground plane. In a microstrip line considering electric field distribution, shown in Figure 14(b), most of the electrical field is concentrated within the substrate, while a smaller portion distributes in the air above the substrate. Therefore we aimed to build a cavity underneath the line to position the sample under test in the highly confined electric field. However, fabricating the cavity and transmission line on one layer was not feasible. Another challenge was to seal the cavity to avoid any leakage that interfered with our response.

Therefore, design optimization was performed to facilitate the process of creating the microfluidic system, the fabrication was completed, and the glucose sensing device was proposed to overcome these limitations. For this purpose, the most simple structure was introduced. The following sections present the processes dedicated to designing and fabricating a microfluidic microwave system while highlighting the sensitivity of the characterization method we have developed.

3.2.1. Materials and methods

- The substrate: The proposed sensor was fabricated on FR4 substrate for low-cost purposes. FR4 is a fire-retardant epoxy resin. This substrate, with a thickness of 1.6 mm, was used for the sensing device. It has a relative permittivity of 4.4 and tanδ of 0.02. Moreover, FR4 is considered to be biocompatible.

- The microwave circuit: The proposed microwave sensor is based on a microstrip line. It was appropriately designed based on the desired operating frequency and the characteristic of the target materials, and the fabrication method was selected regarding the dimension and design of the device.

- The microfluidic system: It was integrated into the microwave circuit and was optimized based on the realization of microstrip design, and was placed in a highly confined electrical field regarding the field distribution in the microstrip line.

- Glucose water solutions: A series of four water glucose solutions were prepared with glucose concentrations starting from 1000 mg/dL and doubling until reaching the concentration of 8000 mg/dL. This range represents the high concentrations. A similar set of three other water glucose solutions in the physiological range were used, where we defined the variation of glucose concentration with a classification of the human blood glucose level of 100 mg/dL as normal, 200 mg/dL as hyperglycemia, and 300 mg/dL as diabetes (DIABETES ASSOCIATION, 2010), named low concentrations.

Depending on the specific design of the sensor, it was well modeled, then Ansys Electronics Desktop was used as the 3D electromagnetic simulator to analyze the performance in the frequency of the sensor. The modeling results in an easy structure design with accurate results and successfully predicts the device response in terms of magnitude, phase, and frequency responses (ANSYS ELECTRONICS).

3.2.2. The glucose sensor overview

The model of the proposed sensor can be seen in Figure 15. Three 1.6 mm-thickness FR4 layers were used to fabricate the microstrip line-based sensing device. The bottom layer is the ground plane layer (copper) with a length of 80 mm, and the middle layer, known as the substrate layer, has a length of 70 mm. Both of these layers are with a width of 40 mm. The length and width of the fabricated cavity in the middle layer are 40 mm, and 30 mm, respectively. The cavity that will be filled with glucose water solutions to be characterized was built by removing the dielectric. It was aligned to the center of the device underneath the

transmission line, where there is a highly dense electric field concentration for higher sensitivity sensing. In addition, the feed lines (input and output of the device) were fabricated on this layer to connect easily to the SMA connectors. The FR4 substrate used in the middle layer is only for mechanical support of the sensor; it is cheap, and its electrical characteristics have little influence on the results since the cavity with the MUT will be the substrate of the transmission line. A transmission line was patterned on a FR4 substrate on the conducting layer on the top using a precise milling process. Finally, the top layer flipped upside down and soldered to the feed lines connecting the input to the output. The part of the microstrip on the cavity is 1 mm wide. The line is not matched to the equipment; it is 30 ohms since fabricating a 50 ohms transmission line considering the high relative permittivity of water (epsilon ~ 80) was not feasible. As we are not aiming for the level of the signals, only the frequency, hence the mismatch was disregarded.
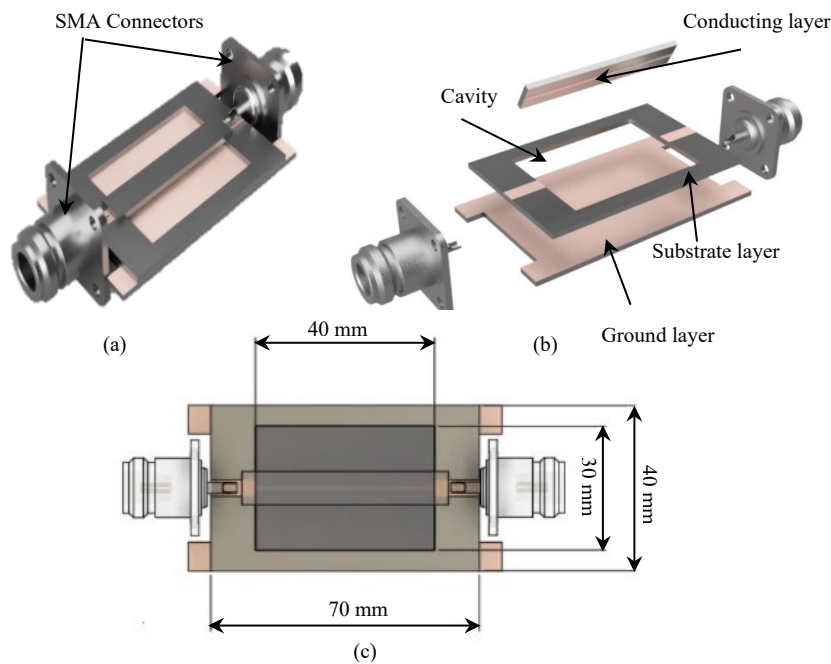
Figure 15. Glucose sensor structure using transmission line and a cavity under it (a) assembled sensor (b) Expanded view of the tree layers (c) Top view of the sensor showing its dimensions.

Here, we used a simple transmission line with a cavity resonator as the glucose sensor, which did not require a complex design. This method is widely used in microwave designs but is novel in sensor applications. The cavity resonator with a height of 1.6 mm, filled with DI water, can act as a quarter wavelength resonator at around 5.2 GHz. Therefore the thickness of

the substrate determines the resonant frequency of the cavity. When the cavity resonates, the signal goes to the ground resulting in a notch (absorption peak) at the frequency response. It is possible to verify changes in the absorption peak as a result of changes in relative permittivity caused by different glucose concentrations in "Experimental Analysis" section 3.5.

When the cavity was filled with the DI water with relative permittivity of ~80 as the substrate of the transmission line, the waveguide at around 5.2 GHz can be obtained from equation (8) where:

$c = 3 \times 10^8 \, m/s$

$f = 5.2 \, GHz \quad \xrightarrow{yields} \quad \lambda_g \approx 6.4 \, mm$

$\varepsilon_r = 80$

Therefore:

$$\lambda_g/4 = 1.6 \, mm$$

3.2.2.1. Equivalent circuit of the cavity resonator

An equivalent circuit model of the proposed sensor is shown in Figure 16(a). In the circuit model, two transmission lines represent the signal line (above) and the ground (below). The cavity with the MUT can be modeled as a resonant cavity between the microstrip line and the ground, generally modeled by an inductance (L) and a capacitance (C). Its loss from the MUT is modeled by the resistance (R). The resonant frequency is:

$$f_r = \frac{1}{2\pi\sqrt{LC}} \tag{12}$$

When this cavity resonates at its resonant frequency, the signal that should be transmitted from the input to the output sees a lower resistance path to the ground, and no signal is transmitted to the output; it goes to the ground at that frequency, forming a notch (or absorption peak) in the frequency response, as shown in Figure 16. Moreover, if the capacitance C changes because of the difference in the glucose concentrations, the frequency also changes.

In order to estimate the equivalent circuit parameters, we needed to model the glucose sample solutions as a dielectric material which was not the scope of this research. The goal was to observe the changes in the resonant frequency. We considered a fixed L=40nH and decreased

the capacitance from C1=10 pF to C1=9 pF; a shift by 100 MHz in the frequency could be observed, which was expected. The simulated frequency response of the equivalent circuit in ADS is shown in Figure 16(b).
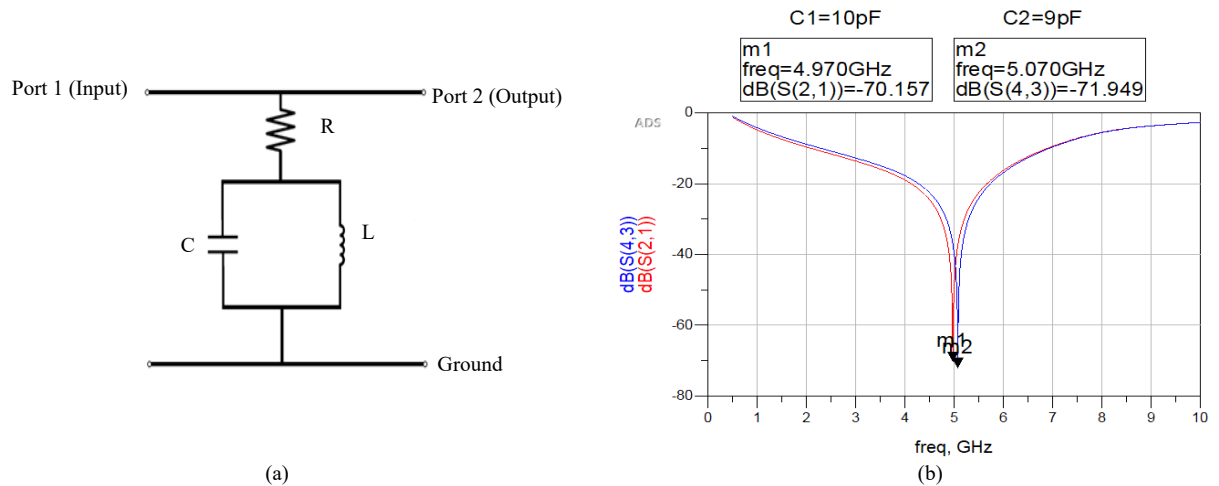
Figure 16. (a) Electrical equivalent model of the cavity (b) the simulation response of this model.

From equation (8), we can conclude that the resonator is not a lumped LC resonator but a quarter-wavelength cavity resonator considering, which will shorten the circuit at its resonant frequency, as explained in the previous section.

3.2.2.2. Electromagnetic field distribution

To verify the intensity of the electric field and its interaction with the MUT, a comparison between electric field distribution according to the position of the MUT in two configurations is shown in Figure 17. In Figure 17(b), the MUT was placed between the microstrip strip and the ground plane. It is easy to observe that the intensity of the electric field inside the MUT in Figure 17(b) is greater than when the MUT was integrated on the top surface of the transmission line resulting in less sensitive responses considering the electric field distribution, shown in Figure 17(a). As illustrated in Figure 17(b), the electric field is more confined and concentrated in the sample when placed as a substrate due to the location of the ground plane and the higher dielectric constant of the substrate. This leads to accurate dielectric measurement considering the position of the MUT between the signal line and the ground plane.
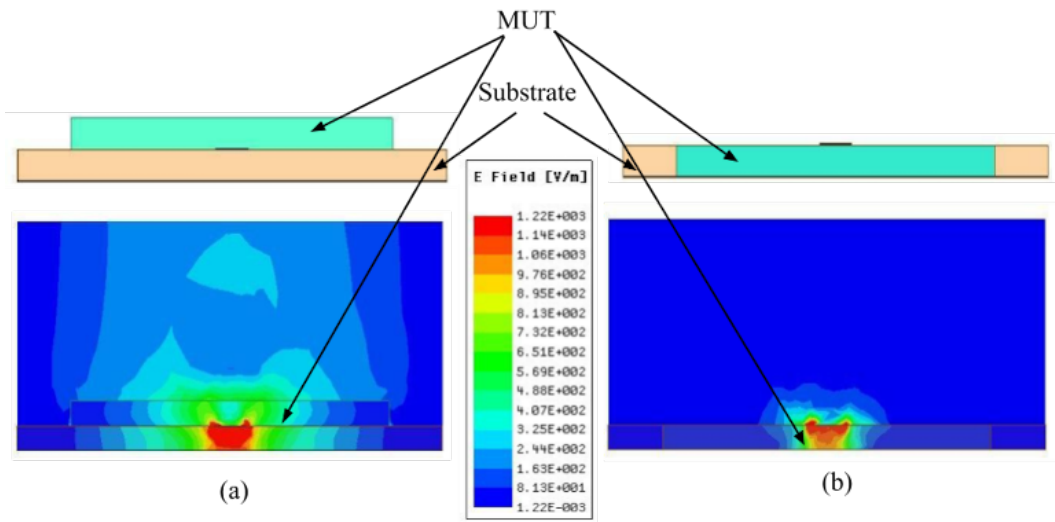
Figure 17. Position of MUT and the electric field distribution. (a) The classic microstrip line-based sensors. (b) Our proposed sensor.

3.3. Electromagnetic Analysis

As proof of concept, a set of simulations have been carried out using Ansys Electronics Desktop as the 3D EM simulator to analyze the performance in the frequency of the sensor using the structure in Figure 18. First, the sensor's frequency response was studied when the cavity was empty without any solutions and then filled with distilled water (DI water) with relative permittivity of 80 tanδ of 0.16, previously characterized by Komarov et al. (KOMAROV; WANG; TANG, 2005). The simulated (dashed orange) and measured (straight orange) frequency response up to 6 GHz of the empty cavity (filled with air) is presented in Figure 19. It is clear that the line is not matched, but the loss is low, as expected for a non-50 Ω-transmission line in air substrate.
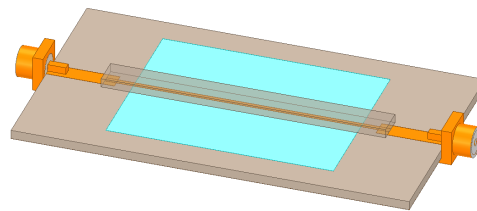
Figure 18. HFSS model of glucose sensing microstrip line-based device.
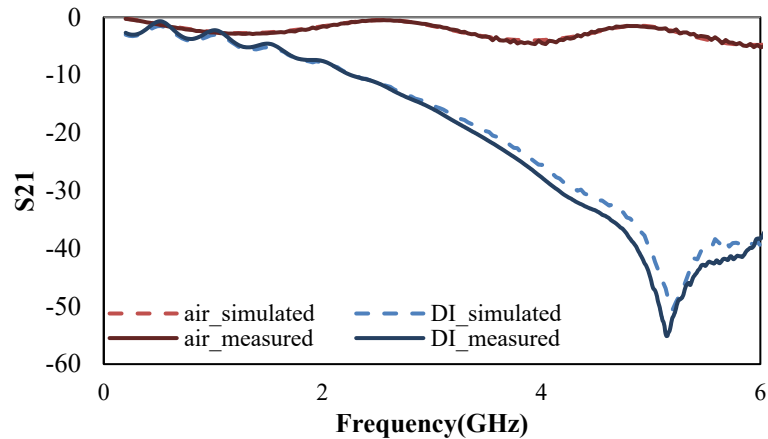
Figure 19. Simulated vs. measured frequency response (S) for empty cavity and filled with DI water.

The cavity was filled with DI water afterward, and the measured frequency response of (straight blue) has been compared to the simulation (dashed blue), also given in Figure 19. It is possible to verify the influence of the DI water, which presents high loss and produces an absorption peak at 5.15 GHz, which is expected from equation (8). And the 1.6 mm-deep cavity represents the length of a quarter of the wavelength at 5.15 GHz, considering a relative permittivity of 80. The simulation results are in very good agreement with the experimental measurements of both air and DI water and validate the simulation of the sensor's behavior in Ansys.

3.4. Measurement Method and Setup

The fabricated sensor and the experimental setup are demonstrated in Figure 20. The performance of our proposed microwave glucose sensors has been characterized in terms of network *S*-parameters using Performance Network Analyzer (PNA)(N5227B, Keysight, USA) with a measurement resolution of 0.1 dB, 1 Hz and 0.5° from 2 to 20 GHz in terms of magnitude, frequency, and phase, respectively. The Short-Open-Load-Through (SOLT) calibration process was required for an accurate measurement. The contact location where the calibration standards were attached (the network analyzer port, the end of a cable, or inside a test fixture) is where the measurement begins and ends. Finally, we conducted our measurements using VNA in two ports. The experiments were performed using glucose water samples with varying glucose concentrations. The device under test (DUT) is connected to VNA ports via coaxial cables. The

experimental setup for the measurement is shown in Figure 20(b), which is composed of VNA, DUT, coaxial probes, and solutions with different glucose concentrations.
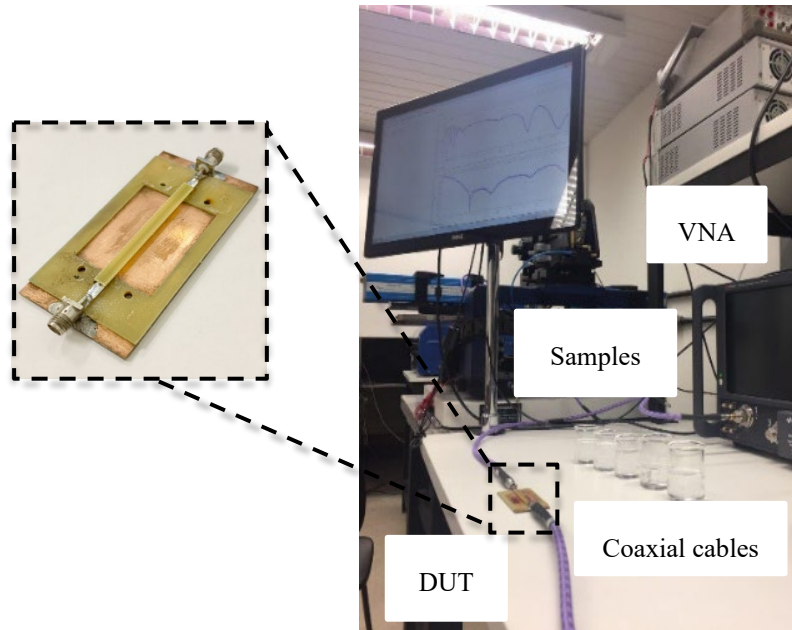
Figure 20. Photograph of (a) the fabricated sensor and (b) Experimental sensor setup with equipment.

In order to validate the functionality of the sensing device, we first measured glucose water solutions of different high concentrations to investigate their permittivity changes regarding the variation in the concentration. Then the study was followed by a series of measurements for low concentrations with the ranges explained in the "Materials and methods" section 3.2.1. All the measurements are performed using the same fabricated biosensor in an ambient environment.

The solutions were measured four times: right after the preparation, after 1-hour rest, 3-hours rest, and 1-day rest; then repeated for several more attempts. In the process, each time, first, the response of the sensor with an empty cavity was measured, then with the cavity filled with DI water to check the reproducibility and repeatability, and finally, filled with the glucose solutions. The solutions were injected one by one manually by syringe and characterized when the liquid was stabilized, then evacuated.

In our experiments, we measured the response by sweeping over a broad frequency range to determine the location of the absorption peak and then to check the accuracy of the

measurements by exposing the sensing device to different solutions. We used the S_{21} scattering parameter of our device to characterize the solutions when the syringe injected the liquid into the sensing area.

3.5. Experimental Analysis

The measured frequency response of the fabricated device for all different glucose solutions described in section 3.2.1 is presented here. The frequency range is between 4.8 and 5.7 GHz, where the structure presents an absorption peak.
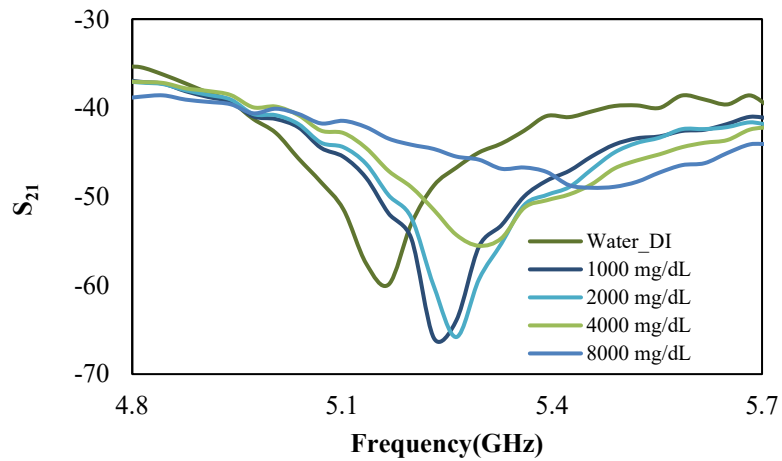
(a)
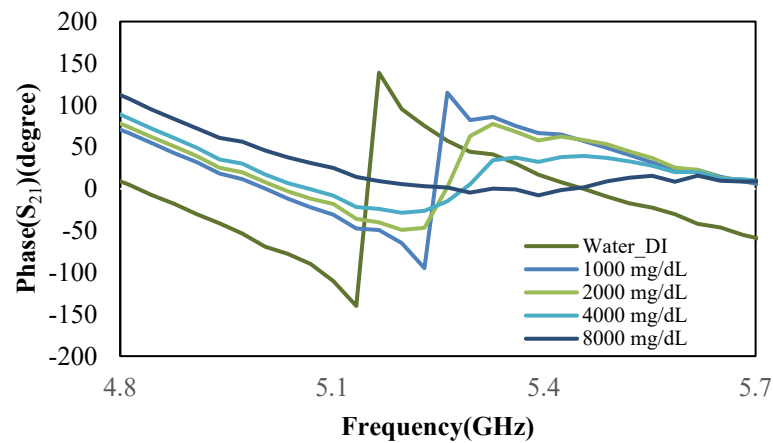
(b)

Figure 21. (a) Measured frequency response of the insertion loss (S_{21}), (b) Measured frequency response of the phase of S_{21} for the glucose solutions with concentrations ranging from 1000 to 8000 mg/dL.

Figure 21(a) shows the frequency response of the solutions for all different glucose solutions with high concentrations ranging from 1000 mg/dL to 8000 mg/dL. It can be seen that glucose concentration causes a change in the magnitude and the frequency of the absorption peak. When the concentration of glucose is increased, a noticeable reduction of the insertion loss and shift in the absorption peak toward higher frequencies can be observed. It is clear that the frequency of the absorption peak is changing because the relative permittivity of the solution is changing. Thus so is the phase of S_{21} illustrated in Figure 21(b).

(a)

(b)

(c)
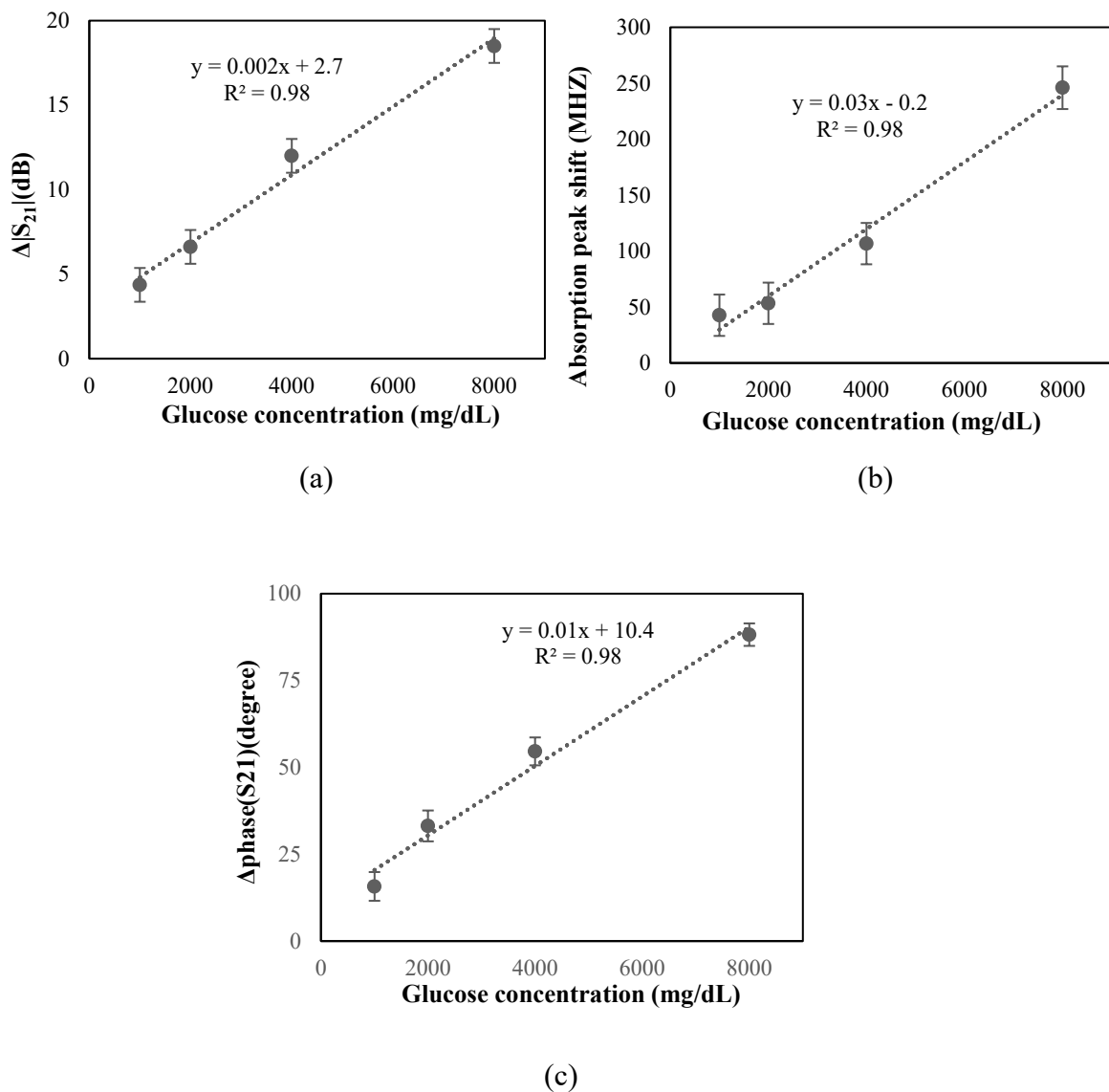
Figure 22. (a) The changes in measured ΔS_{21} at the absorption peak, (b) The shift of absorption peak, and (c)The increase of the phase at 5.3 GHz versus glucose concentrations.

To further examine the sensitivity, the changes in the magnitude of S_{21} versus the glucose concentration ranging from 1000 mg/dL to 8000 mg/dL with respect to the DI water

are plotted in Figure 22(a). Additionally, the corresponding shift in absorption peaks versus the glucose concentration in the above-mentioned range with reference to DI water is shown in Figure 22(b). Both results demonstrate a nearly linear response of the sensor for the considered range of glucose concentrations. Furthermore, the phase increases monotonously with the increase of concentrations, e.g., at 5.3 GHz, as shown in Figure 22(c). The magnitude reduces 2.6×10^{-3} dB/(mg/dL), the frequency of the absorption peak shifts 3.2×10^{-2} MHz/(mg/dL), and the phase changes 1.2×10^{-2} °/(mg/dL).
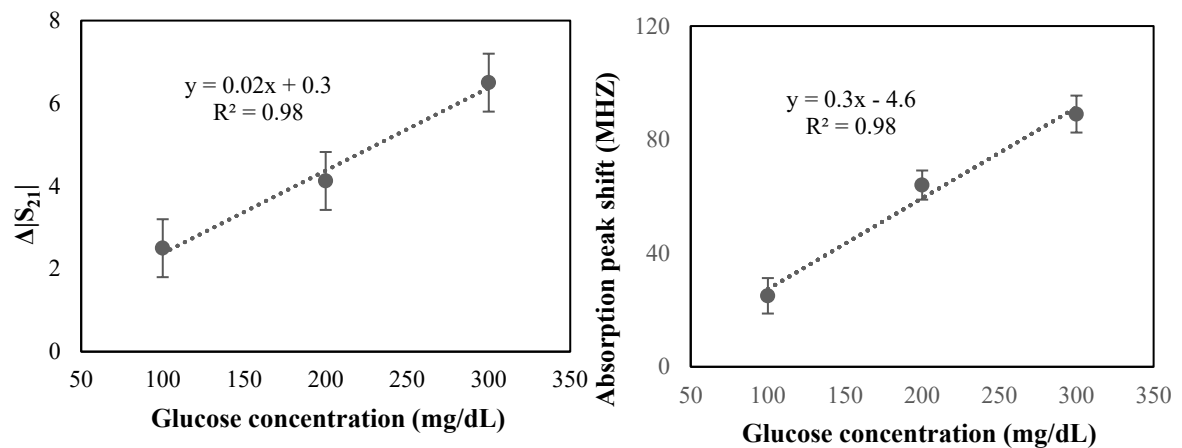
(a)

(b)
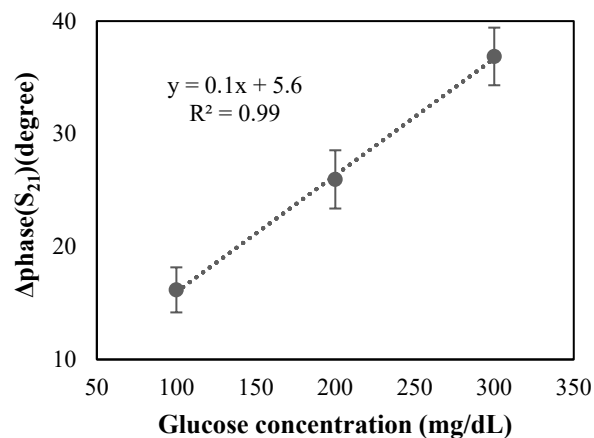
(c)

Figure 23. The measured (a) $\Delta |S_{21}|$, (b) Absorption peak shift, and (c) Phase shift versus glucose concentrations in the physiological range.

Even though the calibration graphs above contributed to the accuracy of glucose concentration estimation, high sensitivity in a smaller glucose concentration change in the

physiological range was desired. Therefore the experiment followed by measuring glucose solutions in the physiological range in the human body. A series of three water glucose solutions with the glucose concentration varied from 100 mg/dL (as a normal level) to 300 mg/dL (as a very high level) has been prepared. The same procedure has been used to measure lower concentrations in the same frequency range.

The result demonstrates that the biosensor can detect very small changes in glucose content, and the linear fitting of the obtained results is presented using error bars in Figure 23. As expected, the absorption peak frequency using these solutions is a little lower than for those using solutions with higher concentrations due to the glucose content. The sensitivity in this case is 2.5×10^{-2} dB/(mg/dL) for the magnitude of S_{21}, 12.5×10^{-2} °/(mg/dL) for its phase, and 32×10^{-2} MHz/(mg/dL) for the frequency. Therefore, our sensor can also distinguish different concentrations in the physiological range in repeated measurements.

The results of the repeated measurements for each sample were presented with error bars for both high and low concentration of glucose solutions. Table 3.1 shows the summary results of sensitivities (s), including the minimum (s_{min}), maximum (s_{max}), and average (s_{avg}) sensitivities of the proposed sensor for high and low glucose concentrations.

Table 3.1. Sensitivity (s) in terms of S_{21}, Absorption Peak, and Phase Measurement for both Ranges of Glucose Concentrations

		Sensitivity per mg/dL		
		S_{min}	S_{avg}	S_{max}
High concentration	$|S_{21}|$ (dB)	1.1×10^{-4}	2.6×10^{-3}	5.1×10^{-3}
	Absorption peak (MHz)	1.6×10^{-2}	3.2×10^{-2}	4.1×10^{-2}
	Phase (°)	4.8×10^{-3}	1.2×10^{-2}	2.8×10^{-2}
Low concentration	$|S_{21}|$ (dB)	3.2×10^{-3}	2.5×10^{-2}	4.7×10^{-2}
	Absorption peak (MHz)	15×10^{-2}	32×10^{-2}	49×10^{-2}
	Phase (°)	11.1×10^{-2}	12.5×10^{-2}	13.6×10^{-2}

3.6. Chapter Summary and Discussion

In this chapter, a glucose sensing platform was introduced based on a microwave sensor integrated with a microfluidic system for label-free detection and content sensing of glucose water solutions. The proposed sensor detects variations in the glucose concentration of the sample by measuring shifts in the absorption peak and phase due to the changes in relative permittivity. Our sensing device distinguishes the variation of glucose around 5.2 GHz due to the thickness of the chosen substrate.

Table 3.2 summarizes the experimental results of glucose-measuring sensors using planar transmission lines stated in the literature and that of our proposed sensor. The studied frequency range and concentration range and the average sensitivity values with respect to the concentration range for each sensor are also presented in this table. As can be observed, a few of them use the resonant frequency as the sensing parameter, while others use the return loss (S_{11}) or insertion loss (S_{21}).

Table 3.2. Comparison with the State-of-the-art Microstrip-based Glucose Sensors

Ref.	Position of the sample with respect to TL	Glucose Concentration (mg/dL)	Sensing parameter	Sensitivity Per mg/dL	Studied Frequency range (GHz)
(PARSAMYAN et al., 2018)	Top	0-250	$\lvert S_{21}\rvert$	9.8×10^{-2} dB	5.5-6.5
(JUAN et al., 2019)	Top	0-10000	$\lvert S_{21}\rvert$, Q	8.4×10^{-2} dB 0.658	2-7
(EBRAHIMI et al., 2020)	Top	0-500	$\lvert S_{11}\rvert$, fr	5×10^{-3} dB 5×10^{-3} MHz	2.4-2.6
(HUANG et al., 2019)	Under	78-5000	$\lvert S_{11}\rvert$	1.8×10^{-3} dB	1.4–1.9
This work	**Under**	**100-300** **1000-8000**	$\lvert S_{21}\rvert$, fr	**2.5×10^{-2}dB 32×10^{-2} MHz** **2.6×10^{-3} dB 3.2×10^{-2} MHz**	**4.8-5.7**

To accurately detect glucose concentrations in the physiological range, the sensitivity provided in the literature (including ours) regarding the magnitude of the signal should be high. For instance, the uncertainty of advanced equipment such as the VNA is, from 2-10 GHz, 0.2 dB. It means that considering an intermediate sensitivity, reported in the literature in Table 3.2, of 0.005 dB/(mg/dL), one would only be able to detect variations in a concentration higher than 40 mg/dL. If we need to detect a variation of 50 mg/dL (and sometimes less than that), this sensor is at the limit. Lower sensitivities would only detect higher variations in glucose concentration.

In view of this, a sensor based on the change of the relative permittivity can be more interesting either in terms of phase or frequency shift. For lower concentrations of glucose (lower than 500 mg/dL), our proposed sensor has the highest sensitivity in terms of frequency, almost 60 times more than the resonator (EBRAHIMI; SCOTT; GHORBANI, 2020). Considering the same variation of 100 mg/dL, our sensor would provide 32 MHz of frequency variation, which is easy for most equipment to measure. Even the worst sensitivity presented as 0.003 MHz/(mg/dL) would provide a 300 kHz of frequency variation, still easy to measure. This makes our proposed sensor an appropriate choice for a microwave sensor for glucose concentration measurements compared to state-of-the-art sensors.

As demonstrated in this study, microwave-based sensors integrated with microfluidic systems could differentiate glucose concentration in a frequency range of up to 6 GHz. This integration allows the miniaturization of the sensor. Here, we focused on choosing a large cavity size to accommodate wave propagation and, from the fabrication perspective, easily fill the cavity with the solutions by syringe and adequately evacuate them. The volume of the sample required in our sensor is 1920 µl. The volume was directly related to the cavity size (40 mm × 30 mm); however, the cavity can be scaled down as the solution has a high relative permittivity. It can be as narrow as the transmission line width and can be large enough to accommodate propagation, e.g., 5 mm × 20 mm, significantly reducing the volume of the sample to 160 µl. It also allowed label-free microwave investigation of bioanalytes by studying the changes in the relative permittivity of biomolecules such as glucose in aqueous solutions in small volumes.

Our proposed sensor contributes to the detection of glucose concentration even when the sensing range is small. However, the detection of glucose is still ambiguous for real-time label-free sensing. The real challenge is detecting glucose concentration in the blood without neglecting the effect of other physiological parameters.

This chapter aims to improve the efficiency of the design of the microwave biosensor capable of conducting glucose measurements based on the changes in the relative permittivity, including the optimization of the structural design and performance of the biosensor. Improving the creation of a microfluidic system involves implementing and establishing a new fabrication method. This method was based on the realization of the microfluidic system integrated as a part of the sensor as a substrate for miniaturization purposes and to improve manufacturing efficiency. The result of this study provides the detection sensitivity of the biosensor and demonstrates that:

- A variation of the relative permittivity of the MUT leads to a variation in absorption peak and phase.

- The use of MUT as substrate increase the electromagnetic interaction, hence the dielectric extraction measurements.

In addition, as a point of care testing, our device is considered to be simple, easy to operate, and sensitive (0.32 MHz/(mg/dL)).

Moreover, the optimizations of the biosensor in terms of microfluidic system integration and sensitivity have been validated experimentally with water glucose solutions. These studies allow us to carry out more efficient and more reproducible characterization. They also open doors for microwave spectroscopy of more complicated and dynamic biological matters.

To conduct our study, we performed dielectric measurements of biological matters, starting from biomolecules (e.g., glucose) in solutions and moving to more complex biological structures such as cells (living and cancer cells) to explore the applications where microwave biosensing could be helpful for biologists and physicians. Detecting cells in their biological medium in real-time was of great significance in point-of-care applications as an early diagnosis and monitoring tool for diseases. In this regard, the thesis continued designing and developing a novel, sensitive microwave-based sensor suitable for detecting living cells and real-time sensing of single cells passing in microfluidic devices.

Chapter 4. A LABEL-FREE MICROWAVE-BASED CELL-DETECTING BIOSENSOR

In this chapter, we will first introduce the concept of the biosensor dedicated to microwave dielectric measurements of a single biological cell. Then we will show the optimization of the experimental test, the fabrication of the biosensor, and the effectiveness of the integration of the microfluidic system for cell passage of the biosensor to increase its sensitivity.

4.1. Design and Implementation

Initially, a microwave-based sensor with a quarter-wavelength stub resonator was proposed to perform single detection. The fact that parallel stub resonators exhibit an input impedance that depends on their length enables some useful applications. Therefore parallel stub resonators based on microstrip transmission lines are a choice for rapid proof of the microwave biosensing principle for this particular application, and they can be easily fabricated.

Furthermore, in measuring the dielectric properties of a single cell, the high relative permittivity of the MUT played an essential role in our structural design. Measuring materials with a lower dielectric constant than the microwave substrate (such as oil droplets) is not a problem since the lower ε_r will prevail in the sum of the capacitances in a series configuration. However, the key challenge is measuring materials with high ε_r, for instance, water, the major constituent of a biological cell and its culture medium. Thus we proposed a novel structure considering the dielectric properties of cell suspensions.

The proposed design focused on placing the MUT in intense interaction with the electric field for better sensitivity and conducting measurements based on the relative permittivity changes without isolating cells from their medium in their flow stream.

Figure 24 illustrates the biosensor model with a stub, where the microfluidic channel was positioned under its tip. The stub, when designed to be a quarter-wavelength resonator at a certain frequency f_{res}, acts as an impedance transformer according to

$$Z_A = \frac{Z^2_{Stub}}{Z_{end\,of\,stub}} \tag{13}$$

The stub is ended by an open-circuit (∞ impedance); therefore, the impedance seen from point A at f_{res} is 0 (a short-circuit). This provides a transmission zero at f_{res}(absorption peak) according to its length. The length l_{res} of the parallel stub resonator is calculated according to

$$l_{res} = \frac{\lambda}{4} = \frac{c}{4f_{res}\sqrt{\varepsilon_r}} \tag{14}$$

where λ and f_{res} are the guided wavelength and resonant frequency of the stub, respectively, c is the speed of light in a vacuum, and ε_r is relative permittivity. Therefore, an ideal infinite attenuation or absorption peak was obtained when the electrical length of the open stub resonator was a quarter-wave ($\lambda/4$) according to equation (14).
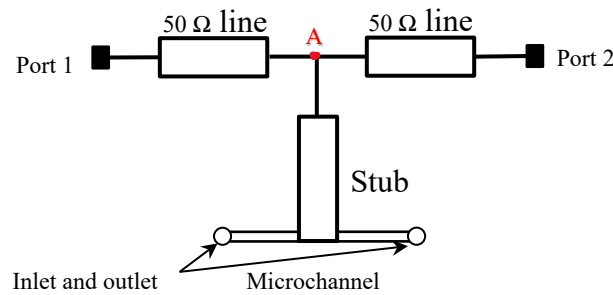
Figure 24. Model of stub resonator for cell characterization.

4.1.1. Materials and Methods

Microfluidic Biosensor

- The biosensor substrate: Here, porous alumina substrate from InRedox (relative permittivity of 6.7 and tanδ of 0.025) was chosen due to its outstanding biocompatibility. It is optically transparent. This feature facilitates the visual detection and direct imaging of cells in the microfluidic channel using optical microscopy. Furthermore, it is simple to fabricate a microchannel with a width small enough to allow the passing of a single cell (10 -20 μm in diameter for most cells) at a time and a small-diameter metal via through it.

- The microwave circuit: The microwave layer is formed by a microstrip transmission line and a parallel stub resonator with a via on its tip, to be placed precisely above the channel.

- The microfluidic channel: It was integrated into the microwave circuit in which the cell suspension flows between the stub tip and the ground plane where the electromagnetic fields are concentrated.

4.1.2. The microfluidic biosensor overview

The proposed biosensor can be seen in Figure 25. The biosensor integrates two layers. The one at the bottom is a microfluidic layer where a microchannel is placed under a microwave layer. The microwave layer composed of the microstrip transmission line, a parallel stub resonator, and a via is used to confine and seal the microchannel filled with cell suspensions to be characterized. The via composed of metallic nanowires extends the tip of the stub resonator to precisely above the channel, as illustrated in Figure 25(a). The ground plane at the back of the microfluidic layer can be seen in Figure 25 (b).
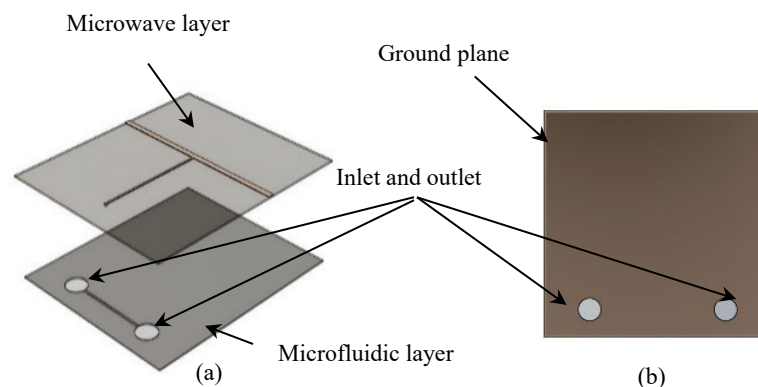
Figure 25. The designed microwave-based microfluidic biosensor: (**a**) Expanded view of the two layers composing the integrated biosensor; (**b**) Bottom view of the assembled biosensor showing the inlet and outlet.

The microfluidic layer that is aligned with the top layer, as shown in Figure 26(a), in which the cell suspension flows orthogonally to the stub, as shown in Figure 26(b); therefore, the cell suspension is the only medium between the tip of the stub and the ground plane. The cell suspension flow in a 50 μm-width channel contributes to maintaining the cell in the sensing region under the stub tip, where all other cells are lined up in a queue to arrive later. A cross-

sectional view of the microfluidic biosensor when the cell suspension flows in is shown in Figure 26 (c).
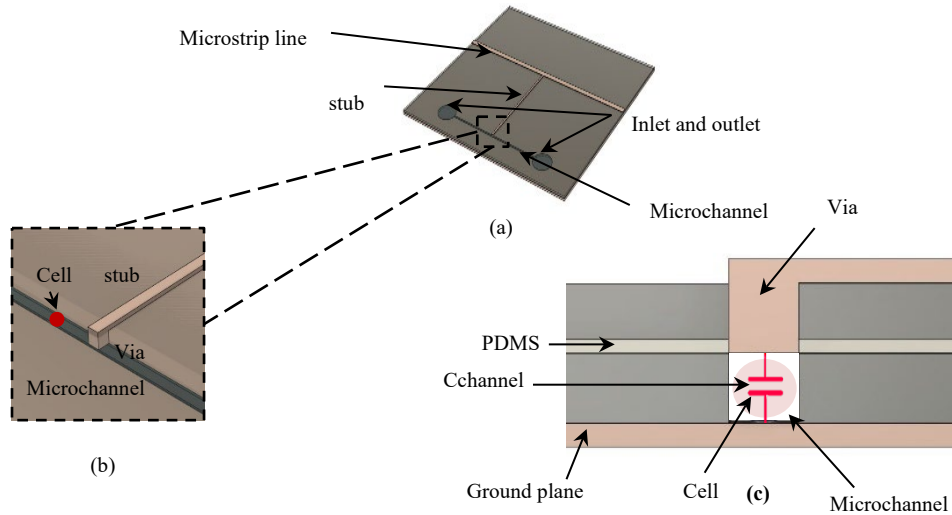
Figure 26. (**a**) View of the assembled biosensor; (**b**) Close-up of the stub tip above the microchannel; (**c**) Cross-sectional view of the microfluidic biosensor when the cell suspension flows in.

4.1.2.1 Equivalent electrical diagram

An equivalent circuit model of our proposed sensor is shown in Figure 27. The circuit is a transmission line with a microwave resonator (the stub) that can be modeled by an inductance (L_{Res}) and a capacitance (C_{Res}) followed by a capacitance at its tip to the ground, related to the microchannel, shown as $C_{Channel}$. Changing this capacitance, the electrical length of the stub is altered; thus, the resonance changes. In fact, when a cell with different permittivity to the surrounding medium enters the sensing region under the stub, it changes this capacitance ($C_{Channel}$). This translates to a change in the transmitted microwave signal phase.
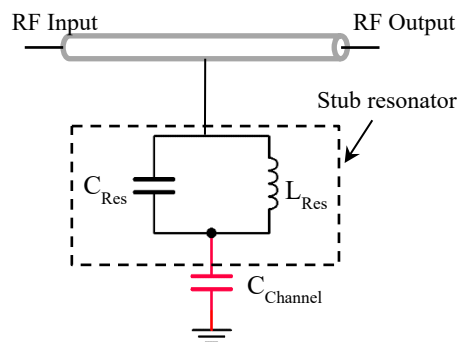
Figure 27. Electrical equivalent model of our proposed biosensor with via on the tip of the stub.

In this case, the quarter wave resonator is formed by the line and a small parallel plate capacitor at its tip. The dielectric of this capacitor is the microchannel itself. The capacitance changes the resonator's frequency when different materials are inside the microfluidic channel. When the microchannel under the tip of the stub is filled with medium (without cells) and cell suspension cell suspensions, the changes in ε_r changes its electrical length, thus changing the frequency of the absorption peak.

The reactance of this capacitor (the channel) in ohm (Ω) is calculated by

$$X_C = \frac{1}{\omega C_{channel}} = \frac{1}{2\pi f C_{channel}} \tag{15}$$

Where ω expresses the angular frequency in rad/s, f is the frequency in hertz, and C is the capacitance in Farads. Considering that the capacitance in Farads can be measured by:

$$C_{channel} = \varepsilon_0 \varepsilon_{MUT} \frac{A}{d} \tag{16}$$

where ε_0 is the permittivity of free space in Farads/meter, ε_{MUT} expresses the permittivity of the material in the microchannel, A represents the area of the resonator's tip in square meters, and d is the thickness of the microchannel in meters.

When the microchannel was filled with the DI water, as an example, with relative permittivity of ~60 at 10 GHz (LIEBE; HUFFORD; MANABE', 1991) as the dielectric of the capacitor, the capacitance can be obtained from equation (16)

where:

$\varepsilon_0 = 8.854 \times 10^{-12}$ Farad/m

$\varepsilon_{MUT} = 60$ $\xrightarrow{yields} C_{channel} \cong 26.5 fF$

A= 50 μm×50 μm

d = 50 μm

With the Capacitance in the range of Femtofarad, an absorption peak (notch) at ~10 GHz when the microchannel was filled with DI water would be obtained. Since water is the major component of all cells and culture media, similar behavior is expected.

4.1.2.2. Impact of the Via fabrication

We checked the sensitivity of our sensor regarding the design architecture of via considering the relative permittivity of the material under test. An equivalent circuit model of the sensor without via is shown in Figure 28.
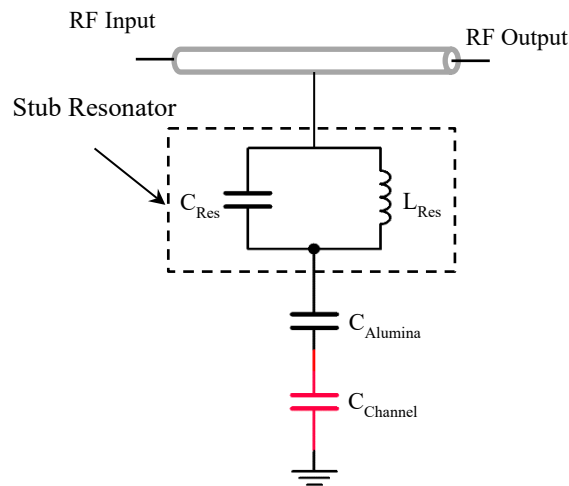
Figure 28. Electrical equivalent model of the sensor without via.
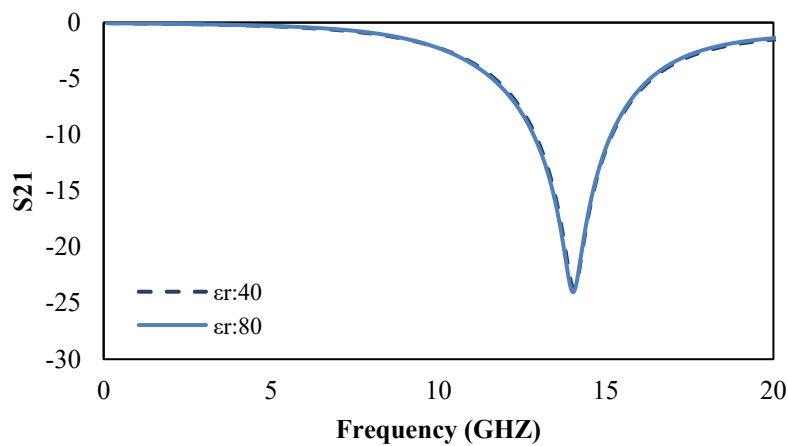
Figure 29. Simulated frequency response of the sensor without via when different materials are inside the microfluidic channel.

If the alumina substrate was placed between the tip of the resonator and the microchannel, without the via, the changes in the total capacitance would be highly attenuated as the cell, and the medium has relative permittivity (ε_r) well higher than the porous alumina due to their water content. With the capacitance of the alumina ($C_{Alumina}$) and the cell suspension

($C_{Channel}$) in series, as illustrated in the equivalent model in Figure 28, the material with lower relative permittivity, hence lower capacitance, attributed to the total capacitance. This means that, in the presence of an alumina layer (ε_r ~7), even a big difference in the relative permittivity of the material in the microchannel from liquid (ε_r ~80) to cell (ε_r ~40) would not affect the total capacitance significantly. The simulated frequency response of the resulting contrasts is shown in Figure 29.

4.1.2.3. Impact of the position of the microfluidic channel

In our proposed design, the via composed of metallic nanowires stretched out the stub tip inside the membrane, confining the electric field between the ground plane and the top of the metallic nanowires inside the sensing region. This means that the electric field only passes through the microchannel and not through the porous alumina substrate and enhances the sensibility of the sensor (FRANC et al., 2012).

Figure 30 illustrates the importance of the position of the channel and gives a better understanding of how the electric field distribution was affected dramatically by the material surrounding the resonator in two different configurations. In the structure shown in Figure 30(a), the 50 μm thick microfluidic channel was located inside the 50 μm thick alumina substrate at the bottom. The 50 μm width via extending the stub tip to the microchannel inside 50 μm thick alumina results in the maximum uniform electric field within the sample; therefore, higher sensitivity in detecting living cells is obtained due to the intense interaction of the field with the biological samples.

In Figure 30(b), the same two 50 μm thick alumina membranes were considered the dielectric substrate between the microstrip and the ground plane. The 50 μm thick microchannel was now placed on top of the stub. The microchannel was filled with distilled water (DI water) (relative permittivity (ε_r) ~80) in these figures. Ansys Electronics Desktop was used as the 3D EM simulator to calculate these quantities.

These figures do not provide a direct comparison between our proposed design and the works in the literature since those works used different substrate materials (glass commonly), most of which used PDMS covers or channels aside from different data extraction methods. The main focus here was to demonstrate the effect of the microchannel position relative to the transmission line. It can be easily seen that the electric field is much more confined in the

sensing region inside the microchannel in our proposed device as opposed to when the microchannel is placed on top of the transmission line. Therefore, for this specific application that detecting a microorganism at the cell level (microscale) is the aim of the study; our proposed sensor provides a much greater intensity of electric field hence more interaction with cells. We can observe a progressive increase in the interaction of the maximum EM field in red when the microchannel is positioned as substrate. The sensing area exactly under the stub tip matches the cell size and is the most sensitive area to permittivity changes. Therefore, this study contributes to defining a new way of designing and fabricating a microfluidic biosensor with maximized sensitivity.
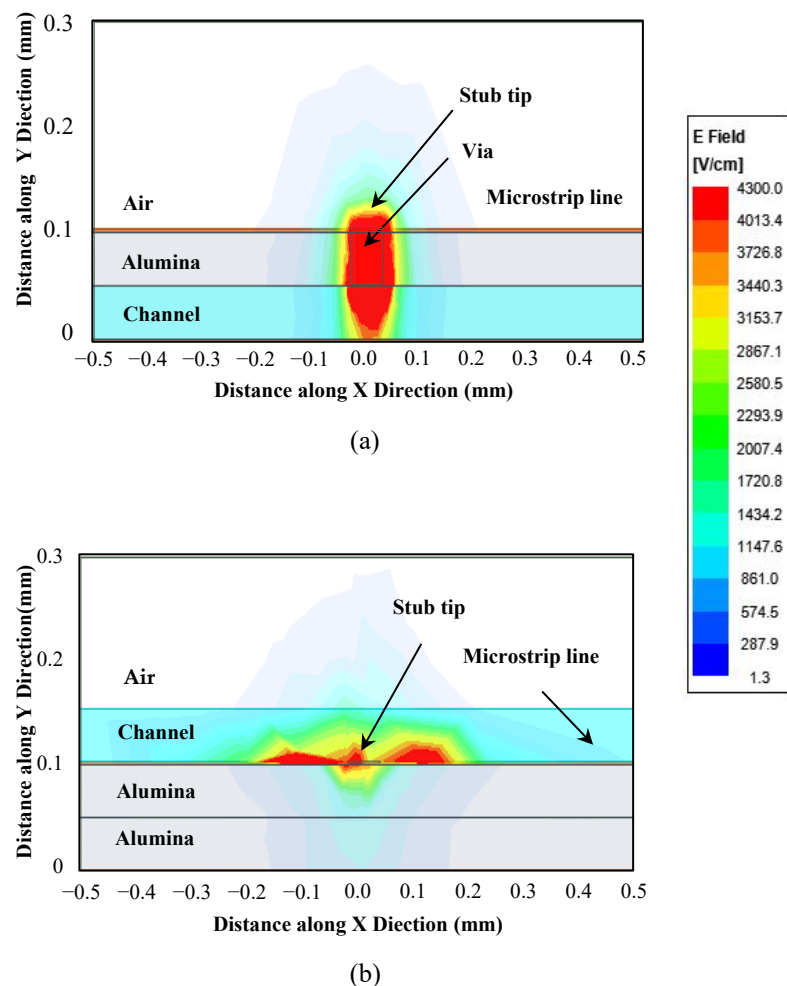
Figure 30. Position of the microchannel and the electric field distribution in (a) the microfluidic biosensor proposed in this work; (b) the sensor with the microfluidic channel above the transmission line.

4.1.3. The fully assembled biosensor overview

Using the carrier, the sensor could be measured by SMA connectors, and expensive probes were avoided, which could be damaged if there was any leak.

- The Carrier substrate: Rogers TMM 6 microwave laminate with a copper thickness of 17 *um* and a dielectric thickness of 2.54 mm was used. It has a relative permittivity of 6 and tanδ of 0.0023. It provided mechanical stability to the structure, especially regarding the liquid injection accesses (inlet and outlet).

-The microwave circuit: The carrier provided 50 Ω coplanar waveguide (CPW) access (input and output of the device).
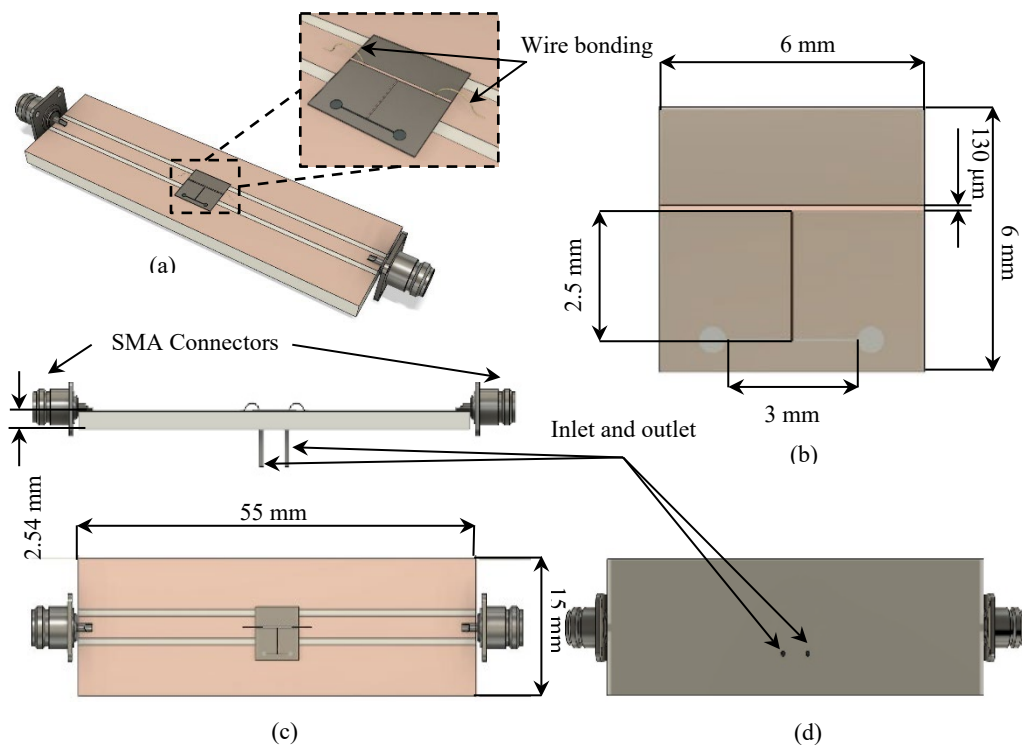
Figure 31. The model of the fully assembled biosensor to the carrier: (a) Close-up of the microfluidic biosensor wire bonded to the carrier; (b) Top view of the microfluidic biosensor showing its dimensions; (c) Top view and lateral view of the fully assembled biosensor to the carrier showing the dimensions of the carrier; (d) Bottom view of the carrier showing the structure of liquid injection accesses.

The TMM6 substrate was 15 mm wide, 55 mm long, and 2.54 mm thick. The microfluidic biosensor, shown in Figure 31, was fabricated with a length of 6 mm and a width of 6 mm, where we have constructed a 3 mm long and 50 μm width microchannel in the bottom layer. On the top alumina layer, we have a 50 Ω microstrip transmission line with a length of 6 mm and width of 130 μm and a quarter wavelength stub with a length of 2.5 mm and a width of 50 μm. A 50 μm × 50 μm square-shaped via was placed on the tip of the stub inside the membrane.

4.2. Sensor Fabrication

The microfluidic biosensor was fabricated using standard microfabrication techniques and divided into two main steps: (1) fabrication of the microfluidic and microwave layers illustrated in Figure 32, and (2) assembly of the two layers to form the microchannel and integration onto the carrier substrate.
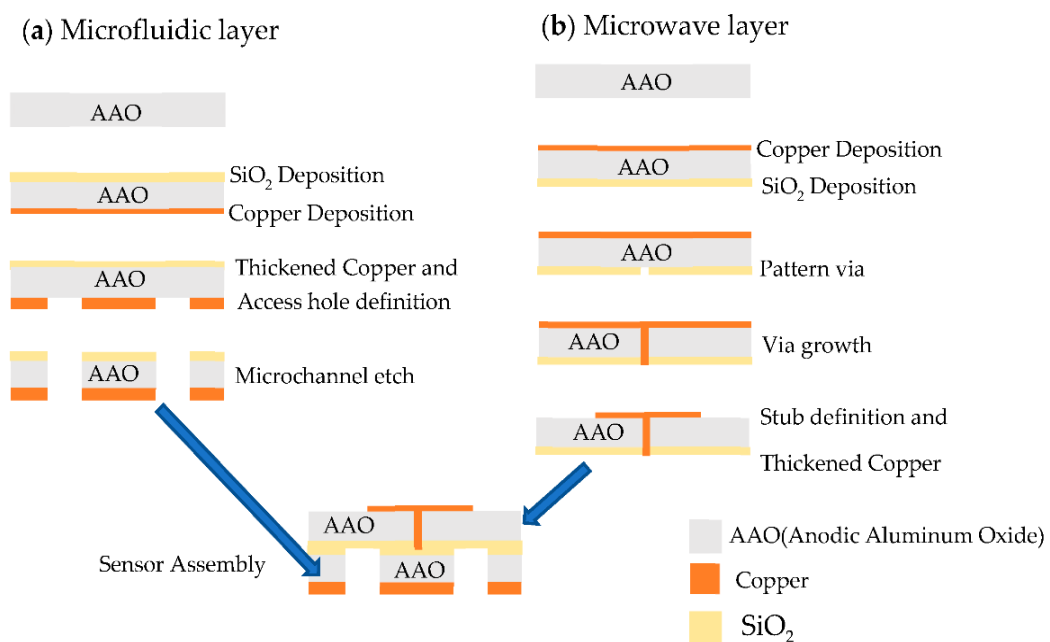
Figure 32. Fabrication steps of the microfluidic and microwave layers for our proposed biosensor.

First, a 20 nm thick copper seed layer was deposited by RF magnetron sputtering for the microfluidic layer. This layer was then patterned with the ground plane geometry by direct laser lithography. The patterned copper was thickened to 3 μm by electroplating. On the other side, silicon dioxide (SiO_2) was deposited by sputtering to be used as a mask for channel etching.

The microchannel geometry was patterned, and the microchannel was etched with a NaOH (50%) solution at 50 °C.

The same copper seed layer and SiO$_2$ layer used in the microfluidic layer were deposited on the top and bottom surfaces of the microwave layer. The SiO$_2$ was patterned with the via geometry, and copper was grown through the porous aluminum to form a via, as described in (PINHEIRO et al., 2018). The copper seed layer was patterned, and the copper was thickened to 3 μm to form the microstrip line and the stub. The two layers were assembled under a microscope using PDMS to seal the channel.

For the assembly of the whole sensor, first, the Gerber files (.gbr) from the DXF HFSS design files were generated for the CPW carrier. The carrier provided 50 Ω coplanar waveguide (CPW) access (input and output of the device). The biosensor prototype was fabricated using the milling machine on a Rogers TMM6 laminate. A few markers were added to the design to facilitate the alignment of carrier and microfluidic biosensor parts in the fabrication process. Two circular holes (The inlet and outlet) were created and drilled through the laminate, which will be aligned to the microfluidic layer using the integrated vision system and prefabricated alignment markers. The microfluidic biosensor was attached to the carrier using electrically conductive silver epoxy. Both ends of the Microstrip line on the microwave layer of the structure were wire bonded to the CPW signal line on the carrier soldered to 50 Ω SMA connectors to ease the VNA connection for measurements.

4.3. Electromagnetic Analysis

Ansys Electronics Desktop was used as the 3D EM simulator to analyze the performance of the biosensor in terms of magnitude, phase, and frequency responses using the modeled structure in Figure 33.
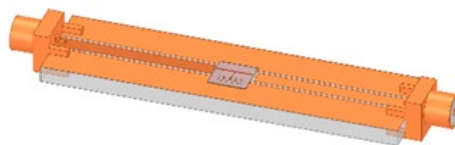
Figure 33. HFSS model of our proposed microwave-based microfluidic sensing device.

As proof of concept, a set of simulations were carried out in which the microchannel was first considered empty and then filled with DI water with relative permittivity of 80. The simulated (dashed orange) and measured (straight orange) frequency response of the empty channel (filled with air) and the measured frequency response of the microchannel filled with DI water (straight blue) compared to the simulation (dashed blue), up to 14 GHz, are presented in Figure 34. The agreement between simulations and measurement is good for both experiments, validating the simulation of the sensor's behavior in Ansys. The differences between the curves are mainly due to the wire bonding connecting the sensor to the carrier.
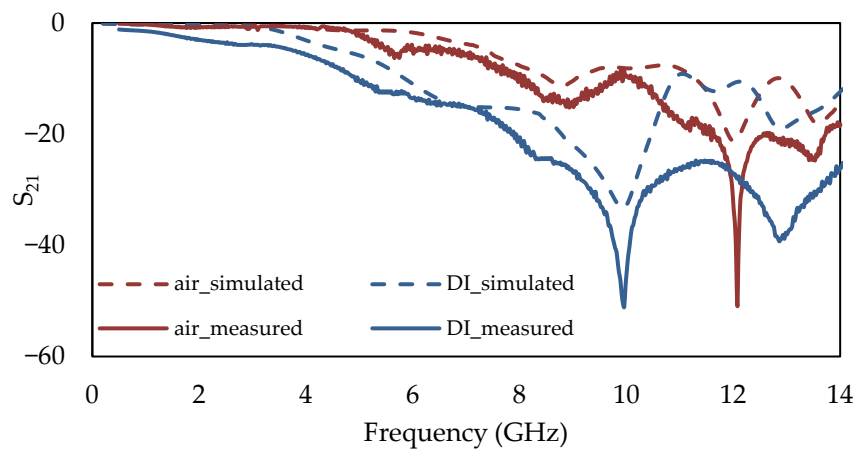
Figure 34. Simulated vs. measured frequency response of the insertion loss (S_{21}) for empty microchannel and filled with DI water.

It is possible to verify that our sensing region provides a capacitive gap with a 50μm microchannel (dielectric) between the thin metals precisely under the via and the ground. In this open stub resonator, when the electrical length is a quarter-wave ($\lambda/4$), an absorption peak (notch) was obtained. When the microchannel was filled with DI water, this produced an absorption peak at ~10 GHz, as discussed in section 4.1.2.1.

4.4. Measurement Method and Setup

The dielectric properties of the biological matters were determined as a function of frequency, as in equation (1). This characteristic was measured in terms of network Scattering

parameters (S-parameters) using a VNA in two ports of configuration over a frequency range of up to 20 GHz. Figure 35 shows the complete experimental setup for the measurement. It is composed of the following:

- An S-parameter measuring device: performance network analyzer (PNA) (N5227B, Keysight, Santa Rosa, CA, USA). The biosensor is connected to PNA ports via coaxial cables.

- A peristaltic pump that precisely controls the constant flow rate in the microfluidic channel with a predetermined speed.

- A microscope to monitor the fluidic channel and the cell suspension flow.

- A high-speed camera to record the sensing area continuously as soon as the cell suspension flowed in the microchannel.
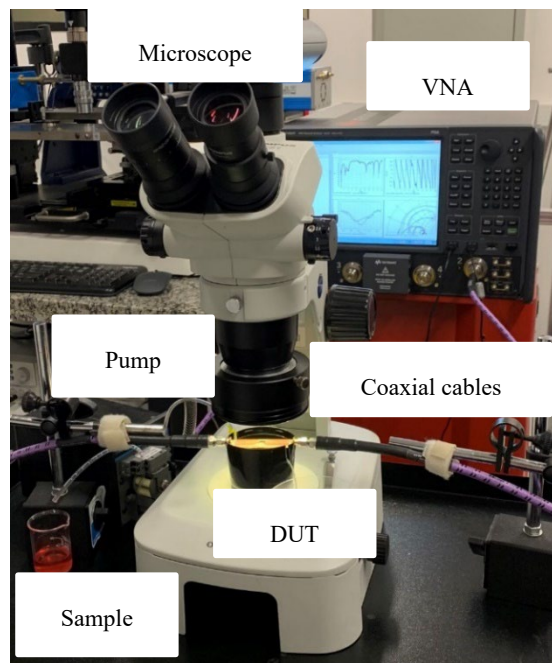
Figure 35. Experimental setup with equipment.

4.4.1. Extraction of dielectric-dependent parameters

The performance of our proposed microfluidic biosensor has been characterized in terms of network S-parameters using a VNA in two ports of configuration after the SOLT calibration process up to 20 GHz. The measurement resolution of 0.1 dB, 1 Hz, and 0.5° in terms of magnitude, frequency, and phase, respectively. We used the S21 scattering parameter

of our device to characterize the cell suspensions. All experiments were carried out under normal laboratory environment conditions.

In the process, each time, first, the response of the sensor with an empty microchannel was measured, then the microchannel was filled with the biological medium continuously as a reference to check the reproducibility and repeatability of the study, and finally, filled with cell suspensions. Furthermore, various duplicated sensors from the same fabrication process were elaborated to validate the performance of the biosensor at several attempts. The liquid flow was controlled using a pump, and the microfluidic channel was monitored with a microscope simultaneously. A high-speed camera recorded the sensing area continuously while the magnitude and phase of S_{21} were measured as soon as the liquid flowed in the microchannel. A similar set of experiments with the same procedure was carried out for the cell suspension in different concentrations.

However, due to the fast speed of the cells being pumped, observing and recording the absorption peak frequency was mainly restricted by the instantaneous response of the vector network analyzer (VNA). In addition, the accurate absorption peak of the cell was obtained by reversing the pumping direction till one single cell arrived at the desired area while the data were recorded. To achieve reliable real-time measurements from the microwave sensor, we evaluated the sensing performance and the sensitivity of the microwave sensor in terms of changes in the phase as a function of time at the absorption peak (~11 GHz).

Therefore, in the second step, to detect a single living cell, we conducted real-time measurements, with an alternative approach, by operating the VNA in continuous wave (CW) mode at the absorption peak with a power level of 0 dBm and an IFBW of 3 kHz to study the phase of S_{21} scattering parameter. The CW mode provided significant control to capture and record the changes due to the speed of the cells proceeding through the microchannel. This led to the detection of the cell due to sufficient sampling of cell suspensions and an accurate determination of the time when the cell passed the sensing area. We described below the principle and the steps essential to this extraction process.

Moreover, to avoid the incident where multiple cells passed the sensing area, the direction of the cell suspension was changed various times randomly while cells moved forward and backward. This operation makes it possible to measure several single cells.

4.5. Experimental Analysis

The fabricated sensor is illustrated in Figure 36. Sample reservoirs are connected to the microfluidic channel via tubing and connectors. A simple pumping flow was used for single-cell detection, and the rate was adjusted. The high-speed camera was used to record microscopic images, and videos were also used to validate the experimental results obtained from the sensor. Measurements were carried out on different measurement days with different samples.

The study continued with the dielectric measurement of living single cells in their culture medium when passing the sensing region in the microfluidic biosensor within the framework of measurements in real-time and assessing its repetitiveness and repeatability. In this section, first, we present the measurements of single living cells in their culture medium, one by one, with the proposed biosensor aiming to evaluate the performance of the biosensor according to the variable nature of the material under test; living cells, and to examine the repeatability of the measurements. Then the experiments were followed by the discrimination of two different cells in the second step.

(a)   (b)
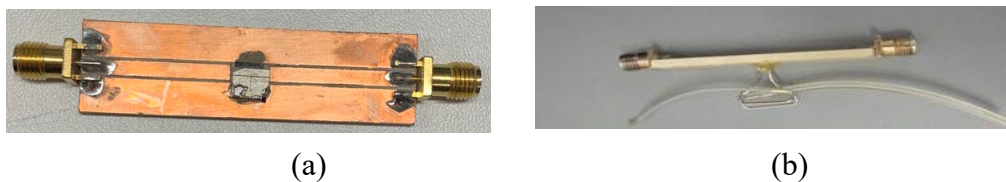
Figure 36. Photograph of (a) Top view of fabricated sensor; (b) Lateral view with liquid injection accesses and tubing.

For all the measurements, the flow speed is maintained throughout the injection, and all the cell solutions have a concentration of 1 million cells/ml. It is optimized for the successful passing of a single cell.

- Cell suspension was injected into the microchannel.

- S-parameters of the biosensor were recorded using VNA.

- Between each measurement, a culture medium was injected to wash the microchannel eliminating the presence of trapped cells.

- S-parameters of the biosensor were recorded using VNA to verify the repeatability.

- Previous steps were repeated several times.

4.5.1. Cells' description and preparation protocol

To evaluate the sensing capability of the proposed biosensor, C1498 cells with a typical diameter close to 20 μm were studied. Their round shape facilitates the visualization process. The C1498 cells (ATCC® TIB-49) were cultivated in a 75 cm^2 tissue culture flask with Dulbecco's Modified Eagle Medium (DMEM) supplemented with 10% Fetal Bovine Serum. The flask was incubated at 37 °C with 5% CO$_2$, and the medium was changed every three days; then, all the contents of a flask (cell and medium) were transferred in a 50 mL tube and centrifuged at 125× g for 10 min. After discarding the supernatant, the pellet of cells was re-suspended with fresh DMEM medium at the dilution ratio of ~2 × 10^5 cells/mL.

Cell suspensions were prepared under ethical standards in the Laboratory of Experimental Hematology, Department of Clinical and Toxicological Analysis, School of Pharmaceutical Sciences, University of São Paulo. Optical methods and image analysis software were used to measure the diameter of cells, as shown in the setup in Figure 37. The cells were placed in their respective fresh culture medium before the measurements.
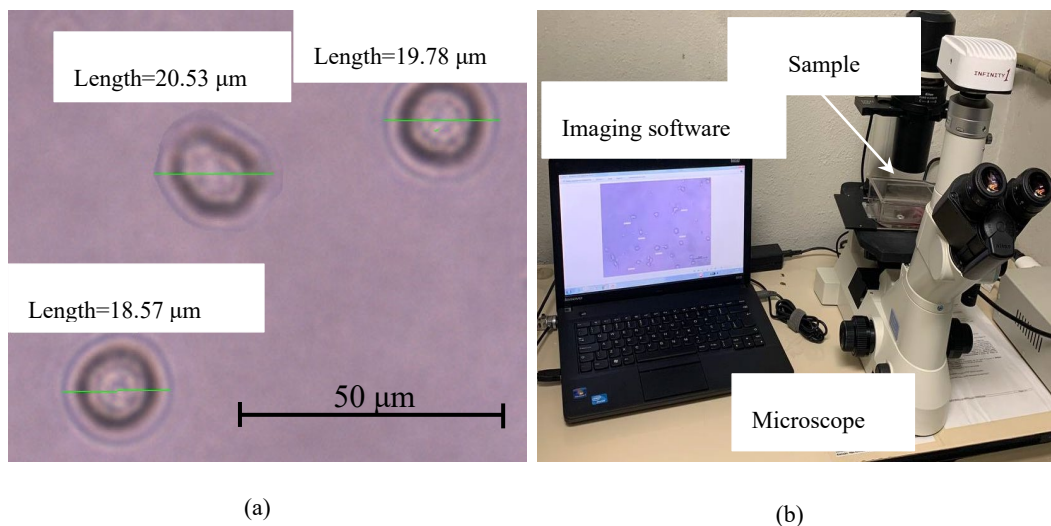
Figure 37. (a) Close-up of the C1498 cell size and shape measurements using optical microscope images treated by image analysis software; **(b)** Complete setup for cell size measurement.

4.5.2. Real-time single-flowing cell detection

To verify the performance of the biosensor, the real-time measurement was divided into two main steps. First, the sensor was loaded only with the biological medium (without cells) to study where the structure presents an absorption peak. Then cell suspension flowed in the microchannel, which was constantly monitored. The moment a single cell traveled through the microfluidic channel, the flow rate of the cell suspension was reduced to ensure the presence of the cell strictly under the stub tip in the sensing region. Then the frequency response of the biosensor was recorded.
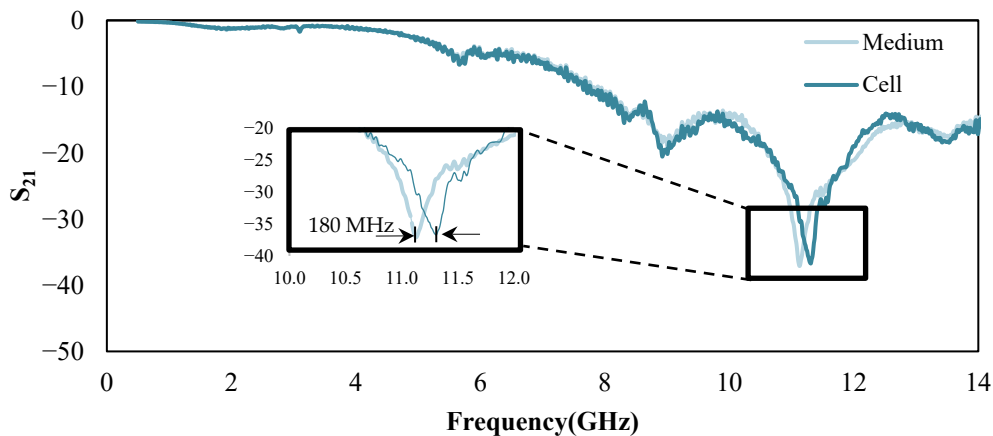
Figure 38. Measured frequency response of the insertion loss (S_{21}) for the medium compared to the single-cell presence under the stub in the sensing region.

Figure 38 shows the frequency response of the medium compared to the instance that a cell is under the stub tip. The presence of a single cell affects the magnitude and frequency of the absorption peak; a shift of 180 MHz in the absorption peak can be observed, as shown in the inset of Figure 38.

In the second step, to detect a single living cell, we conduct real-time measurements, with an alternative approach, by operating the VNA in continuous wave (CW) mode at the absorption peak (~11.1 GHz) by capturing phase. Figure 39 demonstrates pictures taken during the real-time measurements of the cells. Figure 39(a)–(c) are optical microscope images captured by the high-speed camera displaying a C1498 cell (indicated by black circles and arrows) entering the microchannel, crossing the sensing region, and moving forward toward the

outlet, respectively. We confirmed that a single cell passed through the channel, constantly monitoring the microchannel. The same cell was moved backward and forward through the region five times to verify the responses. The real-time phase data for the transmitted signal for each time point shown in Figure 39(a)–(c) were extracted. The shift in the transmitted signal phase was observed in Figure 39(d). A peak confirmed the presence of the cell in the sensing region underneath the stub tip in the microfluidic channel. Figure 39(e) displays an image of three cells during the same pass through the microfluidic channel. The cells are circled in black, traveling from left to right in the microchannel. Figure 39(f) illustrates the real-time phase data for three consecutive cell passes. Each peak value in the phase of S_{21} presented in this figure corresponds to the presence of a single cell. An average of $22.85 \pm 1.65°$ shifts in the phase of the transmitted signal in the presence of the cell in the medium were measured. To avoid the incident where multiple cells passed the sensing area, the direction of the cell suspension was changed various times randomly while cells moved forward and backward. The obtained results eliminated the possibility of overlapping cells' measurement, which was not the case in the present work, and gave us excellent reproducibility.

(a)   (b)   (c)

(d)

(e)

(f)
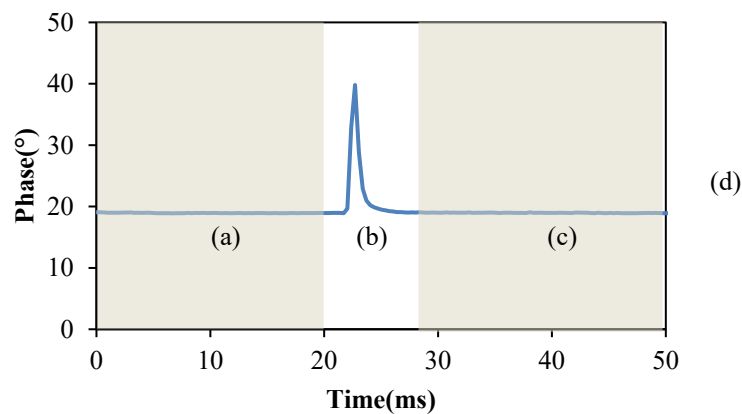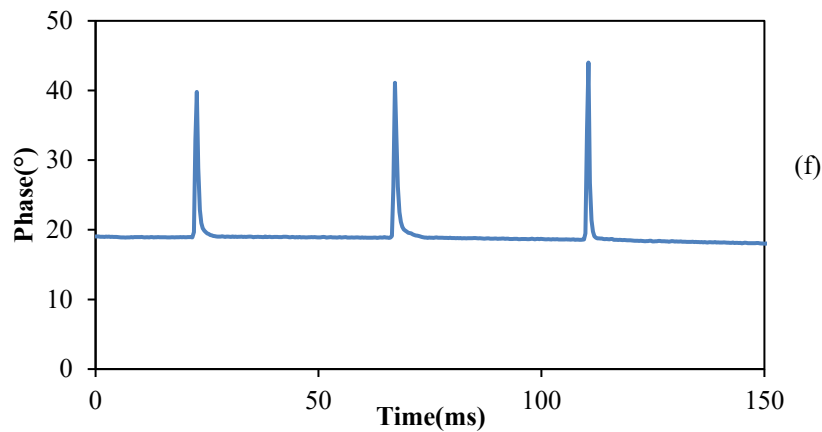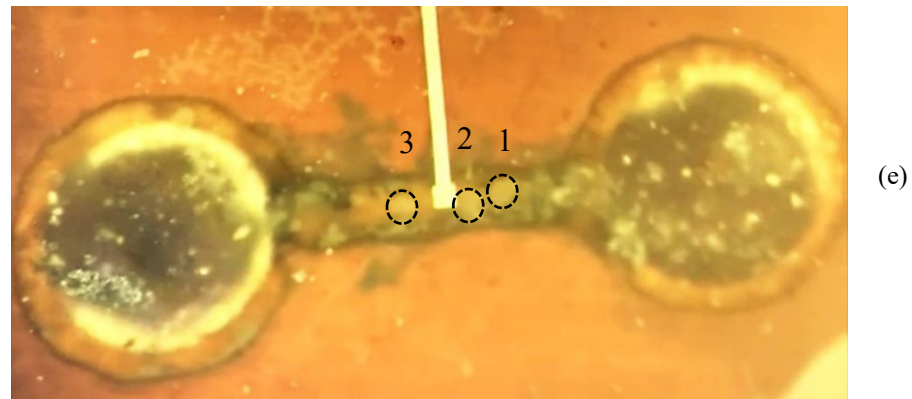
Figure 39. Real-time measurements of a single C1498 cell:

OBS.:

(a–c) are optical microscope images captured by the high-speed camera displaying a C1498 cell (indicated by black circles and arrows) entering the microchannel from the inlet (left), crossing the sensing region, and moving forward toward the outlet (right), respectively;
(d) displays the real-time measurement of phase data of a single cell moving forward in a channel for each time point from (a–c) in 50 ms;
(e) displays an image of three cells (circled in black) during the same pass through the microfluidic channel;
(f) shows the phase data from the biosensor showing a total of 3 consecutive cell passes.

In this experiment, several practical considerations were taken into account during the measurements to eliminate the possibility of overlapped cell measurement in the obtained results above; however, the response of the sensor to the occurrence of the overlapped cells shed light on its accurate performance and what can be accomplished.
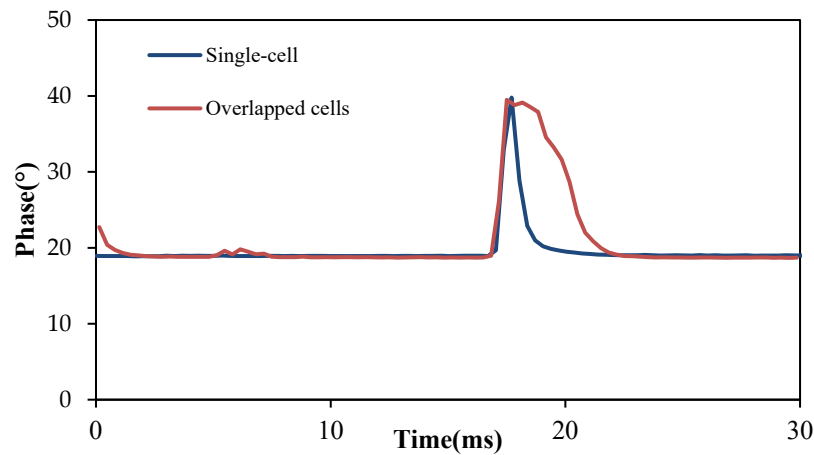
Figure 40. The real-time measurement of phase data of overlapped cells compared to single-cell moving forward in the microchannel.

The phase shift due to the formation of overlapped cells is illustrated in Figure 40. Considering their bigger size, the overlapped cells require more time to pass through the sensing region. This transit time can be measured and correlated to its size. It also qualifies our proposed biosensor as an appropriate choice for cell measurement and size discrimination applications.
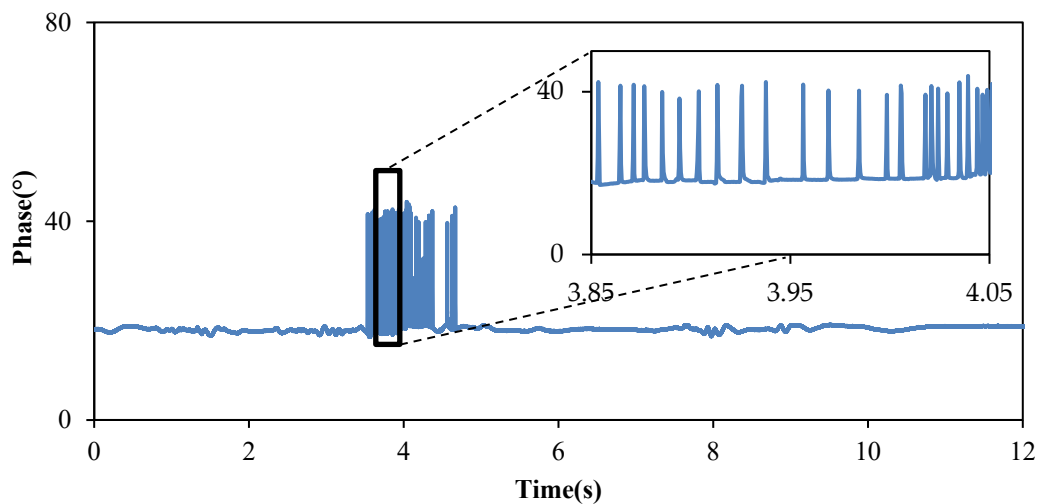
Figure 41. The phase data from the continuous flow of C1498 cell suspensions for 1.2 seconds in between the medium injections.

Another consideration is that even if the flow rate is high, the equipment (VNA) can detect the cell passing through the microchannel because the phase will change for each one. By operating the VNA in continuous wave (CW) mode, the changes in the S-parameter are measured over time at a single frequency. The cell suspension was pumped with different flow

rates and different cell suspension concentrations into the microchannel. Yet, we can detect the cells instantaneously, as illustrated in the inset of Figure 41. Figure 41 shows the phase shift of the transmitted signal in 12 seconds time pass where the sensor was filled with medium. Subsequently, the cell suspension entered the microchannel for 1.2 seconds. The microchannel was then washed with the medium to ensure that all the cells were flushed away and prepare the sensor for subsequent experiments. The inset of Figure 41 confirmed the sensing ability of the sensor, the measurement device, and the experimental setup to detect single cells in a flowing stream in real-time.

4.5.3. Real-time cell discrimination

Following this work, we became interested in the discrimination of different types of cells. Therefore, two different cells of varying sizes were selected. Aside from C1498, Jurkat, Clone E6-1 (ATCC® TIB-152) cells with a typical diameter close to 10 μm were studied. Their round shape illustrated in Figure 42 facilitates the visualization process. The cell preparation was almost the same as the C1498 cells; however, Jurkat cells have different culture medium. They were cultured and expanded in RPMI-1640 supplemented with 10% fetal bovine serum. Cell suspensions were prepared under ethical standards and were placed in their respective fresh culture medium before the measurements.
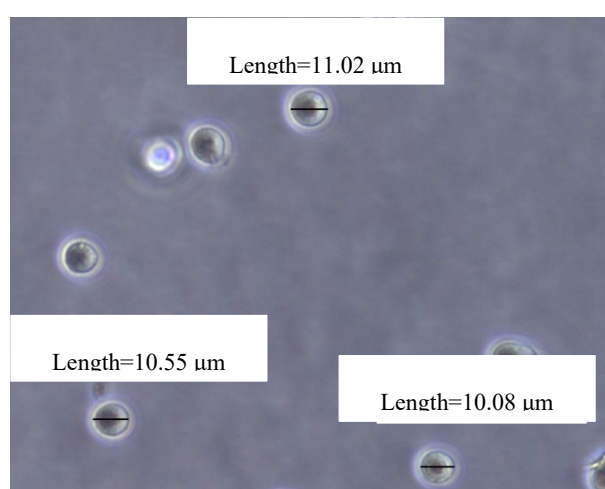
Figure 42. Close-up of the Jurkat cell size and shape measurements using optical microscope images treated by image analysis software.

Although the culture medium of the cells was different, the measurements were done right after mixing the cells in the fresh medium; therefore, it would not interfere with the measurements nor modify their nature. A batch of mixed cells was divided into five 10 ml sub-batches, and dielectric measurement was performed for each case.
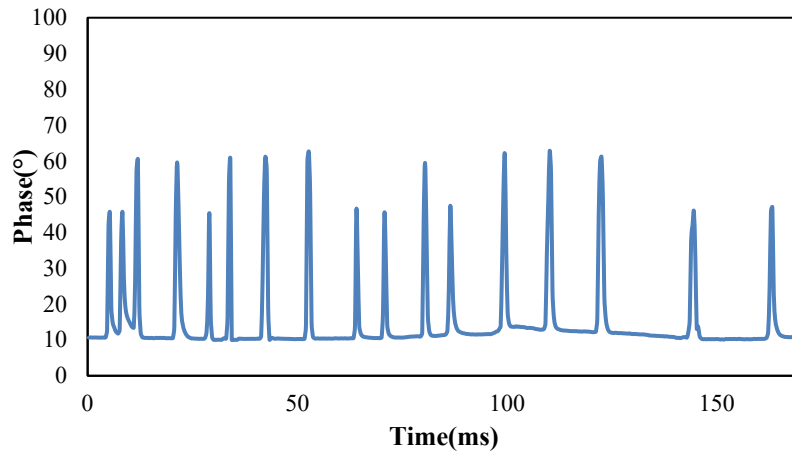
Figure 43. The phase data from the continuous flow of mixed cell suspensions.

Figure 43 shows the measured phase data from the continuous flow of the mixed cell suspensions while the VNA operated in CW mode. A significant difference in the phase shift has been observed between the two cell types. This difference could come from the different relative permittivity of the cells crossing the sensing area. This is due to each cell's constitution and water concentrations, as discussed in (DALMAY et al., 2009).

The feasibility of distinguishing different cells has been studied, and the sensor response demonstrated the possibility of discriminating between different cell types. A summary of phase shifts for two types of cells in a mixed medium and the standard deviation is presented in Table 4.1.

Table 4.1. Sensing abilities of the dispersions and their applications

Cell Type	Average phase shift	Standard deviation
Cell #1	35.125	±1.12
Cell #2	50.078	±1.07

4.6. Chapter Summary and Discussion

In this chapter design and implementation of the cell detection biosensor were presented. Integration and fabrication of a microfluidic channel right underneath the stub tip using metallic nanowire-filled membrane technology in sensing were performed. A microfluidic channel was created to transport the MUT with flowing cells to the sensing area. The optimization of the microfluidic channel involved the study of electromagnetic field distribution. The result of this study allowed us to choose a model which was effective in terms of flow stream detection of cells instead of trapping cells with mechanical components as in the literature. This eliminated the complexity of the fabrication process in terms of including trapping components. Furthermore, isolating cells from their medium was not required. The process of fixation of the cells to biosensors is aggressive to the cell and may modify or destroy its properties.

In this work, we detected the continuous flowing cells, and high sensitivity was achieved in terms of phase due to its particular design. By placing the tip of the microstrip stub resonators above the microfluidic structure through a via, the cell suspension was set to be the medium between the tip of the stub resonator and its ground plane. Therefore, it can be argued that the obtained response of flowing single cells at microwave frequencies in the sensing region is due to the different relative permittivity of the cell with respect to its biological medium crossing the sensing region.

Table 4.2 summarizes the label-free microwave-based sensors for the dielectric characterization of cells using planar transmission lines techniques stated in the literature and that of our proposed sensor. The studied frequency range, design methods, and microwave components are also presented in this table.

Furthermore, various experiments have been carried out with the objective of evaluating the performance of the biosensor for the characterization of single biological cells. First, we presented experiments carried out on single-cell detection in the DMEM medium. These experiments demonstrated the very good repeatability and reproducibility of biosensor measurements. The studies have been carried out on more complex biological situations for cell detection in a flow stream of single cells passing the sensing region with a 12s measurement time frame. The second part presented the experiments for cell discrimination. It has thus been demonstrated that the biosensor is able to follow the changes in the type of single cells

instantaneously. All of the studies carried out indicate that our biosensor is able to perform cellular analysis in a non-destructive way and requires no preliminary preparation.

Table 4.2. Comparison with the State-of-the-art label-free microwave-based sensors.

Ref.	Microwave Topology	Position of the Microfluidic Channel to TL	Flowing or Adherent Cell	Sensing Parameter	Studied Frequency (GHz)
(DALMAY et al., 2010b)	Interdigitated comb capacitor	-	Adherent	$\|S_{21}\|,\|S_{11}\|$ f_r	14.7
(CHEN et al., 2013)	CPW	Top	Flowing	$\|S_{21}\|,\varepsilon_r$	1–40
(ZHANG et al., 2014)	Interdigitated comb capacitor	-	Adherent	f_r, ε_r	5–14
(LIU et al., 2018)	Microstrip resonator	Top	Flowing, mechanically trapped	$\|S_{11}\|,\|S_{21}\|$	2.17
(WATTS et al., 2020)	Microstrip resonator/dielectric resonator	Top	Flowing	$\|S_{21}\|$	9.8
This Work	**Stub resonator/nanowire-filled technology**	**Under**	**Flowing**	**fr, phase**	**11.1**

Finally, establishing this technological method of detection by fabricating the via to integrate the microfluidic channel demonstrates that:

- A difference in the relative permittivity of the cells with their surrounding medium leads to a sensitive detection with a variation of the phase of the transmitted signal.

- A variation in cell types led to a variation of phase, providing different phase shift contrast for discrimination purposes.

This study presented an integrated microwave-based microfluidic biosensor for real-time detecting of flowing cells for cell quantification. The microfluidic channel was integrated into stub resonators using the metallic nanowire-filled membrane technology. The device proposed in the present work distinguished cells measuring the phase shift of the transmitted electromagnetic wave. A variation of as much as $22.85 \pm 1.65°$ degree was observed at ~11.1 GHz. It was demonstrated that the change in the transmitted signal phase is correlated to cells passing through the sensing region. The architecture of this sensor makes it possible to fabricate

the microchannel in between the stub and the ground. Hence, the interaction between the sample and the electric field was stronger, leading to a more effective parameter extraction. This biosensor successfully detects cells in their biological medium in real-time; hence, it can be used as an early diagnosis and monitoring tool for diseases.

Chapter 5. CONCLUSIONS AND FUTURE WORKS

This chapter summarizes the outline of the thesis and provides brief conclusions from the previous chapters. The limitation and challenges of this research will be introduced, and future work will be recommended.

5.1. Conclusions

Biosensors have been trending and overgrowing; however, microwave biosensing methods are not quite available commercially, and conventional methods are still being used.

This thesis proposed simple biosensors based on existing microstrip resonator technology. These biosensors integrated a microfluidic system with a microstrip line for the miniaturization purpose of carrying liquids of biological materials under test. The scientific motivation, problems, and aim of this work were defined to find a solution to a medical issue by microwave biosensors. This thesis used microstrip-based biosensors to approach possible solutions to previously mentioned problems due to their simple and planar geometry of the transmission line.

The first fabricated biosensor provided glucose detection with varying concentrations. The biosensor realization started with microstrip design through modeling and fabrication at an operating frequency of around 5 GHz. Several parameters were considered in the design optimization process, and the cavity resonator design was successfully modified to fit biosensor functionality. The measurements of the sensor were obtained using scattering parameters. Label-free detection of glucose was investigated, and frequency shift and signal attenuation occurred due to changes in analytes concentration. Then the optimization was followed by designing miniaturized biosensors to investigate more complex structures. A quarter wavelength resonator was integrated with a microscale channel to tune the environment at the cell level.

Additionally, modeling investigations on the proposed architectures of the sensors were carried out to make them appropriate for biosensing. Microfluidics systems are made with the same substrate to be integrated with microwave resonators. They were designed in specific

regions only to enhance the sensitivity of the biosensors. Unique adequate geometry of microfluidic systems was proposed for each biosensor to exploit the areas where high field densities are found. Both designs were modeled and analyzed to be fabricated. The fabrication schemes were planned and implemented by two approaches on FR-4 dielectric substrate and alumina substrate. VNA was used to test and validate the fabricated devices. The VNA measurements showed that the microstrip line-based sensors operated correctly according to design parameters.

Consequently, an appropriate form of biosensors was completed and examined. The experimental results of the assembled fabricated biosensors were presented to verify their performance in terms of biological detectability and sensitivity against targeted biological samples. The repeatability of different microwave-based biosensors was evaluated and validated. The result data were discussed and analyzed. The analyzed data showed the potential biomedical application of the proposed biosensors to recognize different concentrations of glucose and detect cells in real-time. The proper position of the microfluidic and the volume of solutions are essential factors in biosensing measurements.

In this thesis, utilizing microwave resonators as biosensors proved to be feasible within the frequency range of the study for healthcare applications. This microwave biosensing method observed a detectable change for each target biological sample change.

5.2. Future Work

The glucose sensor design can be optimized to improve sensitivity and selectivity toward sensing glucose concentration. In the same manner, the sensitivity of the biosensor can be optimized according to the microstrip design. Therefore, optimization of biosensor design and architecture is possible. Size reduction is another recommended work of the optimization process. A miniaturized biosensor will require less sample volume. New substrate materials can be utilized to study their functionality. In terms of selectivity, biorecognition elements can be used, leading to a more successful bio-detection. In future investigations, exploring blood glucose levels in patients with different diabetes conditions to examine the effect of other physiological processes is recommended. Furthermore, different types of biomolecules can be studied.

The biosensing device for cell detection could detect the presence of a single cell with respect to the medium over time; this device can be subject to a dramatic improvement. The next step could be to conduct size measurements and cell differentiation by effectively controlling the flow of the cell using an appropriate pump to provide desired pressure and flow of the cell suspension in the channel. Also, the width of the microfluidic channel can be optimized and further reduced to the typical cell size. Therefore, the bigger cells require more time to pass through the sensing region due to their slower velocity. This transit time can be measured and correlated to the size of the cell. It also qualifies the cell discrimination based on their size. Moreover, designing a microfluidic channel with multiple inlets will facilitate cell discrimination.

Furthermore, the investigation of dynamic biological mechanisms such as blood coagulation based on the changes in the relative permittivity of blood in this process can be the subject of future studies.

The microwave-based microfluidic biosensor design was realized successfully; therefore, commercialization can be beneficial as it will pave the way for non-destructive sensing and facilitate continuous monitoring applications. Finally, microwave-based sensors can be tested not only in healthcare applications but also as industrial sensors with different materials.

REFERENCES

ABEDEEN, Z.; AGARWAL, P. Microwave sensing technique based label-free and real-time planar glucose analyzer fabricated on FR4. **Sensors and Actuators A: Physical**, v. 279, p. 132–139, 15 ago. 2018.

ADHIKARI, K. K.; KIM, N. Y. Ultrahigh-sensitivity mediator-free biosensor based on a microfabricated microwave resonator for the detection of micromolar glucose concentrations. **IEEE Transactions on Microwave Theory and Techniques**, v. 64, n. 1, p. 319–327, 1 jan. 2016.

AFSAR, M. N. et al. The Measurement of the Properties of Materials. **Proceedings of the IEEE**, v. 74, n. 1, p. 183–199, 1986.

ALAHNOMI, R. A. et al. Review of Recent Microwave Planar Resonator-Based Sensors: Techniques of Complex Permittivity Extraction, Applications, Open Challenges and Future Research Directions. **Sensors 2021, Vol. 21, Page 2267**, v. 21, n. 7, p. 2267, 24 mar. 2021.

Ansys Electronics | Complete Electronics Simulation Tools. Disponível em: <https://www.ansys.com/products/electronics#tab1-1>. Acesso em: 9 ago. 2022.

ARLETT, J. L.; MYERS, E. B.; ROUKES, M. L. Comparative advantages of mechanical biosensors. **Nature Publishing Group**, v. 6, p. 203, 2011.

ARTIS, F. et al. Microwaving Biological Cells. **IEEE Microwave Magazine**, v. 16, n. 4, p. 87–96, 2015.

ASAMI, K. Characterization of biological cells by dielectric spectroscopy. **Journal of Non-Crystalline Solids**, v. 305, n. 1–3, p. 268–277, 1 jul. 2002.

ASSOCIATION, A. D. Diagnosis and Classification of Diabetes Mellitus. **Diabetes Care**, v. 33, n. Suppl 1, p. S62, jan. 2010.

BHALLA, N. et al. Introduction to biosensors. **Essays in Biochemistry**, v. 60, n. 1, p. 1, 6 jun. 2016.

BLAKEY, R. T.; MORALES-PARTERA, A. M. Microwave dielectric spectroscopy – A versatile methodology for online, non-destructive food analysis, monitoring and process

control. **Engineering in Agriculture, Environment and Food**, v. 9, n. 3, p. 264–273, 1 jul. 2016.

CARRASCOSA, L. G.; HUERTAS, C. S.; LECHUGA, L. M. **Prospects of optical biosensors for emerging label-free RNA analysis**. TrAC - Trends in Analytical ChemistryElsevier B.V., , 1 jun. 2016.

CHALKLEN, T.; JING, Q.; KAR-NARAYAN, S. Biosensors based on mechanical and electrical detection techniques. **Sensors (Switzerland)**, v. 20, n. 19, p. 26–37, 1 out. 2020.

CHEN, C.; WANG, J. **Optical biosensors: An exhaustive and comprehensive review**. AnalystRoyal Society of Chemistry, , 7 mar. 2020.

CHEN, T. et al. Microwave biosensor dedicated to the dielectric spectroscopy of a single alive biological cell in its culture medium. **IEEE MTT-S International Microwave Symposium Digest**, 2013.

CHEN, Y. et al. Rare cell isolation and analysis in microfluidics. **Lab on a chip**, v. 14, n. 4, p. 626–645, 21 fev. 2014a.

CHEN, Y. F. et al. 40 GHz RF biosensor based on microwave coplanar waveguide transmission line for cancer cells (HepG2) dielectric characterization. **Biosensors and Bioelectronics**, v. 61, p. 417–421, 15 nov. 2014b.

CHIN, C. D.; LINDER, V.; SIA, S. K. **Commercialization of microfluidic point-of-care diagnostic devices**. **Lab on a Chip**The Royal Society of Chemistry, , 22 maio 2012.

CHUNG, Y. K. et al. An electrical biosensor for the detection of circulating tumor cells. **Biosensors and Bioelectronics**, v. 26, n. 5, p. 2520–2526, 15 jan. 2011.

COLE, K. S.; COLE, R. H. Dispersion and Absorption in Dielectrics I. Alternating Current Characteristics. **The Journal of Chemical Physics**, v. 9, n. 4, p. 341, 29 dez. 2004.

COLLIN, R. Foundations for Microwave Engineering: Wiley-IEEE press: Hoboken. p. 944, 2001.

DALMAY, C. et al. Label-free RF biosensors for human cell dielectric spectroscopy. **International Journal of Microwave and Wireless Technologies**, v. 1, n. 6, p. 497–504, dez. 2009.

DALMAY, C. et al. On-chip biosensors based on microwave detection for cell scale investigations. **Communications in Computer and Information Science**, v. 52, p. 51–63, 2010a.

DALMAY, C. et al. Ultra sensitive biosensor based on impedance spectroscopy at microwave frequencies for cell scale analysis. **Sensors and Actuators A: Physical**, v. 162, n. 2, p. 189–197, 1 ago. 2010b.

DALMAY, C. et al. **Development of high frequency microfluidic biosensors for intracellular analysis**. Procedia Engineering. **Anais**...Elsevier Ltd, 1 jan. 2014.

DANIELS, J. S.; POURMAND, N. **Label-free impedance biosensors: Opportunities and challenges**. **Electroanalysis**NIH Public Access, , jun. 2007.

EBRAHIMI, A.; SCOTT, J.; GHORBANI, K. Microwave reflective biosensor for glucose level detection in aqueous solutions. **Sensors and Actuators, A: Physical**, v. 301, p. 111662, 1 jan. 2020.

ESPINA PALANCO, M. et al. Optical Biosensors to Explore Biological Systems. **Biophysical Journal**, v. 110, n. 3, p. 638a–639a, 16 fev. 2016.

FOK, M. et al. A novel microwave sensor to detect specific biomarkers in human cerebrospinal fluid and their relationship to cellular ischemia during thoracoabdominal aortic aneurysm repair. **Journal of medical systems**, v. 39, n. 4, 1 abr. 2015.

FOSTER, K.; SCHWAN, H. Dielectric properties of tissues and biological materials: a critical review. **undefined**, 1989.

FRANC, A. L. et al. Metallic nanowire filled membrane for slow wave microstrip transmission lines. **IEEE 2012 International Semiconductor Conference Dresden-Grenoble, ISCDG 2012**, p. 191–194, 2012.

FRICKE, H.; MORSE, S. THE ELECTRIC RESISTANCE AND CAPACITY OF BLOOD FOR FREQUENCIES BETWEEN 800 AND 4(1/2) MILLION CYCLES. **The Journal of general physiology**, v. 9, n. 2, p. 153–167, 20 nov. 1925.

FRITZ, J. Cantilever biosensors. **Analyst**, v. 133, n. 7, p. 855–863, 24 jun. 2008.

GABRIEL, S.; LAU, R. W.; GABRIEL, C. The dielectric properties of biological tissues: II. Measurements in the frequency range 10 Hz to 20 GHz. **Physics in Medicine and Biology**, v. 41, n. 11, p. 2251–2269, nov. 1996.

GENNARELLI, G. et al. A microwave resonant sensor for concentration measurements of liquid solutions. **IEEE Sensors Journal**, v. 13, n. 5, p. 1857–1864, 2013.

GONZALES, W. V.; MOBASHSHER, A. T.; ABBOSH, A. The Progress of Glucose Monitoring—A Review of Invasive to Minimally and Non-Invasive Techniques, Devices and Sensors. **Sensors (Basel, Switzerland)**, v. 19, n. 4, 2 fev. 2019.

GOVIND, G.; AKHTAR, M. J. Metamaterial-inspired microwave microfluidic sensor for glucose monitoring in aqueous solutions. **IEEE Sensors Journal**, v. 19, n. 24, p. 11900–11907, 15 dez. 2019.

GRENIER, K. et al. Integrated Broadband Microwave and Microfluidic Sensor Dedicated to Bioengineering. v. 57, n. 12, p. 3246–3253, 2009.

GRENIER, K. et al. Microwave signatures of alive B-lymphoma cells suspensions. **2011 IEEE Radio and Wireless Week, RWW 2011 - 2011 IEEE Topical Conference on Biomedical Wireless Technologies, Networks, and Sensing Systems, BioWireleSS 2011**, p. 95–98, 2011.

GRENIER, K. et al. Label-free discrimination of human lymphoma cell sub-populations with microwave dielectric spectroscopy. p. 4p., 10 jun. 2018.

GUARITI, G. et al. Determination of sugar concentration in aqueous solutions using ultra-wideband microwave impedance spectroscopy. **IEEE MTT-S International Microwave Symposium Digest**, 2013.

GUHA, S.; JAMAL, F. I.; WENGER, C. **A review on passive and integrated near-field microwave biosensors**. **Biosensors**MDPI AG, , 23 set. 2017.

HAMZAH, H.; LEES, J.; PORCH, A. Split ring resonator with optimised sensitivity for microfluidic sensing. **Sensors and Actuators A: Physical**, v. 276, p. 1–10, 15 jun. 2018.

HARNSOONGNOEN, S.; WANTHONG, A. Coplanar Waveguide Transmission Line Loaded with Electric-LC Resonator for Determination of Glucose Concentration Sensing. **IEEE Sensors Journal**, v. 17, n. 6, p. 1635–1640, 15 mar. 2017.

HUANG, S. Y. et al. Microstrip Line-Based Glucose Sensor for Noninvasive Continuous Monitoring Using the Main Field for Sensing and Multivariable Crosschecking. **IEEE Sensors Journal**, v. 19, n. 2, p. 535–547, 15 jan. 2019.

HUANG, Y. J. et al. A CMOS cantilever-based label-free DNA SoC with improved sensitivity for hepatitis B virus detection. **IEEE Transactions on Biomedical Circuits and Systems**, v. 7, n. 6, p. 820–831, dez. 2013.

IDF Diabetes Atlas | Tenth Edition. Disponível em: <https://diabetesatlas.org/>. Acesso em: 4 jul. 2022.

JARUWONGRUNGSEE, K. et al. **Microfluidic-based split-ring-resonator sensor for real-time and label-free biosensing**. Procedia Engineering. **Anais**...Elsevier Ltd, 1 jan. 2015.

JUAN, C. G. et al. Concentration Measurement of Microliter-Volume Water-Glucose Solutions Using Q Factor of Microwave Sensors. **IEEE Transactions on Instrumentation and Measurement**, v. 68, n. 7, p. 2621–2634, 1 jul. 2019.

KAATZE, U.; FELDMAN, Y. Broadband dielectric spectrometry of liquids and biosystems. **Measurement Science and Technology**, v. 17, n. 2, p. R17, 23 dez. 2005.

KARP, G.; IWASA, J.; MARSHALL, W. Karp's cell and molecular biology: Concepts and experiments. **Hoboken, NJ : John Wiley & Sons**, p. 832, 2016.

KAUR, G.; TOMAR, M.; GUPTA, V. Development of a microfluidic electrochemical biosensor: Prospect for point-of-care cholesterol monitoring. **Sensors and Actuators, B: Chemical**, v. 261, p. 460–466, 15 maio 2018.

KEISER, G. Overview of Biophotonics. Em: [s.l: s.n.]. p. 1–23.

KIM, H. H. et al. Highly sensitive microcantilever biosensors with enhanced sensitivity for detection of human papilloma virus infection. **Sensors and Actuators, B: Chemical**, v. 221, p. 1372–1383, 24 ago. 2015.

KOMAROV, V.; WANG, S.; TANG, J. Permittivity and Measurements. **Encyclopedia of RF and Microwave Engineering**, 15 abr. 2005.

KRUPKA, J. **Frequency domain complex permittivity measurements at microwave frequencies**. Measurement Science and Technology. **Anais**...Institute of Physics Publishing, 1 jun. 2006.

LA GIOIA, A. et al. Open-Ended Coaxial Probe Technique for Dielectric Measurement of Biological Tissues: Challenges and Common Practices. **Diagnostics**, v. 8, n. 2, p. 40, 5 jun. 2018.

LAZEBNIK, M. et al. A large-scale study of the ultrawideband microwave dielectric properties of normal, benign and malignant breast tissues obtained from cancer surgeries. **Physics in medicine and biology**, v. 52, n. 20, p. 6093–6115, 21 out. 2007.

LECAULT, V. et al. Microfluidic single cell analysis: from promise to practice. **Current Opinion in Chemical Biology**, v. 16, n. 3–4, p. 381–390, 1 ago. 2012.

LEE, H. J. et al. DNA sensing using split-ring resonator alone at microwave regime. **Journal of Applied Physics**, v. 108, n. 1, p. 014908, 14 jul. 2010.

LEE, H. J. et al. A planar split-ring resonator-based microwave biosensor for label-free detection of biomolecules. **Sensors and Actuators B: Chemical**, v. 169, p. 26–31, 5 jul. 2012a.

LEE, H. J. et al. A planar split-ring resonator-based microwave biosensor for label-free detection of biomolecules. **Sensors and Actuators, B: Chemical**, v. 169, p. 26–31, 5 jul. 2012b.

LEE, H. J.; YOOK, J. G. Biosensing using split-ring resonators at microwave regime. **Applied Physics Letters**, v. 92, n. 25, p. 254103, 27 jun. 2008.

LI, C. et al. Principles and Applications of RF/Microwave in Healthcare and Biosensing. **Principles and Applications of RF/Microwave in Healthcare and Biosensing**, p. 1–325, 24 out. 2016.

LI, H. et al. Differentiation of live and heat-killed E. coli by microwave impedance spectroscopy. **Sensors and Actuators B: Chemical**, v. 255, p. 1614–1622, 1 fev. 2018a.

LI, J. et al. Red blood cells aggregability measurement of coagulating blood in extracorporeal circulation system with multiple-frequency electrical impedance spectroscopy. **Biosensors and Bioelectronics**, v. 112, p. 79–85, 30 jul. 2018b.

LIEBE, H. J.; HUFFORD, G. A.; MANABE', T. A MODEL FOR THE COMPLEX PERMITTIVITY OF WATER AT FREQUENCIES BELOW 1 THz. **International Journal of Infrared and Millimeter Waves**, v. 12, n. 7, 1991.

LIU, C. F.; WANG, M. H.; JANG, L. S. Microfluidics-based hairpin resonator biosensor for biological cell detection. **Sensors and Actuators, B: Chemical**, v. 263, p. 129–136, 15 jun. 2018.

LIU, Y.; LU, H. Microfluidics in Systems Biology – Hype or Truly Useful? **Current opinion in biotechnology**, v. 39, p. 215, 1 jun. 2016.

LUCISANO, J. Y. et al. Glucose Monitoring in Individuals With Diabetes Using a Long-Term Implanted Sensor/Telemetry System and Model. **IEEE transactions on bio-medical engineering**, v. 64, n. 9, p. 1982–1993, 1 set. 2017.

LUO, X.; DAVIS, J. J. Electrical biosensors and the label free detection of protein disease biomarkers. **Chemical Society Reviews**, v. 42, n. 13, p. 5944–5962, 10 jun. 2013.

MADURAIVEERAN, G.; SASIDHARAN, M.; GANESAN, V. **Electrochemical sensor and biosensor platforms based on advanced nanomaterials for biological and biomedical applications**. **Biosensors and Bioelectronics**Elsevier Ltd, , 30 abr. 2018.

MASON, A. et al. A resonant co-planar sensor at microwave frequencies for biomedical applications. **Sensors and Actuators A: Physical**, v. 202, p. 170–175, 1 nov. 2013.

MCKINNON, K. M. Flow Cytometry: An Overview. **Current protocols in immunology**, v. 120, p. 5.1.1, 2 fev. 2018.

MEHROTRA, P.; CHATTERJEE, B.; SEN, S. **EM-wave biosensors: A review of RF, microwave, mm-wave and optical sensing**. **Sensors (Switzerland)**MDPI AG, , 1 mar. 2019.

MOLONEY, B. M. et al. Microwave Imaging in Breast Cancer – Results from the First-In-Human Clinical Investigation of the Wavelia System. **Academic Radiology**, 4 ago. 2021.

MURATA, K. I.; HANAWA, A.; NOZAKI, R. Broadband complex permittivity measurement techniques of materials with thin configuration at microwave frequencies. **Journal of Applied Physics**, v. 98, n. 8, p. 084107, 15 out. 2005.

NADERI ASRAMI, P. et al. A novel impedimetric glucose biosensor based on immobilized glucose oxidase on a CuO-Chitosan nanobiocomposite modified FTO electrode. **International Journal of Biological Macromolecules**, v. 118, p. 649–660, 15 out. 2018.

NERGUIZIAN, V. et al. Characterization of several cancer cell lines at microwave frequencies. **Measurement: Journal of the International Measurement Confederation**, v. 109, p. 354–358, 1 out. 2017.

NIELSEN, S. B.; OTZEN, D. E. Quartz Crystal Microbalances as Tools for Probing Protein–Membrane Interactions. Em: **Methods in Molecular Biology**. [s.l.] Humana Press Inc., 2019. v. 2003p. 31–52.

NIKOLOVA, N. K. Microwave imaging for breast cancer. **IEEE Microwave Magazine**, v. 12, n. 7, p. 78–94, dez. 2011.

ORLOFF, N. D. et al. Dielectric characterization by microwave cavity perturbation corrected for nonuniform fields. **IEEE Transactions on Microwave Theory and Techniques**, v. 62, n. 9, p. 2149–2159, 2014.

O'ROURKE, A. P. et al. Dielectric properties of human normal, malignant and cirrhotic liver tissue: in vivo and ex vivo measurements from 0.5 to 20 GHz using a precision open-ended coaxial probe. **Physics in medicine and biology**, v. 52, n. 15, p. 4707–4719, 8 ago. 2007.

ÖZTÜRK, E. et al. Resveratrol and diabetes: A critical review of clinical studies. **Biomedicine & pharmacotherapy = Biomedecine & pharmacotherapie**, v. 95, p. 230–234, 1 nov. 2017.

PARSAMYAN, H. A. et al. DETERMINATION OF GLUCOSE CONCENTRATION IN AQUEOUS SOLUTION BY USING MODIFIED HILBERT SHAPED MICROWAVE METAMATERIAL SENSOR. **Proceedings of the YSU A: Physical and Mathematical Sciences**, v. 52, n. 2 (246), p. 144–148, 15 ago. 2018.

PINHEIRO, J. M. et al. 110-GHz Through-Substrate-Via Transition Based on Copper Nanowires in Alumina Membrane. **IEEE Transactions on Microwave Theory and Techniques**, v. 66, n. 2, p. 784–790, 1 fev. 2018.

PIRES, N. M. M. et al. Recent Developments in Optical Detection Technologies in Lab-on-a-Chip Devices for Biosensing Applications. **Sensors (Basel, Switzerland)**, v. 14, n. 8, p. 15458, 21 ago. 2014.

POZAR, D. M. Microwave Engineering, 4th Edition. **John Wiley &Sons, Inc**, p. 1–756, 2012.

QUAZI, S. Application of Biosensors in Cancers, An Overview. 31 jan. 2022.

REJINOLD, N. S.; JAYAKUMAR, R.; KIM, Y. C. Radio frequency responsive nano-biomaterials for cancer therapy. **Journal of controlled release : official journal of the Controlled Release Society**, v. 204, p. 85–97, 28 abr. 2015.

ROELVINK, J.; TRABELSI, S.; NELSON, S. O. A planar transmission-line sensor for measuring the microwave permittivity of liquid and semisolid biological materials. **IEEE Transactions on Instrumentation and Measurement**, v. 62, n. 11, p. 2974–2982, 2013.

SALITERMAN, S. S. **Fundamentals of BioMEMS and Medical Microdevices | (2006) | Saliterman | Publications | Spie**. Disponível em: <https://spie.org/Publications/Book/631781?SSO=1>. Acesso em: 15 jun. 2022.

SANSONE, L. et al. Label-free optical biosensing at femtomolar detection limit. **Sensors and Actuators, B: Chemical**, v. 255, p. 1097–1104, 1 fev. 2018.

SANTANGELO, M. F. et al. SiPM as miniaturised optical biosensor for DNA-microarray applications. **Sensing and Bio-Sensing Research**, v. 6, p. 95–98, 1 dez. 2015.

SCHWAN, H. P. Electrical Properties of Tissue and Cell Suspensions. **Advances in biological and medical physics**, v. 5, p. 147–209, 1 jan. 1957.

SCHWAN, H. P. Analysis of Dielectric Data: Experience Gained with Biological Materials. **undefined**, v. EI-20, n. 6, p. 913–922, 1985.

SEO, S. et al. High frequency wideband permittivity measurements of biological substances using coplanar waveguides and application to cell suspensions. **IEEE MTT-S International Microwave Symposium Digest**, p. 915–918, 2008.

SHA, L.; WARD, E. R.; STROY, B. A review of dielectric properties of normal and malignant breast tissue. **Conference Proceedings - IEEE SOUTHEASTCON**, p. 457–462, 2002.

SISTA, R. et al. Development of a digital microfluidic platform for point of care testing. **Lab on a chip**, v. 8, n. 12, p. 2091–2104, 2008.

SKOCIK, P.; NEUMANN, P. **Measurement of complex permittivity in free space**. Procedia Engineering. **Anais**...Elsevier Ltd, 1 jan. 2015.

STOKES, D. L.; GRIFFIN, G. D.; VO-DINH, T. Detection of E. coli using a microfluidics-based antibody biochip detection system. **Fresenius' Journal of Analytical Chemistry 2001 369:3**, v. 369, n. 3, p. 295–301, 2001.

SUHITO, I. R.; KOO, K. M.; KIM, T. H. **Recent advances in electrochemical sensors for the detection of biomolecules and whole cells**. **Biomedicines**MDPI AG, , 1 dez. 2021.

TANG, H. et al. Amperometric glucose biosensor based on adsorption of glucose oxidase at platinum nanoparticle-modified carbon nanotube electrode. **Analytical Biochemistry**, v. 331, n. 1, p. 89–97, 1 ago. 2004.

THORSEN, T.; MAERKL, S. J.; QUAKE, S. R. Microfluidic Large-Scale Integration. **Science**, v. 298, n. 5593, p. 580–584, 18 out. 2002.

TURNER, A. P. F.; KARUBE, I.; WILSON, G. S. Biosensors : fundamentals and applications. p. 770, 1987.

VANDER VORST, A.; ROSEN, A.; KOTSUKA, Y. RF/Microwave Interaction with Biological Tissues. **RF/Microwave Interaction with Biological Tissues**, p. 1–330, 21 fev. 2006.

WANG, Q.; ZHAO, W. M. **Optical methods of antibiotic residues detections: A comprehensive review**. **Sensors and Actuators, B: Chemical**Elsevier B.V., , 15 set. 2018.

WANG, S. et al. Cantilever with immobilized antibody for liver cancer biomarker detection. **Journal of Semiconductors**, v. 35, n. 10, p. 104008, 1 out. 2014.

WATTS, C. et al. Microwave Dielectric Sensing of Free-Flowing, Single, Living Cells in Aqueous Suspension. **IEEE Journal of Electromagnetics, RF and Microwaves in Medicine and Biology**, v. 4, n. 2, p. 97–108, 1 jun. 2020.

WOLF, M. et al. Broadband Dielectric Spectroscopy on Human Blood. **Biochimica et Biophysica Acta - General Subjects**, v. 1810, n. 8, p. 727–740, 25 maio 2011.

WU, G. et al. Bioassay of prostate-specific antigen (PSA) using microcantilevers. **Nature Biotechnology**, v. 19, n. 9, p. 856–860, 2001.

YILMAZ, T.; FOSTER, R.; HAO, Y. Broadband tissue mimicking phantoms and a patch resonator for evaluating noninvasive monitoring of blood glucose levels. **IEEE Transactions on Antennas and Propagation**, v. 62, n. 6, p. 3064–3075, 2014.

YOO, S. M.; LEE, S. Y. **Optical Biosensors for the Detection of Pathogenic Microorganisms**. **Trends in Biotechnology**Elsevier Ltd, , 1 jan. 2016.

ZARIFI, M. H. Sensitivity and Selectivity Enhancement in Coupling Ring Resonator Sensors Using Splitting Resonant Frequencies. **IEEE MTT-S International Microwave Symposium Digest**, v. 2018- June, p. 36–39, 17 ago. 2018.

ZHANG, L. Y. et al. Discrimination of colorectal cancer cell lines using microwave biosensors. **Sensors and Actuators, A: Physical**, v. 216, p. 405–416, 1 set. 2014.

PUBLICATIONS DERIVED FROM THIS THESIS

SHAHRI, A. A.; OMIDVAR, A. H.; REHDER, G. P.; SERRANO, A. L. C. A high sensitivity microwave glucose sensor. *Meas. Sci. Technol.*, v.32, p. 075104, 2021. https://doi.org/10.1088/1361-6501/abe1e3

AMANATI SHAHRI, A.; OMIDVAR, A.H.; PAMPLONA REHDER, G.; SERRANO, A.L.C. A microwave-based microfluidic cell detecting biosensor for biological quantification using the metallic nanowire-filled membrane technology. *Sensors,* v. 22, n.9, p. 3265, 2022. https://doi.org/10.3390/s22093265

APPENDIX

Appendix E

Two-Port Network Parameters

A microwave network with two terminals may be analyzed by considering the network as an equivalent two-port. The signals at the terminals or ports of the two-port may be described in terms of voltages and currents and the interaction between these signals in terms of impedances or admittances. Alternatively, the signals may be described in terms of incident and reflected waves and the interaction in terms of scattering.

An arbitrary two-port may be described in several ways. Here we will discuss the two-port in terms of impedance parameters (Z), admittance parameters (Y), chain or ABCD parameters and scattering parameters (S).

For the description in terms of Z, Y or ABCD parameters we refer to Figure E.1(a). For the description in terms of S parameters we refer to Figure E.1(b).

The relation between the voltages and currents in terms of impedance parameters is given by

$$\begin{pmatrix} V_1 \\ V_2 \end{pmatrix} = \begin{pmatrix} Z_{11} & Z_{12} \\ Z_{21} & Z_{22} \end{pmatrix} \begin{pmatrix} I_1 \\ I_2 \end{pmatrix}. \tag{E.1}$$

The relation between the currents and voltages in terms of admittance parameters is given by

$$\begin{pmatrix} I_1 \\ I_2 \end{pmatrix} = \begin{pmatrix} Y_{11} & Y_{12} \\ Y_{21} & Y_{22} \end{pmatrix} \begin{pmatrix} V_1 \\ V_2 \end{pmatrix}. \tag{E.2}$$
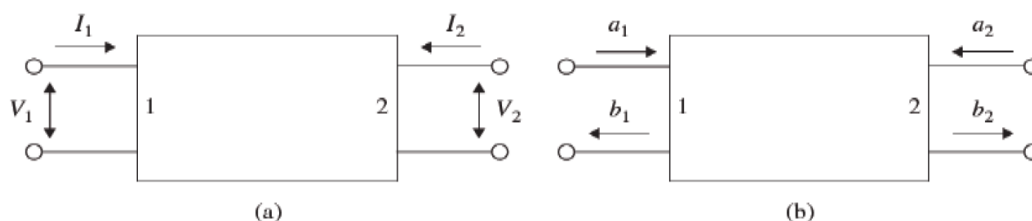
Figure E.1 Two-port definition. (a) Using voltages and currents. (b) Using incident and reflected waves.

Table E.3 Two-port parameter conversion for scattering and voltage- and current-based matrices

	S	
S	S_{11} S_{12}	
	S_{21} S_{22}	
Z	$Z_0 \frac{(1+S_{11})(1-S_{22})+S_{12}S_{21}}{(1-S_{11})(1-S_{22})-S_{12}S_{21}}$	$Z_0 \frac{2S_{12}}{(1-S_{11})(1-S_{22})-S_{12}S_{21}}$
	$Z_0 \frac{2S_{21}}{(1-S_{11})(1-S_{22})-S_{12}S_{21}}$	$Z_0 \frac{(1-S_{11})(1+S_{22})+S_{12}S_{21}}{(1-S_{11})(1-S_{22})-S_{12}S_{21}}$
Y	$Y_0 \frac{(1-S_{11})(1+S_{22})+S_{12}S_{21}}{(1+S_{11})(1+S_{22})-S_{12}S_{21}}$	$-Y_0 \frac{2S_{12}}{(1+S_{11})(1+S_{22})-S_{12}S_{21}}$
	$-Y_0 \frac{2S_{21}}{(1+S_{11})(1+S_{22})-S_{12}S_{21}}$	$Y_0 \frac{(1+S_{11})(1-S_{22})+S_{12}S_{21}}{(1+S_{11})(1+S_{22})-S_{12}S_{21}}$
ABCD	$\frac{(1+S_{11})(1-S_{22})+S_{12}S_{21}}{2S_{21}}$	$Z_0 \frac{(1+S_{11})(1+S_{22})-S_{12}S_{21}}{2S_{21}}$
	$\frac{1}{Z_0} \frac{(1-S_{11})(1-S_{22})-S_{12}S_{21}}{2S_{21}}$	$\frac{(1-S_{11})(1+S_{22})+S_{12}S_{21}}{2S_{21}}$

The relation between the incident and reflected waves is given by

$$\begin{pmatrix} b_1 \\ b_2 \end{pmatrix} = \begin{pmatrix} S_{11} & S_{12} \\ S_{21} & S_{22} \end{pmatrix} \begin{pmatrix} a_1 \\ a_2 \end{pmatrix}. \tag{E.4}$$

The Z, Y, ABCD and S matrices may be converted into each other. The interrelations between the voltage- and current-based matrices are given in Table E.1.

The interrelations between the scattering and voltage- and current-based matrices are given in Tables E.2 and E.3.